Homology Search Guidance by the Yeast Recombination Enhancer

Dissertation

zur Erlangung des Doktorgrades

der Fakultät für Biologie

der Ludwig-Maximilians-Universität München

vorgelegt von

Benjamin Anstett, M.Sc. Molecular Biosciences

Februar 2017

Eidesstattliche Versicherung und Erklärung

Hiermit versichere ich, Benjamin Anstett, an Eides statt, dass ich die vorliegende Dissertation "Homology Search Guidance by the Yeast Recombination Enhancer" selbstständig und ohne unerlaubte Hilfe angefertigt habe. Ich habe weder anderweitig versucht, eine Dissertation einzureichen oder eine Doktorprüfung durchzuführen, noch habe ich diese Dissertation oder Teile derselben einer anderen Prüfungskommission vorgelegt.

München, den……………..   ……………………………………..

                                                                    (Unterschrift)

Die vorliegende Arbeit wurde zwischen Januar 2012 und Februar 2017 unter der Anleitung von Prof. Dr. Stefan Jentsch am Max-Planck-Institut für Biochemie in Martinsried durchgeführt.

Per aspera ad astra

Table of Contents

1 Summary

Homologous recombination (HR) is an essential mechanism to repair DNA double-strand breaks (DSBs) and to maintain genome integrity. HR uses an intact homologous donor sequence as a template to repair a DSB and has been extensively studied for decades. The probably best understood model system to investigate HR is the mating type system of the budding yeast *S. cerevisiae*, which allows a yeast cell to switch its mating type (*MATa* or *MATα*) and undergo diploidization with a cell of the opposite mating type. To initiate the mating type switch, a site-specific DSB is induced by HO endonuclease in the mating type locus on chromosome III. Repair of the break is then performed via recombination with one of two donor loci, depending on the mating type of the cell. The correct donor is chosen with a surprisingly high efficiency. This donor preference is mainly facilitated by the cis-acting recombination enhancer (RE) element. In *MATa* cells the RE is activated and bound by trans-acting factors like Fkh1. A chromosomal loop is proposed to form between the RE and the mating type locus, enabling efficient recombination with the correct donor locus located upstream of the RE. However, it is still not understood how this chromosomal loop is formed and which factors contribute. Generally, chromosomal loops are relevant, as chromosome and nuclear architecture are known to shape HR. Furthermore, the influence of the RE on homology search remained largely enigmatic.

This study sheds light onto the mechanism of RE-guided homology search (the search for a homologous sequence), using chromatin immunoprecipitation (ChIP) of the recombinase Rad51 as well as recombination efficiency measurements in *S. cerevisiae*. I demonstrate that the RE can be uncoupled from the mating type system and acts as a general recombinational enhancer of nearby donor sites during HR when placed at different genomic sites, independent of the DSB-inducing endonuclease. Furthermore, the RE guides ongoing homology search reflected by the Rad51 nucleoprotein filament, which assists in the recognition of the homologous donor site. Moreover, this study corroborates the essential function of Fkh1 and its phosphothreonine-binding forkhead associated (FHA) domain for the regulation of donor preference. Well-known factors involved in DSB repair like RPA and Mph1 are identified as Fkh1 interaction partners via a mass spectrometry based approach. I propose that these factors mediate the potential loop formation between the RE and the DSB via a phosphorylation-dependent interaction with Fkh1 bound to the RE. Finally, a role in donor preference regulation can be assigned to the checkpoint kinase Mec1.

In summary, this study does not only provide evidence for a general role of the RE as a facilitator of recombination, but also gives intriguing insights on a multi-factorial Fkh1 anchor pad at the DSB site that contributes to the function of the RE.

2 Introduction

2.1 DNA damage

DNA carries the unique genetic code that contains the instructions to generate proteins, cellular structures and organisms. The whole set of DNA of an organism is the genome, which enables the organism to develop, live and reproduce. During DNA replication the genome is duplicated and passed to daughter cells, whereas the distinctive genetic information is preserved.

The stability of DNA is constantly facing multiple threats: creation of abasic sites and deamination mostly caused by spontaneous hydrolysis[1], endogenous processes like replication[2] and transcription[3], exogenous events like radiation and chemical agents and oxidative damage[1,4-6] (Figure 1). In total, the lesions a human genome experiences per day sums up to 10^5 changes[5]. Moreover, long exposure to UV radiation like sunlight can double this amount of DNA damage[5]. DNA damage contributes to premature aging and development of cancer and harms the overall genomic integrity[5] (Figure 1 B). Therefore, cells developed sophisticated DNA damage repair pathways to counteract this quandary. Multiple pathways have been characterized during decades of DNA damage research[7]. Simultaneously, a large range of DNA lesions has also been identified[7] (Figure 1 A). DNA damage includes base substitutions, intra- and interstrand-crosslinks, micro-insertions or -deletions and different types of DNA strand breaks[8]. Due to the fundamental role of DNA as the carrier of genetic instructions, repair pathways like mismatch repair (MMR), base-excision repair (BER), nucleotide-excision repair (NER) as well as homologous recombination (HR) are highly conserved mechanisms from microorganisms to humans[9,10]. Altogether, these pathways constitute the DNA damage response (DDR) that signals and repairs DNA lesions, preventing cell death as well as development of diseases associated with DNA damage[7,8].
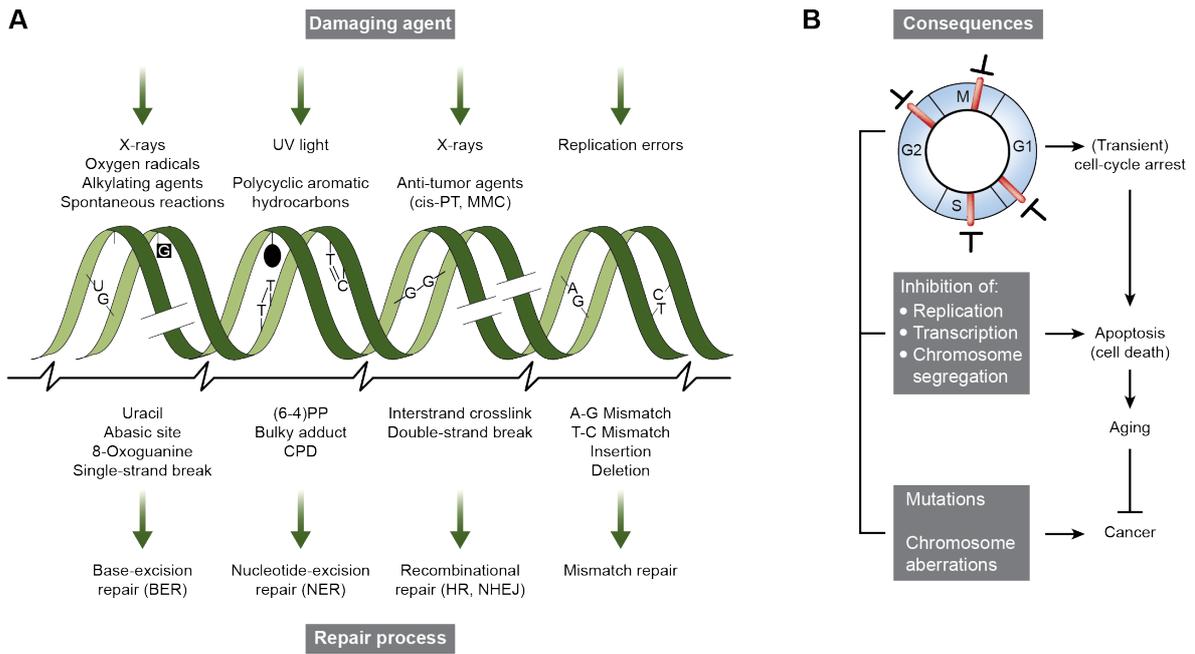
Figure 1 | **DNA damage, its repair mechanisms and consequences.**
(A) DNA damage is caused by a wide range of exogenous and endogenous damaging agents. Common lesions are base modifications like guanine oxidation (causing 8-Oxoguanine) and cytosine deamination (generating uracil). UV light can cause bulk adducts like 6,4 photoproducts ((6-4)PP) as well as cyclobutane pyrimidine dimers (CPD). Stalled or collapsed replication forks during DNA replication as well as ionizing radiation like X-rays can also generate DNA strand breaks (single- and double-strand breaks) and DNA insertions/deletions, respectively. Several pathways evolved to counteract these cytotoxic lesions.
(**B**) A signaling cascade known as the DNA damage response is activated by the DNA damage mentioned in (A), coupling cell cycle progression to damage repair. In the long view DNA damage causes two different consequences: first, if endogenous processes like replication or transcription are constantly impaired by DNA damage, cell death is triggered, which can contribute to premature aging. Second, surviving cells permanently accumulate genetic changes like point mutations and chromosomal aberrations, supporting the development of cancer.
Adapted from[11].

2.2 DNA double-strand breaks and repair mechanisms

2.2.1 The impact of double-strand breaks

DNA break damage is composed of two different lesions: single-strand breaks (SSBs) and double-strand breaks (DSBs). SSBs can occur as a result of replication stress and endogenous metabolic reactions as well as exogenous sources, like radiation and chemotherapeutics[12]. Ionizing radiation (IR), for example, produces radiolysis radicals which attack the sugar-phosphate backbone of DNA[13,14]. Furthermore, topoisomerases induce SSBs as reaction intermediates[15]. If two such DNA nicks are localized within one helical turn in complementary DNA, a DSB can be generated[12,16]. Concerning IR, there are approximately 10 SSBs for each DSB induced[17]. In total, roughly 1 % of SSBs in a cell are converted to DSBs, that is about one DSB per 10^8 bp per cell cycle[12,18]. A single persisting DSB is enough to block DNA replication and trigger cell cycle arrest[19-21], demonstrating the detrimental effect of DSBs. Therefore, several genetic syndromes could be assigned to DSB repair, including cancer[11,22]. However, besides occurring randomly within the genome, DSBs are also deliberately induced by several organisms to allow genetic rearrangements. A prominent example is meiosis, a process occurring in all sexually reproducing organisms[23]. Meiotic DSBs are generated by the evolutionarily conserved endonuclease Spo11[23,24]. Also yeast cells are capable of generating a specific DSB via homothallic switching (HO) endonuclease, allowing them to switch their mating type to initiate sexual reproduction[25] (see section 2.3.1). Furthermore, in vertebrates developing lymphocytes trigger antibody diversification through V(D)J recombination. Here, RAG (recombination activating gene) endonuclease induces a DSB and repair is completed by somatic recombination[26,27].

DSB repair is essential for the cell to maintain genome integrity. Failure to repair DSBs is coupled to chromosome rearrangements or chromosome loss and can even lead to cell death[28]. Therefore, repair pathways evolved to counteract the cytotoxic potential of DSBs and will be further elucidated in the next sections. The pre-dominant DSB repair mechanisms are non-homologous end joining (NHEJ) and homologous recombination (HR, Figure 2). These pathways are evolutionarily conserved among eukaryotes and therefore, description of these mechanisms will be given only for yeast proteins. Mammalian proteins will be indicated in brackets, if they are not direct homologs or mentioned differently.

2.2.2 Signaling of DSBs

A proper protection of the genome requires the detection of all kinds of structural alterations of DNA. Therefore, a variety of molecular complexes evolved to sense and signal DNA damage[29].

The occurrence of DSBs activates the highly conserved DNA damage checkpoint, which couples the repair of DSBs to cell cycle progression. A DSB is recognized and sensed by the heterotrimeric Mre11-Rad50-Xrs2 (MRX, mammalian MRN: Nbs1 instead of Xrs2) complex[30]. MRX has a high affinity to bind to DNA ends[31] and localizes at DSB ends[32]. In addition, MRX functions in initial degradation (resection) of a DSB (see section 2.2.4)[28] and maintains the tethering of the DSB ends to each other[33,34]. A functional checkpoint response then requires the kinases Mec1 and Tel1 (mammalian ATR and ATM, respectively), both well known as key players of the DNA damage checkpoint[35]. Resection via MRX generates single-stranded DNA (ssDNA), which is then rapidly covered by the heterotrimeric ssDNA-binding protein RPA (replication protein A). The ssDNA-RPA complex plays two critical roles: 1) it recruits the phosphatidylinositol 3' kinase-like kinase (PIKK) Mec1 through its regulatory subunit Ddc2 (ATR-interacting protein, ATRIP in mammals)[36]. 2) it recruits and activates the Rad17 clamp loader which subsequently loads the PCNA-related 9-1-1 (Rad9-Rad1-Hus1) complex onto DNA[29]. Colocalization of the 9-1-1 complex and Mec1-Ddc2 then allows interactions at the damaged DNA. Mec1 phosphorylates Rad17 and 9-1-1, which is important for downstream signaling[29]. Phosphorylated Rad9 (mammalian 53BP1) is activated and amplifies this initial signal by stimulating Mec1 phosphorylation of the effector kinases Rad53 and Chk1 (mammalian CHK2 and CHK1, respectively), giving rise to a global checkpoint response (see below)[29,37].

In contrast to Mec1, Tel1 activation depends on the MRX complex, which is required for Tel1 recruitment to the site of DNA damage through a direct interaction between Tel1 and Xrs2[38-40]. Once Tel1 is loaded at DSBs by MRX, it also supports the function of MRX in resection in a positive feedback loop[40]. Consequently, Tel1 promotes the appropriate association of MRX with DNA, which is required for the tethering of the broken DNA ends. This function is independent of Tel1's kinase activity, pointing towards an additional structural role for Tel1 for the stabilization of the binding of MRX to DSBs[40,41]. Similar to Mec1, Tel1 also phosphorylates Rad53[42]. Subsequently, the checkpoint signal is strongly amplified and leads to a response including cell cycle arrest, transcription of damage inducible genes as well as activation of DNA repair[40]. DSB repair can then be performed via NHEJ (section 2.2.3) or HR (section 2.2.4).

2.2.3 Non-homologous end joining

Non-homologous end joining (NHEJ) repairs DSBs via direct ligation of the broken DNA ends[43]. Although initially only assigned to eukaryotes, it is now understood that also prokaryotes use a similar NHEJ pathway to repair DSBs[44,45]. In contrast to HR, NHEJ is not limited to any cell cycle phase[43] (compare section 2.2.4). A key selective advantage of NHEJ is its high flexibility in terms of that it allows joining of the two broken ends of almost any kind of DSB[43].

In order to initiate NHEJ, a DSB is recognized and sensed by the MRX complex as well as the ring-shaped heterodimeric Ku70/80 (Ku) complex[30,46,47]. Subsequently, proteins of both complexes bind DNA ligase IV and its co-factor Lif1 (mammalian XRCC4[48]) and position them at the break[49,50]. The next step is the critical alignment and base pairing of the free DNA overhangs to initiate ligation[43,49,51]. A recent study identified the synapsis of the DNA ends to be a two-stage process: initially DNA ends are tethered in a long-range complex by the Ku complex, followed by the formation of a short-range complex and detailed alignment by DNA ligase IV[52]. The broken ends are then aligned closely and ligation can be initiated. The early-formed joining complex can probably tolerate incompatible overhangs[53]. However, ligation cannot continue directly. Instead, modifications are conducted to permit ligation. Coordinated processing of incompatible ends requires the recruitment of several factors like the endonuclease Fen1 (mammalian ARTEMIS) or the gap-filling polymerase Pol4 (mammalian Polμ and Polλ)[54,55]. DSBs are accurately repaired by NHEJ on a regular basis. Nevertheless, the flexibility of NHEJ to modify free DNA ends makes this mechanism susceptible for small insertions or deletions[43].

Besides the classical and above described NHEJ, broken DNA ends can also be re-joined via a process named microhomology-mediated end joining (MMEJ, also: alternative NHEJ, Alt-NHEJ)[56,57]. Unlike classical NHEJ, an initial degradation of the 5' end of each side of a DSB is required for MMEJ. Studies in the budding yeast *Saccharomyces cerevisiae* (*S. cerevisiae*) showed that the endonucleolytic activity of the MRX complex together with Sae2 (mammalian CtIP) is responsible for this process[57,58], which reveals microhomologies at both sides of the DSB. A microhomology of only 6 nt (1 nt in mammals) is sufficient to align the free DNA ends and to continue with the repair process. Removal of heterologous 3' flaps is performed by the Rad1-Rad10 (mammalian XPF-ERCC1) nuclease to allow replicative polymerase δ (Pol θ in mammals) to fill in the gaps[59,60]. Ligation of the broken ends and therefore completion of MMEJ is likely carried out by DNA ligase I (DNA ligase III in mammals[61])[57]. However, MMEJ is only considered to be a backup survival pathway[57] due to deletions the pathway can introduce. When

applicable, cells repair DSBs via NHEJ or HR. The choice between these two pathways is tightly regulated and mainly coupled to the initial DNA end resection step[62]. In the next section I will describe HR in detail and highlight the differences and advantages of HR compared to NHEJ.

2.2.4 Homologous recombination

Homologous recombination (HR) is a key pathway to maintain genomic integrity and relies on an undamaged homologous DNA sequence as donor template to repair a DSB[10,63] (Figure 2). The advantage of HR is that the genetic information can be accurately restored upon DSB repair. Therefore, HR is generally considered to be an error-free repair pathway[5], which also discriminates it from NHEJ. HR typically uses an independent homologous DNA molecule as a repair template (chromosomes, sister chromatids)[63]. A previous study showed that the preferred template is the sister chromatid[64], whereas the underlying mechanism is likely sister chromatid cohesion[65]. Thus, HR is in principle restricted to the S and G2 phase of the cell cycle when a sister chromatid as a donor template is available[63].

As mentioned in section 2.2.3, pathway choice between NHEJ and HR is primarily coupled to the DNA end resection process, which takes place most effectively in the S and G2 phase[66]. HR as well as MMEJ needs resected DNA to commence, whereas NHEJ efficiency is decreased, probably due to the poor binding of the Ku complex to ssDNA[67]. The balance between these three DSB repair pathways was shown to be controlled by one of the key resection factors, Sae2, which is regulated by CDKs (cyclin-dependent kinases)[66]. Following a DSB, resection then first starts with a short-range resection of the first few hundred base pairs by the MRX complex and Sae2 (Figure 2 A)[30]. Mre11 offers an exonuclease as well as a weak endonuclease activity, the latter one being promoted by the physical interaction between MRX and Sae2[58]. Following the initial resection by MRX and Sae2, further long-range DNA degradation is then provided by the exonuclease Exo1 and the helicase-containing complex Sgs1-Top3-Rmi1 (STR; mammalian BLM-TOPO3α-RMI1-RMI2) together with the endonuclease Dna2[68,69]. The resulting ssDNA is rapidly covered by RPA, thereby preventing the formation of secondary structures[70] and inhibiting MMEJ[71]. RPA impedes the loading of the recombinase Rad51 onto ssDNA and therefore, the core recombination mediator Rad52 is needed to overcome this inhibitory effect[72,73]. Rad52 then binds Rad51 as well as RPA and facilitates the exchange of both proteins. Subsequently, Rad51 binds to ssDNA and forms a dynamic nucleoprotein filament, also known as the presynaptic filament[72]. This filament then performs the search for a homologous donor sequence (homology search) to enable error-free recombination

with the broken DNA[74-76]. Most frequently the intact DNA sequence to repair the break is located on the sister chromatid, which makes HR the favored pathway during G2 phase[10]. Nonetheless, non-allelic donor sequences on the same or other chromosomes can also be used by HR[74,77]. Once the matching DNA sequence is found, the Rad51 filament invades the homologous double-stranded counterpart and forms the typical displacement loop (D-loop) structure, thereby initiating the recombination reaction[63]. Subsequently, Rad51 is removed from the heteroduplex DNA by the Rad54 motor protein to initiate DNA synthesis by DNA polymerase δ[78,79]. The intermediate D-loop structure represents the branching point of multiple HR sub-pathways, which will be applied depending on the cellular context (Figure 2)[63]: break-induced replication (BIR), synthesis-dependent strand annealing (SDSA) and the formation of double Holliday junctions (dHJ), representing the classical DSB repair (DSBR) pathway[63]. DSBs arising by replication fork collapse have only one free end and are repaired via BIR (Figure 2 B)[80], involving the DNA helicase Pif1[81]. Despite restoration of chromosome integrity, it can lead to loss-of-heterozygosity (LOH) of the information distal to the DSB[63,80]. If a second end is present, the favored repair pathway in mitotic cells is SDSA (Figure 2 C)[63]. In this case the extended D-loop is reversed, which allows the annealing of the newly synthesized strand with the resected strand of the second DSB end. When the recombinase Dmc1 is recruited in meiotic cells, the capturing of the second DSB end inside the D-loop is favored, resulting in the formation of a dHJ (Figure 2 D)[63,82]. HJs have to be removed timely to ensure faithful chromosome segregation. Therefore, multiple endonucleases like Mus81 and Mms4 (EME1 in mammals), Slx1-Slx4 or Yen1 (GEN1 in mammals) are available to resolve these structures and to trigger genetic exchange via crossovers and non-crossovers, respectively[83]. In mitotic cells, crossover formation is strongly suppressed by HJ dissolution via the STR complex, resulting only in a low abundance of crossovers[84].

Besides the above-mentioned Rad51-dependent mechanisms, there is also another Rad51-independent pathway to repair DSBs, which uses homologous repeats to bridge DSB ends: single-strand annealing (SSA, Figure 2 E)[85]. SSA resembles MMEJ, as they both involve an annealed intermediate to synapse a DSB[85]. In case of SSA however, this intermediate is caused by re-annealing of RPA-coated ssDNA between flanking repeats, mediated by Rad52[86]. Like MMEJ, SSA causes a deletion rearrangement by removal of the 3' flaps via the Rad1-Rad10 nuclease in concert with the mismatch repair protein complex Msh2-Msh3[85]. While relatively mutagenic, SSA might be of high relevance to restore a broken chromosome with DSB ends unable to be resolved by homology-directed repair or MMEJ. Scenarios, which favor SSA would include absence of the sister chromatid or the state of the cell cycle[85]. However, the requirement of SSA inside cells remains unclear.
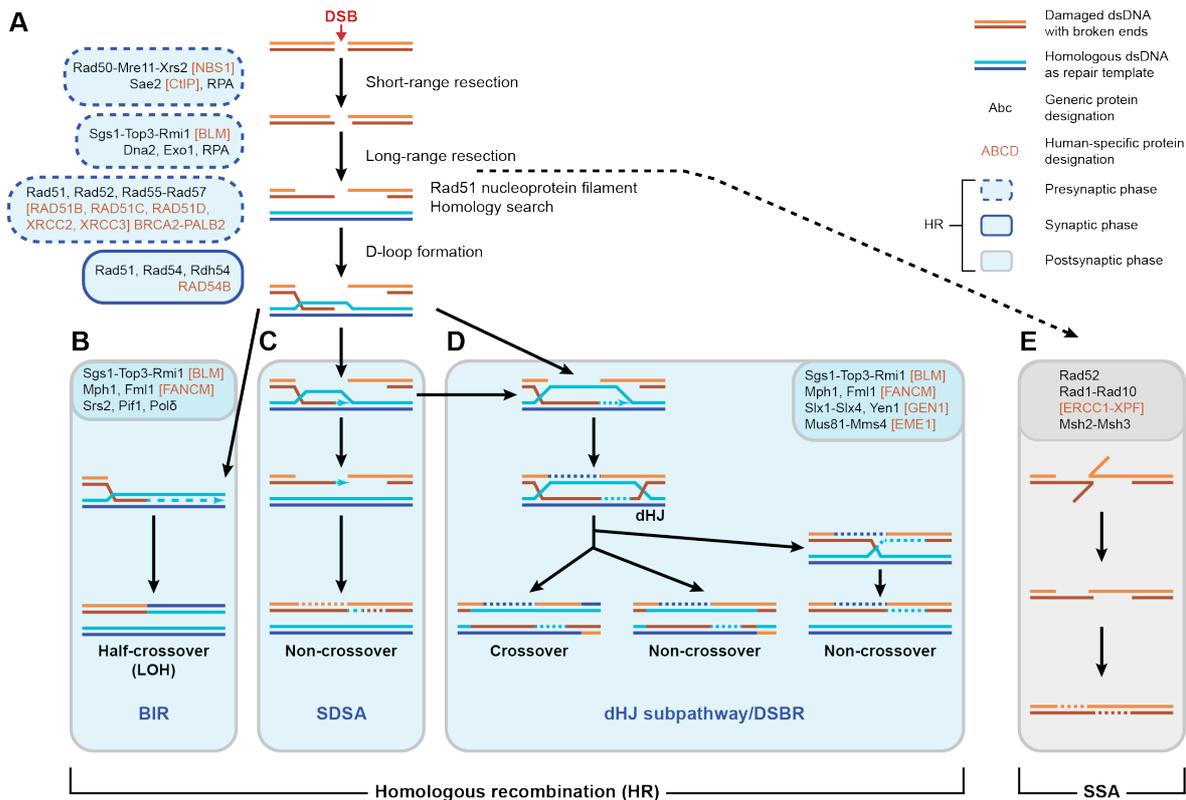
Figure 2 | **Recombination-based DSB repair mechanisms.**
(A) During S and G2 cell cycle phases, homologous recombination (HR) is the favored DSB repair pathway. Initially, DSBs undergo DNA end resection by multiple enzymes. Short-range resection is followed by long-range resection resulting in ssDNA, which is rapidly covered by RPA. Recombination mediators then facilitate the exchange of RPA for Rad51, which then together with ssDNA forms the nucleoprotein filament. This Rad51 filament then performs the homology search and invades the homologous donor template. A D-loop is formed and signifies the branching point for a set of different HR pathways.
(B) The repair of one-ended DSBs emerging at replication forks is conducted by break-induced replication (BIR), which leads to loss of heterozygosity (LOH).
(C) DSBs induced in mitotic cells are subjected to synthesis-dependent strand annealing (SDSA). Here, crossovers are avoided due to reversion of the D-loop.
(D) Meiotic DSBs result in double Holliday junction (dHJ) formation. This structure is cleaved by a variety of nucleases, mediating crossovers or non-crossovers.
(E) Rad51-independent single-strand annealing (SSA) uses homologies on opposing sides of a DSB to repair the break, supported by the strand-annealing activity of Rad52. Rad1-Rad10 nuclease removes large overhangs. SSA is a mutagenic pathway and should only be used as a backup (indicated by dashed arrow).
Adapted from[63].

2.2.5 Chromatin architecture and HR

A variety of studies revealed genomic organization from different organisms and how they are positioned in territories[87-90]. For mammalian cells it was shown that the nucleus is compartmentalized by chromosomal territories[90-93]. In the budding yeast nucleus, chromosomes show the so-called Rabl configuration with centromeres tethered to the spindle pole body (SPB) and telomeres tethered to the nuclear envelope, whereas

telomeres of shorter arms are located in a territory closer to the SPB than those in longer arms[94-96]. Besides centromeres and telomeres, a third nuclear landmark is the nucleolus, which is a crescent-shaped structure located in spatial proximity to the nuclear periphery[97]. In yeast, the nucleolus forms a dense region containing the rDNA repeats located on chromosome XII and it is assumed to act as a near absolute barrier, blocking interactions between the ends of chromosome XII[98].

Generally, spatial proximity plays a crucial role when the cell faces a DSB. For NHEJ it was shown that chromosomal translocations are mostly dictated by the spatial proximity of chromosomes[99-101]. Similar findings have been made for DSB repair by HR, whose efficiency is strongly related to the general nuclear architecture. The reason for this is the intrinsic ability of the Rad51 filament to conduct homology search more efficiently, the lower the spatial distance to the target DNA is[76,102]. Importantly, architectural features like the naturally occurring cohesin-mediated sister-chromatid cohesion or alignment of homologous chromosomes thereby pre-define an identification of the desired donor sequence, due to DSB and donor homology already being in close proximity[2,65,103,104]. In accordance with this finding, the recombination efficiency to repair a DSB generally decreases with an increasing distance of an engineered donor to the DSB[76]. Moreover, when multiple homologous sequences are provided throughout the genome, recombination between homologies on the same chromosome is more efficient[105,106]. These findings are again well explained by the general nuclear architecture of yeast cells, whereby intra-chromosomal interactions pre-dominate over inter-chromosomal interactions[98]. Additionally, multiple studies showed that recombination efficiency between homologous sequences located proximal to centromeres is higher than between donor sites located on chromosomal arms[76,96,107]. Indeed, by using a Rad51 ChIP-based approach our laboratory revealed that the Rad51 filament is guided by centromeres, represented by small Rad51 signals surrounding the regions of centromeres of all other yeast chromosomes[76]. Furthermore, when homologous alleles are located at subtelomeric regions, the recombination between them is higher when the respective chromosome arms reside in closer spatial proximity[96]. In addition, increased mobility of a DSB as well as the unbroken chromosomes might further contribute to find more distantly located homologies[108,109]. The sum of these findings led to the important conclusion that recombination efficiency between two homologous sequences is not a direct consequence of the linear distance between two homologous sequences, but rather due to the proximity of DNA in a three-dimensional setting[104].

2.3 The *S. cerevisiae* mating type switch as a model system to study homologous recombination

2.3.1 The *S. cerevisiae* mating type system

S. cerevisiae is a budding yeast and serves as model organism to study HR. Hence, major findings about HR were obtained from *S. cerevisiae* studies[25]. The propagation of *S. cerevisiae* happens vegetatively, but cells display a simple sexual differentiation, defined by their mating type, which is determined by two different alleles of the mating type (*MAT*) locus: *MATa* or *MATα* (Figure 3 A). Like many other fungi, *S. cerevisiae* has the ability to switch its mating type within a colony to mate with the opposite mating type, resulting in a *MATa* or *MATα* cell[110]. This process of mating type switching is known as homothallism[111]. The mating between two different haploid cells enables them to undergo self-diploidization (Figure 3 A). This diploid state provides the cell with a couple of evolutionary advantages such as the ability to conduct meiotic recombination or spore formation under nutritionally limiting conditions[25].

The *MAT* locus is located in the middle of the right arm of chromosome III. The mating type specific alleles, *MATa* and *MATα*, can be divided into five regions, W, X, Y, Z1 and Z2, whereas only the Y region is specific for *MATa* and *MATα* (Figure 3 B)[25]. This ~700 bp region contains the mating type specific open reading frames that regulate the cell's sexual identity[112-114], and mainly encode for proteins that act as transcriptional activators or repressors (Figure 3 B)[110]. Shared regions between *MATa* and *MATα* include the recognition site for the site-specific HO endonuclease, which induces a DSB within the *MAT* locus to enable the cell to switch its mating type (see sections 2.3.2 and 2.3.3).

MATα cells express two specific proteins, Matα1 and Matα2 (Figure 3 B). Together with the constitutively expressed Mcm1 protein, they activate a set of α-specific genes[115]. Among those is also the sequence coding for the mating pheromone α-factor[25,116]. Furthermore, the Matα2-Mcm1 complex represses a-specific genes that produce the opposite mating pheromone a-factor (encoded by *MFA1* and *MFA2*). Repression is further supported by the general transcriptional repressor Tup1 as well as the co-repressor Ssn6[117-119]. A knockout of the bidirectional promoter controlling Matα1 and Matα2 leads to an a-like behavior of cells as a-specific genes are constitutively expressed in the absence of Matα2[25]. Additionally, α-specific genes are not transcribed when Matα1 is not present[120]. In contrast, *MATa* cells express the mating type specific proteins Mata1 and Mata2 (Figure 3 B).

A   Diploidization

B   The *MAT* locus
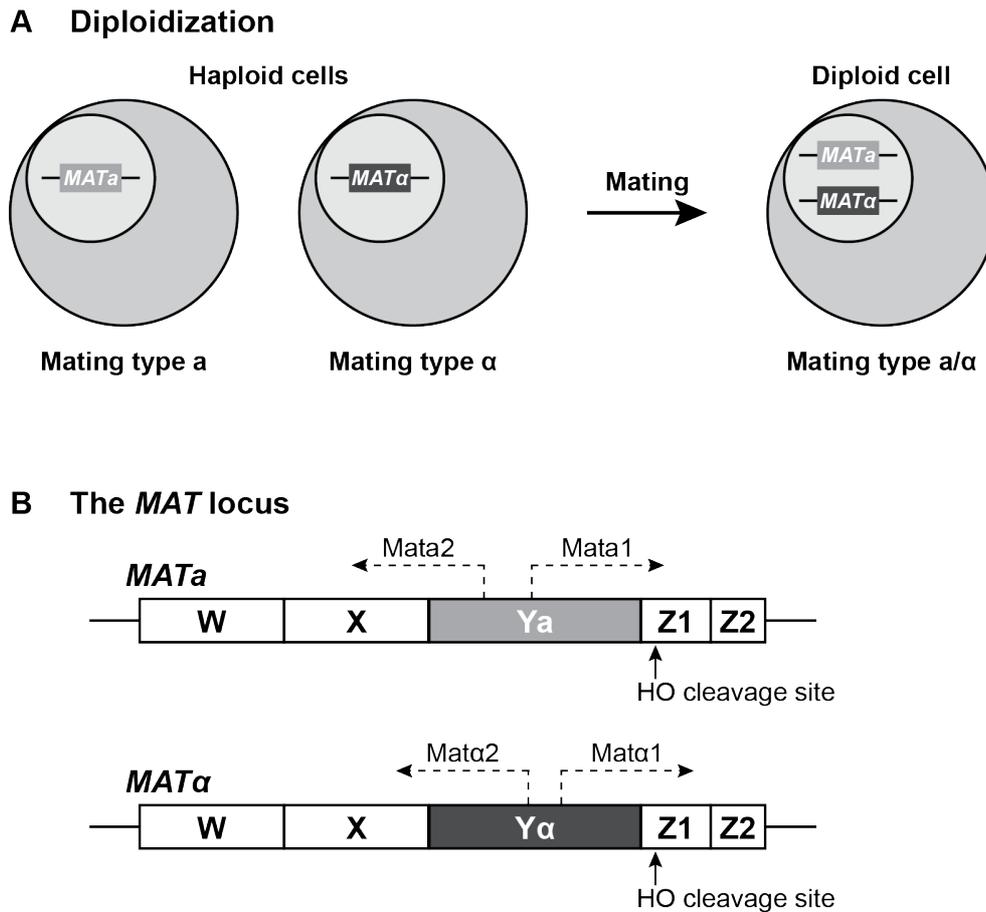
Figure 3 | **The *S. cerevisiae* mating type system.**
(A) Haploid *S. cerevisiae* cells display a simple sexual differentiation, determined by their mating type: *MATa* and *MATα*. Two haploid cells can undergo self-diploidization, resulting in a diploid cell (*MATa/α*).
(B) The mating type locus of *S. cerevisiae* on chromosome III consists of five regions: W, X, Y, Z1 and Z2. The difference between the *MATa* and *MATα* locus is defined by the Y sequence, which is specific for the mating type (Ya or Yα) and contains mating type specific open reading frames and their promoters. *MATa* cells express Mata1 and Mata2 and *MATα* cells Matα1 and Matα2. A shared sequence between both mating type loci is the recognition site for the HO endonuclease.

Whereas haploid cells are able to mate with the opposite mating type, this process is abolished in diploid cells, because of the formation of a very stable co-repressor consisting of Mata1 and Matα2 (Figure 4 A)[116,121]. This repressor allows the expression of diploid-specific genes and simultaneously turns off a set of haploid-specific genes[25]. On the one hand, the Mata1-Matα2 repressor turns off the transcription of Matα1, the activator of α-specific genes and on the other hand it allows the expression of Matα2, the repressor of a-specific genes (Figure 4 A). Therefore, diploid cells are non-mating cells[25].

2.3.2 Mating type switching via homologous recombination

Mating type switching depends on the presence of two donor mating type sequences, located at either end of chromosome III: *HMLα* (hidden *MAT* left), located at the left arm,

and *HMRa* (hidden *MAT* right), located at the end of the right arm. Following DSB induction by HO endonuclease these sequences act as donors during *MAT* switching[122,123]. Depending on the mating type of the cell one of these sequences will be copied into the *MAT* locus in an HR process known as gene conversion. Here, *MATa* cells use the *HMLα* locus to repair the break and *MATα* cells the *HMRa* locus, whereas the mating type specificity of the respective donor is transferred to the *MAT* locus. *S. cerevisiae* cells show a remarkably high efficiency of ~90 % to use the correct donor for recombination (Figure 4 B and section 2.3.3)[25].

A   Control of expression of mating type specific genes
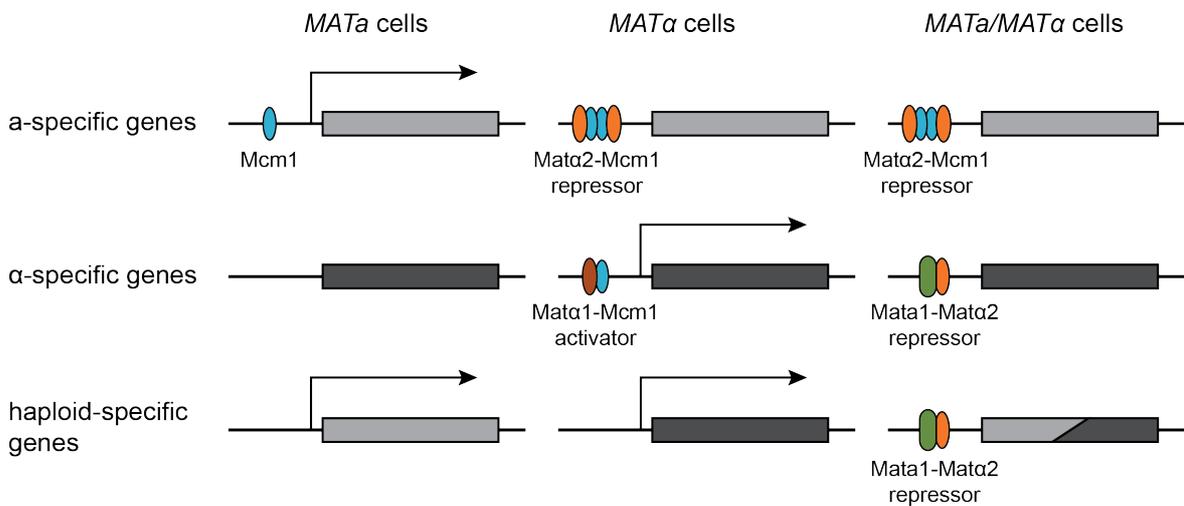
B   Donor usage
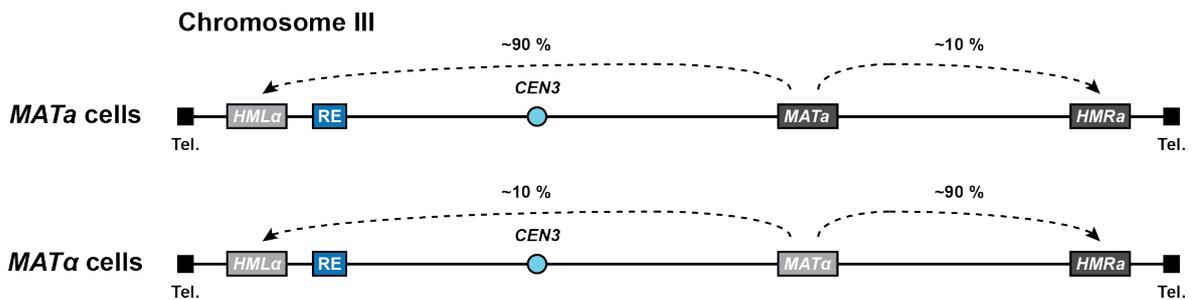
C   Donor silencing
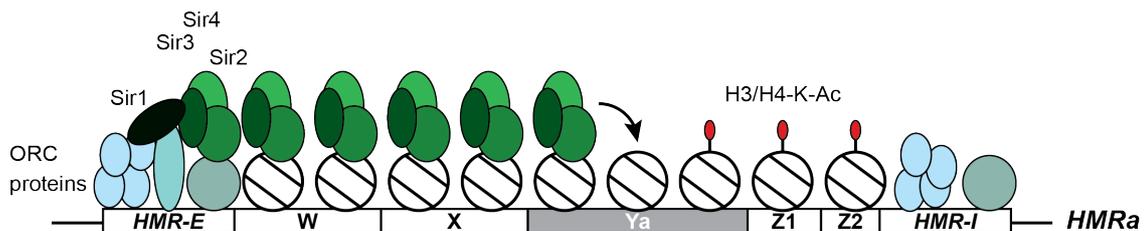
Figure 4 | **Activation and silencing of the mating type system.**
(A) Control of mating type specific genes. a-specific genes are expressed in *MATa* cells, mediated by Mcm1 as an activator. In contrast, in *MATα* and diploid (*MATa/MATα*) cells Mcm1 and Matα2 act as a repressor of a-specific genes. α-specific genes need to be activated by the Matα1-Mcm1 complex. Their expression is silenced in diploid cells by the Mata1-Matα2 repressor, which also performs general regulation of haploid-specific gene expression: Mata1-Matα2 turns off the transcription of the α-activator Matα1 and allows the expression of the a-repressor Matα2.
(B) Donor usage in the mating type system. *MATa* cells preferentially use the *HMLα* locus to conduct mating type switching. In contrast, *MATα* cells show a high preference for the *HMRa* locus. In both mating types, the correct donor is chosen with an efficiency of 90 %.
(C) Silencing of the *HMRa* donor locus. The locus is flanked by two silencing sequences, *HMR-E* and *HMR-I*. ORC (origin recognition complex) proteins bound to *HMR-E* recruit Sir1 that subsequently recruits the Sir2-Sir3-Sir4 complex. Sir2 deacetylates lysines on the N-terminal tails of histones H3 and H4, which allows Sir3-Sir4 to bind and stabilize the position of the nucleosome. Sir2 then continues to deacetylate the next nucleosomes and silencing spreads further. The silencing here is only progressing in one direction. Actually, silencing spreads from both flanking sequences, *HMR-E* and *HMR-I*. Silencing is similar for the *HMLα* locus.
A and C are adapted from[25].

Yet, mating type switching via gene conversion relies on a twofold intrinsic problem: 1) mating type information at *HML*/*HMR* must not be expressed to maintain a definite mating type and 2) HO endonuclease must not induce a DSB at its recognition sites at *HML*/*HMR* to allow both loci to function as intact donors. Intriguingly, the single solution for both of these issues is the packaging of *HML* and *HMR* sequences into an unusual, silent chromatin configuration. *HMLα* as well as *HMRa* are surrounded by a pair of distinct silencer sequences, designated *HML-E*, *HML-I*, *HMR-E* and *HMR-I* (Figure 4 C)[25]. A set of trans-acting factors interacts with these sequences to repress transcription of either locus. Among these factors are the four silent information regulator (Sir) proteins (Sir1-4) as well as several chromatin modifiers. Together with the sequences surrounding *HMLα* and *HMRa* they produce short regions (~3 kb) of heterochromatin, whereby *HMLα* and *HMRa* are packed within highly ordered nucleosomes[124,125]. Therefore, they are neither accessible for HO nor for any transcriptional activator[126,127]. One of the major factors in this silencing process is the deacetylase Sir2, which is required for deacetylation of several lysines on the N-terminal tails of histones H3 and H4 (Figure 4 C)[128]. Whereas none of the four Sir proteins directly bind to DNA, they interact with each other and bind to histones H3 and H4, thereby providing the base for the silencing mechanism performed by Sir2[129,130]. Interestingly, there seem to be differences in the strength of the silencing between *HMLα* and *HMRa*. In detail, *HMR-E* was found to be enough to silence a couple of usually transcribed genes when they were inserted at the place of the Ya region, whereas *HMR-I* was not enough to fulfill this task[131,132]. In contrast, each *HML-E* and *HML-I* alone are sufficient to silence *HMLα* as well as other genes placed nearby[25,133]. Further studies also showed that the distance between the *E* and *I* sequences is also important for the efficiency of their silencing ability. When the mating type sequences between *E* and *I* are replaced with a *LEU2* gene, transcription of the gene is turned off. If

LEU2 is just inserted within the mating type sequences, thereby increasing the distance between *E* and *I* to more than 3 kb, *LEU2* is expressed at low levels, thereby enabling cells to grow in media lacking leucine[25]. In summary, silencing plays an essential role for mating type switching. It facilitates the cell to maintain its correct mating type and to choose the correct donor to efficiently convert its mating type from *MATa* to *MATα* and vice versa.

2.3.3 Mating type switching as a model to study homologous recombination

The configuration of the yeast mating type system makes it an exquisite system to study homologous recombination at a defined DSB. Whereas treatment of cells with DNA damaging agents results in bulk DNA damage, induction of multiple DNA repair pathways and often ends with cell death, the mating type system represents a very specialized site-specific chromosomal DSB repair event. However, the *HO* locus is only expressed in haploid cells and at the G1 phase of the cell cycle[134]. To overcome this limitation, a system was developed, in which expression of HO is galactose-inducible and independent of the cell cycle[135]. With this approach a DSB can be induced simultaneously in all cells and DNA products can be further investigated[126]. As a consequence, the ability to synchronously induce a single and site-specific DSB within the mating type switching system in *S. cerevisiae* contributed major findings about DSB-induced mitotic recombination, including the kinetics and genetic requirements of molecular steps during DSB repair[25,76,136,137]. In vitro, a 24 bp degenerated recognition site is enough to induce a DSB by HO endonuclease[138]. It was shown that *MAT* switching induced by HO is a slow process, whereas it takes 1 h to finish recombination and end up with a new mating type, independent of the time during the cell cycle[25,126]. Following DSB induction, resection takes place as described above (see sections 2.2.2 and 2.2.4) and Rad51 binds to the resected ssDNA to form the nucleoprotein filament, which then performs the search for the homologous donor to repair the break. This process could be monitored by our laboratory using a Rad51 ChIP-on-chip system[76]. Interestingly, the Z side of recipient and donor seems to initiate the copying process, although the shared homology between *MAT* and its donors at this side is relatively small: *MAT* and *HMLα* share 230 bp, whereas *MAT* and *HMRa* share 327 bp. In contrast, the overlap in the W/X region is roughly 1400 bp[25]. *MAT* switching does not only replace the mating type specific Y region, but also partially includes the neighboring homologous sequences[139]. Notably, crossovers are rare events during mating type switching (see section 2.3.4.2)[25]. This seems to depend mainly on two helicases, Sgs1 and Mph1. Sgs1 is part of the STR complex (see section 2.2.4) and acts

as a dissolvase to remove dHJs that could otherwise lead to crossovers. The role of Mph1 in this process is not that clear, but it seems to be required to choose the SDSA pathway, which in contrast to the classical DSBR pathway does not lead to crossovers (compare Figure 2 C).

2.3.4 Donor preference is guided by a recombination enhancer

The preferential usage of the opposite donor sequence compared to the cell's mating type is also called donor preference and consequently, the entire mechanism, by which a specific donor is chosen, regulation of donor preference. Surprisingly, donor selection is not dictated by the Ya or Yα sequence of the donor loci. When a *MATa* strain is used in which the mating type specific information was switched between donor loci (*HMLa* and *HMRα*), *HML* is still chosen with an efficiency of 85-90 %[140,141]. Furthermore, replacement of the whole *HMLα* locus with a copy of the *HMRa* locus still did not change the donor preference upon DSB induction[141]. Hence, it is not the mating type specific sequence within a donor locus that determines which donor is chosen to repair the break. Instead, the location of the donor is responsible for the directionality of the *MAT* switching. Therefore, the existence of one or more cis-acting sequences, which act outside of the donor loci to guide donor choice, was assumed[25]. It seems like the cell uses *HMRa* as a default donor and active regulation is only conducted for the *HMLα* locus. *MATa* cells deficient for the *HMLα* donor site use the *HMRa* donor instead to repair the DSB. The cells remain *MATa*, but are viable. In contrast, *MATα* cells show a significant decrease in viability when only provided with an *HMLα* site[142-144]. The hypothesis of a cis-acting element was confirmed when an incremental deletion of the sequence 17 kb downstream of *HMLα* revealed a 700 bp sequence, whose deletion abolished *HMLα* usage in *MATa* cells[142]. *HMLα* donor usage in cells lacking this sequence decreases to 10 % instead of the normal 90 %. In *MATα* cells, deletion of this region does not have an effect of the correct donor usage. As this region is essential for the correct donor usage in *MATa* cells and enhances the recombination, it was named recombination enhancer (RE) element (Figure 5 A)[142]. Whereas the entire RE is defined as a 2.5 kb spanning sequence, the core region of 700 bp (also termed left RE) is enough to guide the *HMLα* usage in *MATa* cells. The core RE consists of the five subdomains A-E (Figure 5 A). Deletion of domain B does not show an effect on *HMLα* donor usage in *MATa* cells, whereas deletions of subdomains A, C and D completely abolish recombination with *HMLα* and instead recombination efficiency using *HMRa* increases to 90 %[25]. A common feature shared by regions A, D and E is that they contain one or more binding sites for Forkhead Homolog 1 (Fkh1, Figure 5 A), a forkhead familiy transcription factor (see section 2.3.4.2)[145].

Strikingly, replacement of the RE with multimers of either subdomain A, D or E retains the RE activity[145].

2.3.4.1   Silencing and activation of the RE

Although the RE sequence is present in yeasts of both mating types, it seems only to be active in *MATa* cells. When mating type switching is induced, the RE does not regulate *HMLα* donor usage through a global change of transcriptional activity of neighboring genes on the left arm of chromosome III[25]. Instead, the chromatin state within the region harboring the RE (in total 2.5 kb) changes (Figure 5 A). In *MATa* cells, this region shows an open chromatin conformation, whereas in *MATα* cells the RE is covered by highly positioned nucleosomes that do not extend into neighboring genes[146,147]. This change in chromatin conformation is mediated by the Matα2-Mcm1 repressor complex that also represses transcription of a-specific genes[148,149]. The C subdomain of the RE harbors a 31-bp consensus Matα2-Mcm1 binding site (DPS1)[25]. In addition, the right part of the RE contains another Matα2-Mcm1 binding sequence (DPS2)[150]. Besides Matα2-Mcm1, the general repressor Tup1 acts as a co-repressor to silence the RE[151]. Consequently, mutations in the C region lead to a shift in donor usage in *MATα* cells[147,151]. Intriguingly, mutations in Mcm1 which compromise Mcm1 binding to the RE also abolish *MATa* donor preference[147] and along that line, chromatin structure at the RE is different in those cells although Matα2 is not expressed[147]. In contrast, Matα2 is not expressed in *MATa* cells and Mcm1 alone binds to and activates the RE. In addition, the Swi4/6 (SBF) complex binds to a conserved SCB (Swi4/6 cell cycle box) within subdomain C and activates the RE as a co-activator of Mcm1[152]. Therefore, the binding of Mcm1 to the RE does not only repress RE function in *MATα* cells together with Matα2, but is also essential for the activation of the RE in *MATa* cells (Figure 5 A).

2.3.4.2   Mechanistic insights into RE function

The RE enables mating type switching to be a highly directional process. Although a large amount of genetic data on the function of RE sequences exists, mechanistic insights into how this translates into donor preference regulation are still limited.

A   The RE locus
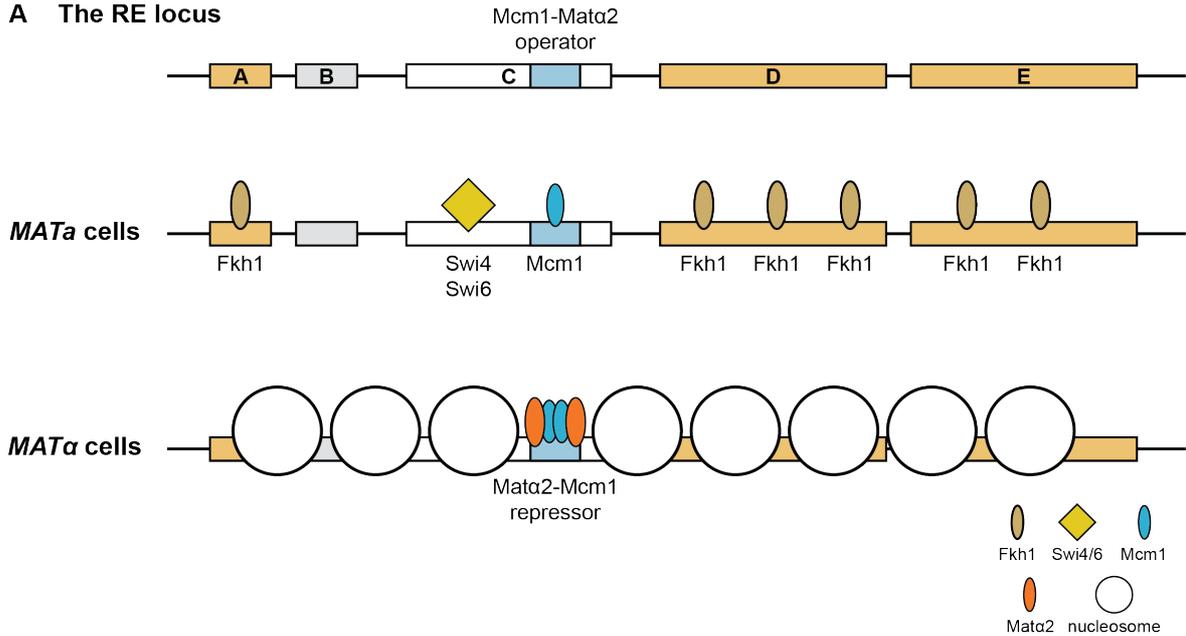
B   RE activation/repression in *MATa* and *MATα* cells
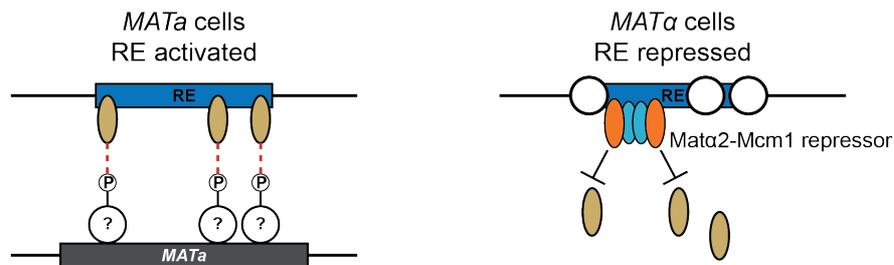
Figure 5 | **Regulation of the RE.**
(A) The RE consists of 5 subdomains, A-E. C contains an Mcm1-Matα2 binding site and domains A, D and E share the feature of Fkh1 binding sites. Domain B was not shown to have a function for the RE. In *MATa* cells, the RE is activated by Mcm1 and its co-activator Swi4/Swi6 and has an open conformation. Trans-acting factors like Fkh1 can then bind to the RE. In *MATα* cells the Matα2-Mcm1 repressor complex binds to the RE and leads to the positioning of nucleosomes (white circles) at the RE, whereas the RE is inactivated. Adapted from[25].
(B) Fkh1 binds to the activated RE in *MATa* cells and likely interacts with phosphothreonines of target proteins at the *MAT* locus upon a DSB (not indicated here). A physical bridge is assumed to form between the RE and the *MAT* locus. In *MATα* cells, the Matα2-Mcm1 repressor binds to the RE, thereby inhibiting Fkh1 binding.

Besides the silencing and activation factors binding at the RE, subdomains A, D and E contain binding sites for the transcription factor Fkh1 (Figure 5 A). Due to the compact chromatin state in *MATα* cells, Fkh1 only binds to the RE in *MATa* cells[152]. Fkh1, together with its paralog Fkh2, regulates the expression of the *CLB2* cluster genes, which are important for cell cycle progression[153]. In addition, Fkh1 and Fkh2 are also involved in developmental regulation and bind to multiple chromosomal elements with distinct specificities[154]. Deletion of both *FKH1* and *FKH2*, but not a single knockout alone, leads to pseudohyphal growth. Therefore, one protein can complement for the loss of the other one. However, although one Fkh2 binding site was identified within the A subdomain of

the RE, a role in the regulation of donor preference could not be assigned to Fkh2[145]. Fkh1 and Fkh2 share the structural feature of a forkhead associated (FHA) domain. FHA domains were shown to interact with phosphoserine and phosphothreonine residues in target proteins, but exhibit a surprisingly high affinity for phosphothreonines and only barely interact with phosphoserines[155,156]. Upon mating type switching Fkh1 binds to the RE and its FHA domain is assumed to interact with phosphorylated threonines of factors binding to the DSB at the *MAT* locus[157]. It is thought that this interaction forms a physical bridge or a chromosomal loop between the RE and the *MAT* locus, thereby bringing the *HMLα* locus in close proximity to the DSB site at the *MAT* locus (Figure 5 B and compare section 2.2.5)[150,157]. Consistent with this hypothesis it makes sense that crossovers are rare events during mating type switching (compare section 2.3.3)[25] as this would result in chromosomal translocations. The essential function of the FHA domain for the suggested loop formation was shown when it was fused to LexA and the RE was replaced with LexA binding sites[157]. This setup was enough to trigger the correct donor choice upon DSB induction in *MATa* cells. This mechanism is only possible in *MATa* cells, as the RE is blocked in *MATα* cells, thereby preventing Fkh1 binding. Data from our laboratory obtained from Rad51 ChIP-on-chip experiments show that Rad51 enriches early after DSB induction around the position of the RE[76]. This early enrichment was only seen in *MATa* cells, but not in *MATα* cells. Deletion of the RE in *MATa* cells abolished the early enrichment of Rad51, but had no effect in *MATα* cells. These data further support the hypothesis of a chromosomal loop between the RE and a DSB. As already mentioned in section 2.2.5, efficient DNA repair also depends on the spatial proximity between a donor and the DSB. Basically, the RE is located far away (~160 kb) from the *MAT* locus. A loop between the RE and the DSB in the *MAT* locus would therefore increase the probability of Rad51 filament probing at the RE, reflected in an early and strong Rad51 enrichment in this region. Generally, the mechanism of donor preference regulation is only partially understood. Deletion of *FKH1* strongly decreases *HMLα* usage in *MATa* cells from 85 to 35 %, but the recombination is not completely abolished[152]. It is suggested that other factors are involved in the regulation of donor preference, facilitating the genetic exchange between the DSB and a sequence next to the RE. Therefore, details of the coupling between the RE and the DSB have to be investigated (see section 4.2).

Intriguingly, it was shown that the choice of a preferred donor is not strictly limited to the *MAT* system. In a previous study a DSB was induced by HO in a *leu2* allele on chromosome V and two donor sites were present in the cell: one *LEU2* gene next to the RE on chromosome III and a *leu2-K* allele 100 kb proximal to the centromere on chromosome V[158]. In *MATa* cells, where the RE is active, the probability to repair the DSB with the inter-chromosomal *LEU2* gene was 50 %. A deletion of the RE decreased usage

of this site to 15 %[158]. Therefore, the RE also influences donor choice when *HMRa* is not the preferred donor site. Conservation of the RE was demonstrated for *Saccharomyces sensu stricto* species[145], but not for other species. Although the presence of two homologous donor loci on the same chromosome as the DSB and the donor preference mediated by the RE are special features of DNA repair by homologous recombination, the influence of the RE on homology search offers the opportunity to study the influence of donor preference regulation and therefore chromosomal loops onto DSB repair in general. Thus, a more comprehensive investigation of the RE outside the *MAT* system is needed, which also helps to understand which factors are really required for its function (see section 4.1).

3 Aims of this study

Homologous recombination has been studied for decades using the mating type switching system of *S. cerevisiae* as a model system, which represents a specialized site-specific chromosomal DSB repair event. It has long been a question how cells choose the correct donor sequence to repair the DSB and efficiently switch their mating type. The identification of the recombination enhancer (RE) gave first insights into this regulation of donor preference. Although extensive studies regarding the genetics and the functions of the RE sequences exist, insights into the mechanism how this translates into donor preference regulation are still limited.

This study aims to address two questions regarding donor preference regulation: 1) whether the RE also guides homology search during the process of HR outside of the mating type switching system. For mating type switching, the RE facilitates correct donor choice. An influence of the RE onto homology search and DSB repair in general would corroborate the influence of nuclear architecture onto homology search.
2) which factors contribute to the regulation of donor preference. A chromosomal loop is proposed to form between the RE and the DSB to enhance recombination efficiency. Therefore, the identification of factors involved in this process is necessary to reveal details of this possible link between the RE and the DSB on a mechanistic level.

To shed light into the regulation of donor preference I will use the power of genetics in the model organism *S. cerevisiae* combined with chromatin immunoprecipitation (ChIP) as well as a previously developed assay to measure recombination efficiency. Importantly, Rad51 ChIP enables the visualization of ongoing homology search and can give insights into the guidance of homology search by the RE. Furthermore, I will identify protein factors mediating the potential coupling between the RE and the DSB via a mass spectrometry-based approach.

4 Results

4.1 The recombination enhancer guides homology search and supports homologous recombination

4.1.1 The RE guides homology search following DSB induction independently of the *MAT* system

Ongoing homology search during HR can be monitored via Rad51 ChIP[76]. In brief, a single site-specific DSB is induced by HO endonuclease and the assembly of the Rad51 nucleoprotein filament as well as the homology search are monitored by Rad51 enrichment at different chromosomal sites. High Rad51 enrichment close to the DSB site reflects the formation of the Rad51 presynaptic filament after break induction. Lower enrichments measured at sites outside the area of DNA end resection reveal the homology sampling of the Rad51 filament, i. e. the transient probing of chromosomal loci in a sub-population of cells at a given time. In Rad51 ChIP experiments combined with whole genome tiling arrays (ChIP-on-chip), the Rad51 signal could be monitored up to 500 kb away from the DSB site[76,159].

The *S. cerevisiae* mating type system on chromosome III was already previously used as a tool to study homologous recombination (see section 2.2.4), where a DSB is induced via overexpression of HO endonuclease[76,160]. Upon DSB induction, Rad51 signals can also be detected at the RE element at the left arm of chromosome III in *MATa* strains. The RE was identified as a 700 bp cis-acting element[25,142] and was recently shown to determine mating type-dependent chromosome folding[150]. In this way the RE mediates proximity between the DSB and the *HMLα* donor locus during mating type switching, likely through protein-protein interactions between itself and *MATa*-bound factors[76,157] (see section 2.3.4.2).

Previous studies investigated the function of the RE using the mating type system[157,158] (see section 2.3.3). It was recently shown by our laboratory that the HO recognition site can be placed at random positions in the genome and that an HO-induced DSB still led to Rad51 enrichment at the RE[76]. I wondered if the RE can be uncoupled from the mating type system, but still perform its enhancing function. In order to prove that the RE-guided homology search is independent of the *MAT* system, I generated a strain harboring SceI endonuclease under the control of the galactose promoter. SceI is a mitochondrial endonuclease, responsible for intron homing in yeast mitochondria[161,162]. The strain harboring the *SCEI* sequence was compared to a strain harboring the *HO* sequence instead (Figure 6 A). An SceI system to induce specific DSBs and homologous recombination was previously used in yeast[76] as well as in mammalian cells[162]. In my

studies, a single and site-specific DSB was achieved by insertion of a 30 bp SceI or a 36 bp HO recognition site at randomly chosen genomic sites. All strains were *MATa* and deleted for the endogenous HO recognition sequence on chromosome III. Therefore, break induction solely depended on the integrated sequences. Direct comparison of Rad51 enrichment in strains with either an HO- or an SceI-induced DSB was achieved by break induction on chromosome IV at 491 kb. In addition, to prove the independence of the chromosomal location of the DSB, another strain carrying an SceI recognition site on chromosome XV was constructed (Figure 6 B).
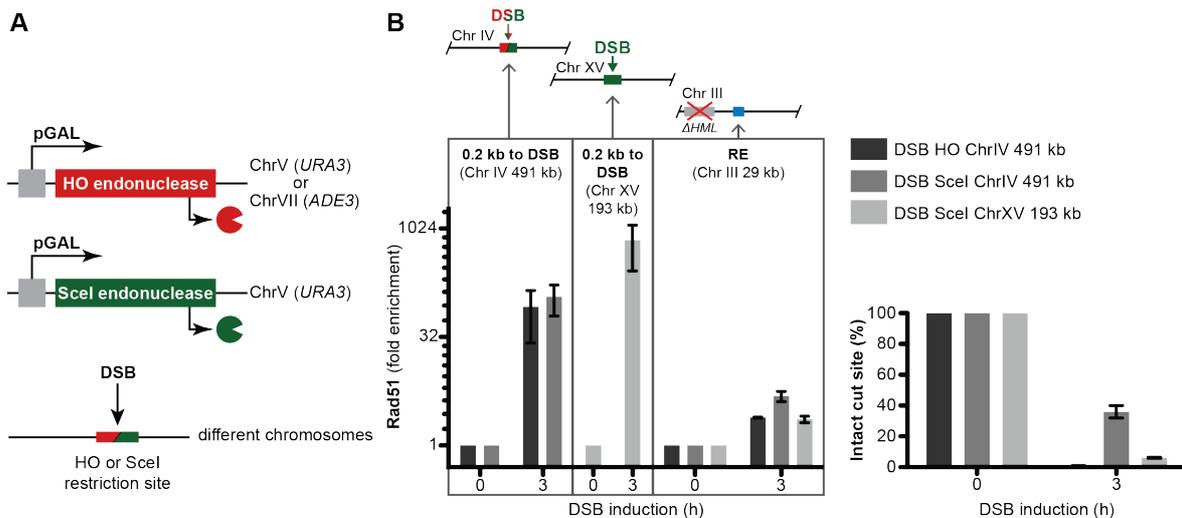
Figure 6 | **RE guides homology search independently of the *MAT*-induced DSB system.**
(A) Scheme of the HO or SceI expression system. HO endonuclease was integrated into the *ADE3* locus on ChrVII. To compare HO to SceI DSB induction, their coding sequences were introduced into the *URA3* locus following a standard PCR-based strategy for chromosomal integration[163,164]. Both enzymes were expressed under the control of the *GAL1* promoter.
(B) A single DSB was induced by HO or SceI either on ChrIV at 491 kb or on ChrXV at 193 kb. Rad51 enrichment was calculated after Rad51 ChIP, followed by qPCR analysis. Rad51 is significantly enriched at the respective DSB site. An additional primer pair binding at 29 kb on ChrIII was used to determine the Rad51 enrichment at the RE. The efficiency of the induced DSBs was measured by using a primer pair spanning the DSB site, only giving a qPCR signal if the HO or SceI recognition site is intact. Rad51 enrichment data are depicted on a log2 scale, whereas the cut site efficiency is depicted on a linear scale. Data represent mean ± SEM of three independent experiments. The qPCR data were normalized to a control locus on ChrX and additionally to the time before DSB induction (0 h).

As expected, DSB generation resulted in strong Rad51 enrichments directly around the break site. Therefore, Rad51 filament formation is independent of the endonuclease inducing the DSB. Notably, although Rad51 enrichments in the strains harboring SceI are comparable to strains with an HO-induced DSB, SceI cuts within its recognition site less efficiently (Figure 6 B). Strikingly, Rad51 does not only enrich at the RE in the HO-induced strain, but also in the strain harboring an SceI-induced DSB. Thus, by moving the DSB away from the *MAT* locus on chromosome III and inducing it via SceI, a system

independent of the mating type switching was established. Also the genomic position of the DSB is not crucial for Rad51 binding to the RE.

Next, I wondered whether the effect of the RE to guide homology search could be transferred to another chromosome. Therefore, the RE was amplified from chromosome III and integrated either on chromosome IV at 1148 kb or on chromosome XIII at 282 kb. Due to break induction on chromosome IV at 491 kb by HO endonuclease I could not only test for intra-chromosomal, but also for inter-chromosomal guidance of homology search. Rad51 enrichment after DSB induction was calculated following Rad51 ChIP-qPCR. In a first step the Rad51 enrichment was studied in the presence of the endogenous RE on chromosome III (Figure 7 A). In addition to monitoring Rad51 accumulation at the RE, a primer pair binding 40 kb upstream of the DSB reflecting ongoing homology search was used.
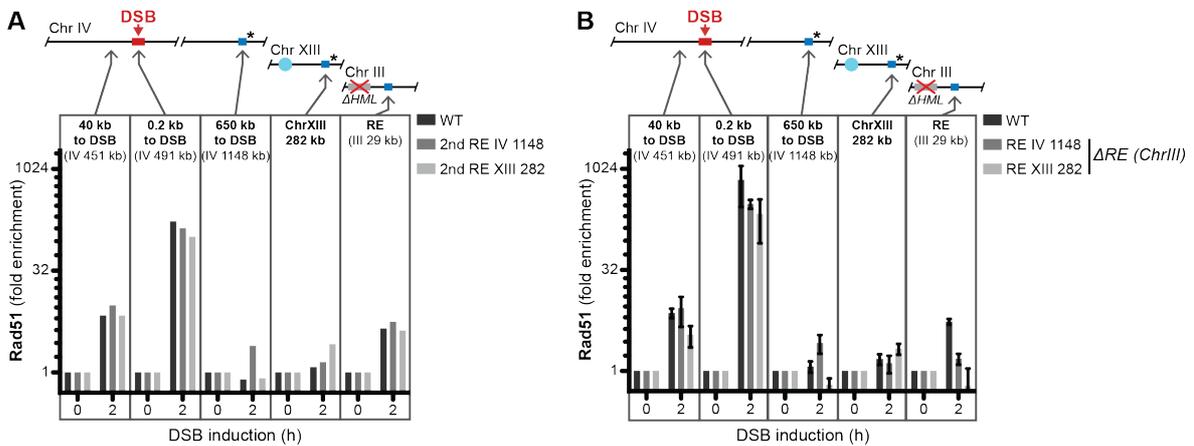
Figure 7 | **The RE guides the Rad51 nucleoprotein filament also to other positions in the genome.**
(A) Integration of a second RE (blue square with asterisk) into different genomic positions leads to Rad51 nucleoprotein filament probing at these sites. A second RE was either inserted on chromosome IV 1148 kb or chromosome XIII 282 kb. A DSB was induced on ChrIV at 491 kb via HO overexpression.
(B) Deletion of the endogenous RE does not lead to a further increase in Rad51 enrichment at the RE. The RE on chromosome III was deleted and DSB induction was again performed via HO overexpression.
Rad51 enrichment was calculated following Rad51 ChIP-qPCR analysis. Enrichment data are depicted on a log2 scale. qPCR primers were used for the indicated positions. (A) represents data from a single experiment. For (B), data represent mean ± SEM of three independent experiments. The qPCR data were normalized to a control locus on ChrX and additionally to the time before DSB induction (0 h).

Two hours after DSB induction, Rad51 enrichment was detected in both strains at the positions where the second RE was inserted. In addition, Rad51 also accumulated at the endogenous RE on chromosome III, meaning that the homology search was probing both RE sites, chromosomes III, IV and XIII, respectively. To circumvent distraction of ongoing homology search due to the presence of a second RE, the endogenous RE was deleted

in a second approach and the Rad51 enrichment again calculated after Rad51 ChIP-qPCR (Figure 7 B). As expected, Rad51 enrichment at the RE on chromosome III was only obtained in the wildtype strain. Rad51 enrichment at the positions on chromosomes IV and XIII did not further increase compared to the situation when the endogenous RE was still present (compare Figure 7 A). These findings clearly show that the RE guides homology search not only to its endogenous position on chromosome III, but also to any other genomic position, when transplanted to another chromosome.

Altogether, these data thus point towards a more general mechanism, whereby the RE guides homology search.

4.1.2 The RE guides homologous recombination independently of the *MAT* system

In *MATa* cells, the RE plays an essential role in mating type switching[76,142,162]. A DSB in the *MAT* locus in *MATa* cells results in 90 % usage of the *HMLα* locus, located at the left arm of chromosome III, close to the telomeric region. Vice versa, *MATα* cells use the *HMRa* locus in 90 % of *MAT* DSBs, located at the end of the right arm of chromosome III[157,163,164]. A knockout of the RE in *MATa* cells disrupts the natural mating type system and cells will use the incorrect *HMRa* locus for up to 90 %. Hence, the RE is crucial for the *MAT* system to ensure proper recombination during mating type switching. To test if the RE also supports recombination independent of the mating type switch system, I applied a previously developed recombination assay[76]. This assay makes use of the recombination between two homologous DNA sequences, which are naturally not present in *S. cerevisiae*. Therefore, a plasmid, based on constructs for PCR-based tagging with green fluorescent protein (GFP)[163,164], was constructed to integrate the sequence encoding for the GFP. The 36 bp HO recognition site was cloned into the middle of the GFP encoding sequence. For the other recombination allele, an incleavable variant of the HO recognition site, containing two point mutations[165], was inserted. Both constructs were integrated according to the protocol for a PCR-based strategy[163,164]. Following a DSB induced by HO, this assay allows to determine the recombination efficiency between the two recombinant alleles (Figure 8 A). For this purpose, cells were plated on galactose containing medium to induce the DSB via overexpression of HO. Recombination could then be measured by counting the colonies on the galactose containing plates compared to the amount of colonies on glucose plates. Constant expression of HO endonuclease on galactose plates leads to permanent DSB induction. Therefore, NHEJ is not sufficient to repair the break and the readout of this assay monitors recombination. The GFP encoding sequence harboring the intact HO recognition

site was integrated on chromosome IV at 491 kb. The construct bearing the incleavable HO recognition site was used as a donor sequence and integrated at different sites (one per strain).

If the RE is involved in recombination and guides homology search towards the left arm of chromosome III, the recombination efficiency is supposed to be rather high compared to other positions in the genome. Indeed, *MATa* cells with a donor site integrated next to the RE at 30 kb on chromosome III show a recombination efficiency of up to 70 % (Figure 8 B). Two controls were used to ensure that the recombination close to the RE is not just a random probing of the nucleoprotein filament. One donor site was integrated around 650 kb away from the DSB, at 1148 kb. This distance is larger than the observed spreading of homology search around the break site[76] and therefore, results in a low recombination rate of 13 %. Another homologous site was placed next to the centromere of chromosome XIII at 282 kb, leading to an average recombination efficiency of 35 % (Figure 8 B). Notably, the recombination efficiency in this case was higher than that observed for the intra-chromosomal recombination event on chromosome IV, despite inter-chromosomal recombination normally being very inefficient[102]. A reason for this finding is likely the short distance of both DSB and donor sequence to the centromeres of the respective chromosomes. Due to centromere-clustering[166,167], both loci gain close spatial proximity, and it has been previously shown that this is a major determinant for recombination efficiency (see section 2.2.5)[76,96,102]. The same assay was performed in *MATα* cells (Figure 8 C). As already mentioned, the RE is silenced in *MATα* cells. Therefore, recombination with a donor site next to the RE was significantly reduced compared to *MATa* cells (Figure 8 C) due to the RE being unable to change chromosomal conformation[150]. For the donor site on chromosome IV, the recombination efficiency does not change compared to *MATa* cells. Note that efficiency for the chromosome XIII locus is decreased, which might reflect a different chromosomal rearrangement when *MATα* cells are compared to *MATa* cells. However, an RE-dependent difference in chromosomal conformation was only shown for chromosome III[150]. These data show that the RE is involved in recombination and increases recombination with nearby donor sites, as this is also the case for the *HMLα* locus[25].
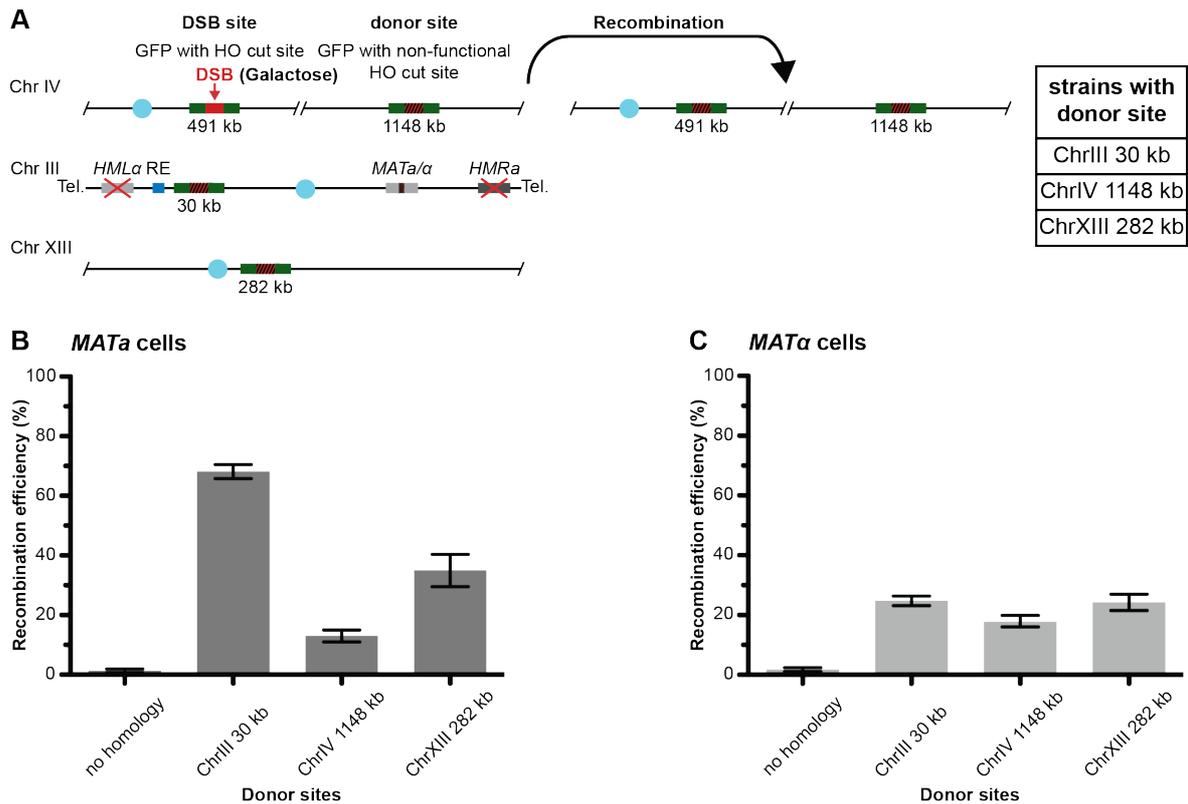
Figure 8 | RE influences recombination efficiency in *MATa* cells.
(A) Scheme representing the recombination efficiency assay. A construct containing the GFP encoding sequence and an HO recognition site inserted in the middle of this sequence was integrated at ChrIV 491 kb by a PCR-based strategy[163,164]. This construct served as the DSB site. A second construct, also containing the sequence encoding for GFP, but with a mutated HO recognition site, was inserted at different sites in the genome. All strains contained the cleavable construct plus one donor site either at ChrIII 30 kb, ChrIV 1148 kb or ChrXIII 282 kb. The endogenous HO recognition site within the *MAT* locus on ChrIII was mutated and not cleavable.
(B) Recombination efficiency in *MATa* cells. As control, an additional strain was used without a homologous donor site.
(C) Recombination efficiency in *MATα* cells.
Recombination efficiency data are depicted on a linear scale. Data represent mean ± SEM of three independent experiments. Cells were plated on glucose and galactose containing medium to induce the DSB. Colonies were counted and normalized to cells growing on glucose.

To further understand the effect of the RE on homology search, I tested if the RE could also guide homology search when integrated at different positions in the genome, next to a donor site. Therefore, in the next approach a second RE was inserted 1 kb downstream of a donor site, either on chromosome IV 1148 kb or on chromosome XIII 282 kb (Figure 9 A). For both positions, an increase in recombination efficiency was observed, when the RE was inserted next to them (Figure 9 A). For chromosome IV 1148 kb the recombination efficiency increased from 12.8 to 17.6 % (relative increase of 37.5 %) and for chromosome XIII 282 kb from 32.6 to 48 % (relative increase of 47 %, Figure 9 C). Note that the endogenous RE on chromosome III was still present in these strains, meaning that homology search was probably distracted by the presence of this second RE. To circumvent this fact and to get the actual recombination efficiency data, when

there is only one RE present, the endogenous RE was deleted and the same approach was conducted to calculate the recombination efficiency at different genomic positions (Figure 9 B).
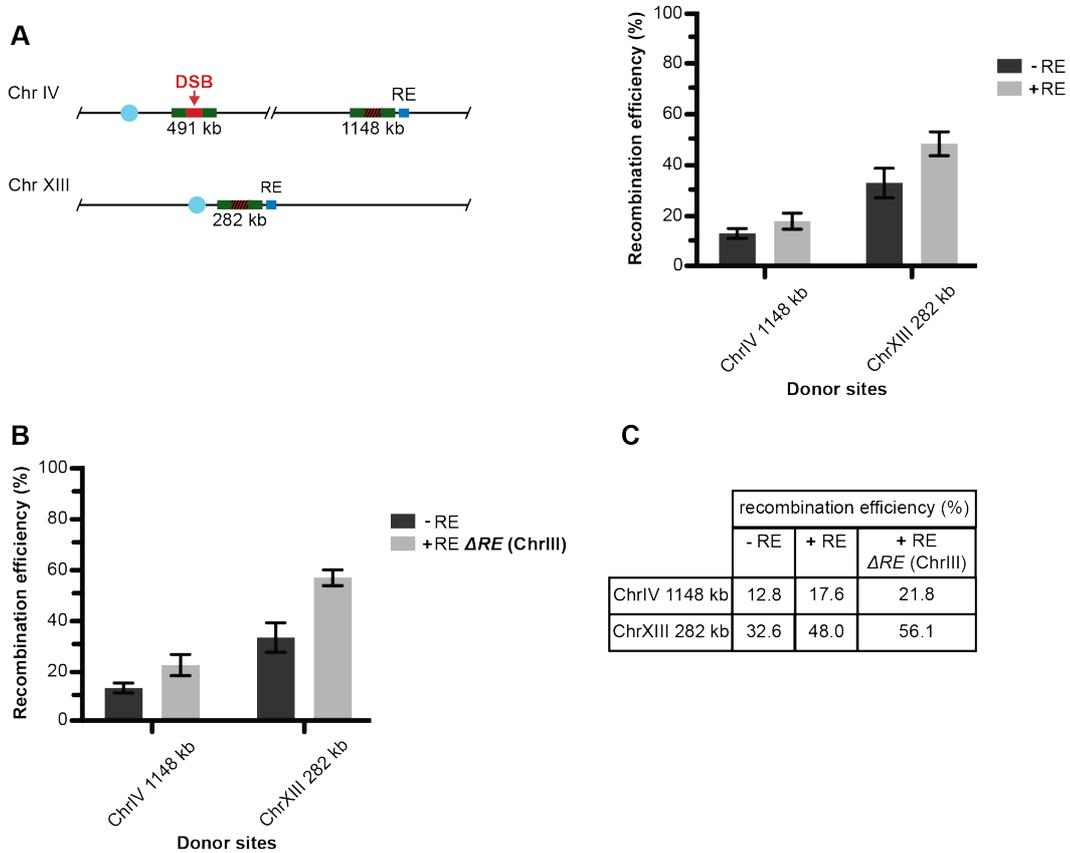
Figure 9 | RE increases homologous recombination also on other chromosomes.
(A) Recombination efficiency is increased when the RE is integrated next to a homologous donor site. The scheme represents the setup for the experiment. All strains contained one DSB site plus one additional donor site. A 754 bp sequence, representing the RE, was amplified from genomic DNA and inserted next to a donor site. The DSB was induced on ChrIV 491 kb. The endogenous RE on ChrIII was still present in this experiment. The endogenous HO recognition site within the *MAT* locus on ChrIII was mutated and not cleavable.
(B) The efficiency of homologous recombination increases further when the endogenous RE is deleted. Strains were carrying one DSB site (ChrIV 491 kb) and one donor site each.
(C) This table represents the calculated recombination efficiencies for (A) and (B). The increase in recombination efficiency for position ChrIV 1148 kb was 37.5 % with the ChrIII RE present and 70 % without. For the donor site at ChrXIII 282 kb, the efficiency increased by 47 % with the endogenous RE and 72 % when the ChrIII RE was deleted on top.
Recombination efficiency data are depicted on a linear scale. Data represent mean ± SEM of three independent experiments. Cells were plated on glucose and galactose containing medium to induce the DSB. Colonies were counted and normalized to cells growing on glucose.

Indeed, when the endogenous RE on chromosome III was deleted, the recombination efficiency increased even more. Without the distraction of a second RE, the homology search is guided by only one RE, leading to a higher usage of the donor site at the indicated position. The relative increase in recombination efficiency for chromosome IV 1148 kb is now 70 % (from 12.8 to 21.8 %) and for chromosome XIII 282 kb 72 % (from

32.6 to 56.1 %, Figure 9 C). These data perfectly fit to the results obtained in section 4.1.1, when Rad51 enriched at sites proximal to the RE on chromosomes IV and XIII (compare Figure 7). In addition, these recombination data correlate with recently published results, where the RE was also inserted next to a donor site and promoted repair efficiency between two loci[102].

4.1.3 The distance between the RE and the homologous donor dictates recombination efficiency

Upon DSB damage, the Rad51 nucleoprotein filament forms directly at the break site and can commence homology search. When measured with Rad51 ChIP-on-chip, the Rad51 signal decreases with the distance to the DSB site[76,159]. This effect can also be seen in Rad51 ChIP-qPCR experiments[76]. Therefore, I wondered if I could see a similar effect with the RE guiding homology search to other chromosomes. When measuring recombination efficiency, a larger distance between the RE and a donor is expected to result in lower repair efficiency. In order to approach this hypothesis, I used the recombination efficiency assay as previously described (see section 4.1.2). A DSB was induced on chromosome IV at 491 kb and one donor site per strain was integrated either at 1148 kb on chromosome IV or at 282 kb on chromosome XIII. To verify if the repair efficiency depends on the distance between the RE and the donor site, one RE per strain was integrated at varying distances to the donor, while the endogenous RE was deleted (Figure 10). First, I investigated different positions of the RE to the donor site on chromosome IV at 1148 kb (Figure 10 A). When placed 1 kb downstream to the donor, repair efficiency increased compared to the wildtype strain, where only the RE on chromosome III is present (compare section 4.1.2). With increasing distance of the RE from the donor site, the recombination efficiency significantly decreased. Even when integrated 27 kb downstream of the donor at 1175 kb, the DSB can still be repaired slightly more efficiently compared to the control strain lacking the RE at the donor. To consolidate this finding, I used the same setup for the donor site on chromosome XIII 282 kb (Figure 10 B). Here, the RE was integrated at four different positions upstream or downstream of the donor site, one per strain. Again, the highest repair efficiency was obtained with the RE directly (1 kb downstream) at the homologous site. Recombination efficiency decreased with an increasing distance between the RE and the donor. Indeed, the lowest repair rate could be seen when the RE was placed 27 kb downstream of the donor.
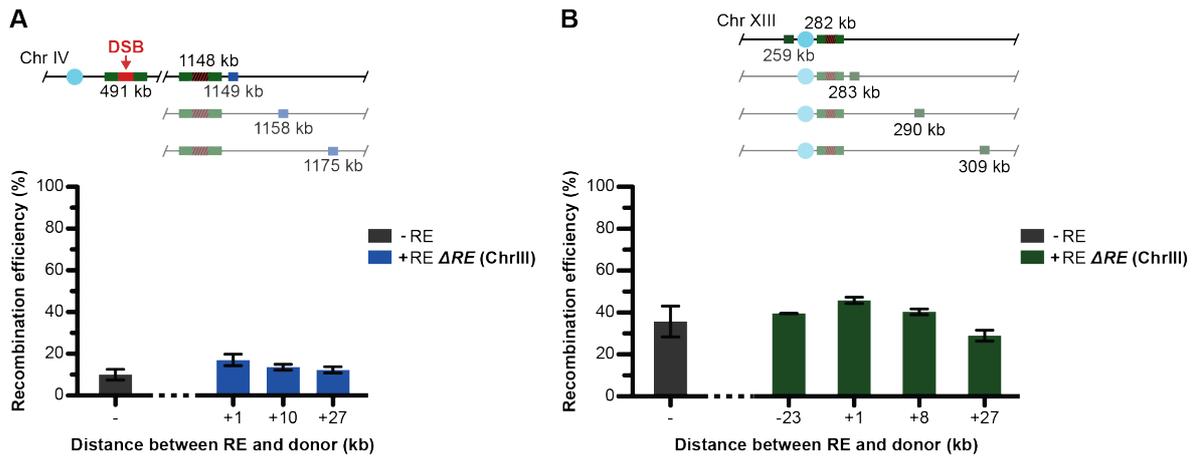
Figure 10 | Recombination efficiency depends on the distance between the RE and a donor.
(A) A donor site was integrated at ChrIV 1148 kb and a DSB was induced on ChrIV at 491 kb. A 754 bp sequence from ChrIII, encoding the RE, was amplified from genomic DNA and one RE per strain (blue square) was inserted at the indicated positions. As a control, a strain carrying only the endogenous RE (-RE) was used. The other strains carried an *RE* deletion.
(B) A donor site was integrated at ChrXIII 282 kb, whereas a DSB was induced at ChrIV 491 kb. The 754 bp sequence from ChrIII encoding the RE was amplified from genomic DNA and one RE per strain (green square) was inserted at the indicated positions. As a control, a strain carrying only the endogenous RE (-RE) was used. The other strains carried an *RE* deletion.
Recombination efficiency data are depicted on a linear scale. Data represent mean ± SEM of two independent experiments. Cells were plated on glucose and galactose containing medium to induce the DSB. Colonies were counted and normalized to cells growing on glucose.

Knowing that the distance between the RE and the donor site is important for recombination processes, I wanted to figure out if the distance between the RE and a DSB site would also determine repair efficiency. In order to approach this issue I used a recombination efficiency assay, in which each strain contained a donor site next to the endogenous RE. The repair efficiency of a break was expected to correlate with the distance between the DSB and the RE and the donor site, respectively. A DSB was induced at different positions in the genome, one per strain (Figure 11 A). The recombination efficiency in a strain still bearing the endogenous RE was compared to another strain lacking the RE, only harboring the donor site (Figure 11 B). When the RE is still present, all DSBs at different genomic sites lead to similar repair efficiency, ranging from 67-77 %. Surprisingly, upon removal of the RE on chromosome III, the remaining usage of the donor site nearby varies a lot, depending on the site where the DSB was induced. A strain with a DSB on chromosome IV at 491 kb leads to a repair efficiency of 22 %, whereas a strain with a break on the same chromosome, but at 1148 kb, drops to 10 %. Looking now at the DSBs induced on chromosomes XIII and XV, a significantly higher repair rate is achieved lacking the RE (50 % for chromosome XIII and 33 % for chromosome XV). Importantly, these data showed that despite varying repair capacities with different DSB locations, presence of an RE element next to the donor site made all recombination events equally efficient.

Still, it remained unclear why recombination rates were so different in the absence of an RE. A likely reason could be the general nuclear architecture, which is known to be a major determinant for recombination[96]. To test this model, I calculated the spatial distance between DSB and donor site for each of the different pairs based on available 3D modeling data of the yeast nucleus[98] (Figure 11 C). However, no correlation between 3D distance and repair efficiency could be observed using these four genomic positions.
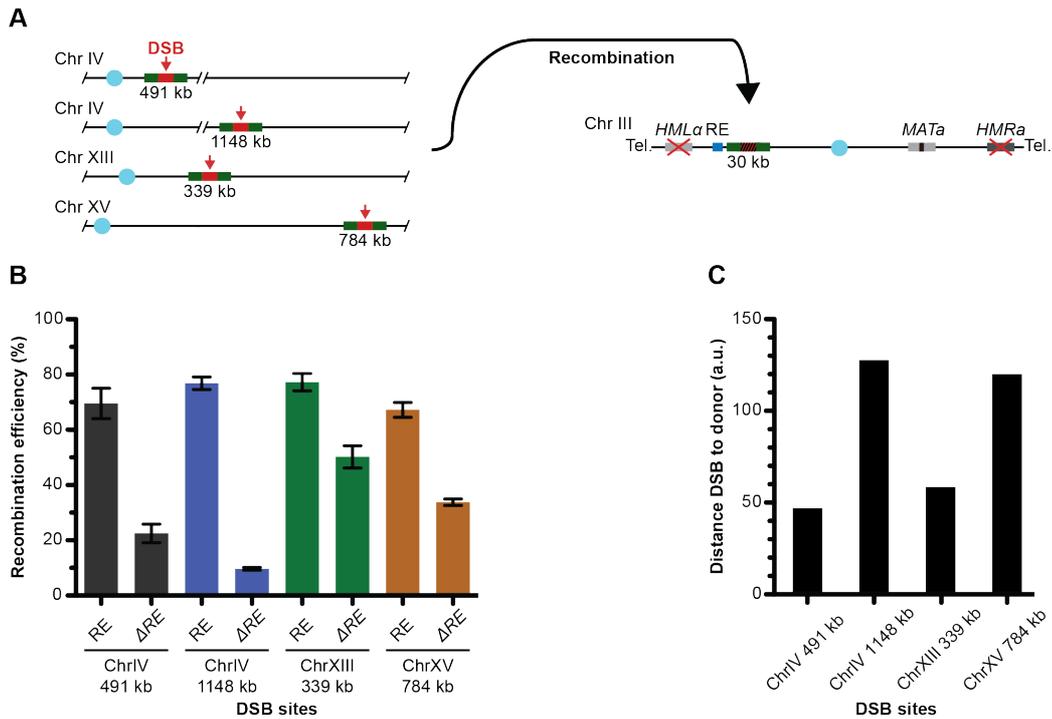
Figure 11 | **The distance between the RE and a DSB does not correlate for selected DSB sites.**
(A) Scheme representing the experimental setup. A donor site was integrated next to the RE on ChrIII at 30 kb. One HO recognition site per strain was inserted at different positions in the genome. Following DSB induction, cells could only repair the break by using the donor site on ChrIII. The endogenous HO recognition site within the *MAT* locus on ChrIII was mutated and not cleavable.
(B) Recombination efficiency of strains with different DSB sites. The repair efficiency of strains with the RE was compared to RE-deleted strains. Recombination efficiency data are depicted on a linear scale. Data represent mean ± SEM of three independent experiments. Cells were plated on glucose and galactose containing medium to induce the DSB. Colonies were counted and normalized to the cells growing on glucose.
(C) Relative distance between the DSB and donor site. Distances were calculated based on previously published data modeling the *S. cerevisiae* genome[98].

Yet, the calculations are based on measurements of a static genome without DNA damage. In fact, a DSB leads to a distinctly increased mobility of the cut chromosome, facilitating homology search to complete homologous recombination[108,109]. A chromosomal movement has the advantage of exploring a larger volume of the nucleus in order to find a homologous sequence to repair the DSB. In addition, it was also shown for non-cut chromosomes to show an increased movement[108]. Thus, DSB-dependent specific

changes in the nuclear architecture might be a hypothetical model to explain the lacking correlation between spatial distance and the observed recombination efficiency.

4.1.4 The left part of the RE guides homology search

Identified originally as an approximately 700 bp sequence at the left arm of chromosome III[142], it has been shown that the RE is a larger region of roughly 2.5 kb[150]. In fact, the RE region can be split into a left and a right portion, whereas the left part contains the originally 700 bp sequence. The RE was found to be a composite element with its left part playing a role for donor selection in *MATa* cells and its right part being responsible for the mating type-specific conformation of chromosome III, which might help to guide subsequent donor selection[150]. Hence, I wanted to know if the right part also plays a role for donor preference regulation. To test this hypothesis, either the left or the right part or, as a control, the whole RE was deleted (Figure 12). In a first approach another recombination assay was performed (Figure 12 A). A donor site was inserted next to the RE at 26.9 kb, outside the deleted region. When the recombination efficiency is compared between wildtype RE cells and deletions, it strongly decreases when the left or the total RE is deleted. Deletion of the right part of the RE does not reduce repair efficiency, indicating that the right RE is not involved in the homologous recombination process. To check if Rad51 nucleoprotein filament probing is impaired, Rad51 enrichment was calculated following Rad51 ChIP-qPCR (Figure 12 B). Equal Rad51 enrichment was obtained for all strains 40 kb upstream of the DSB, indicating ongoing homology search. Looking at Rad51 next to the RE on chromosome III, enrichments could only be monitored in a strain carrying a deletion of the right part of the RE, but were lost when the left or the whole RE was deleted. These data confirm the results already obtained for the recombination assay in Figure 12 A. In summary, the guidance of homology search and the completion of homologous recombination only depends on the left part of the RE, but not on the right part.
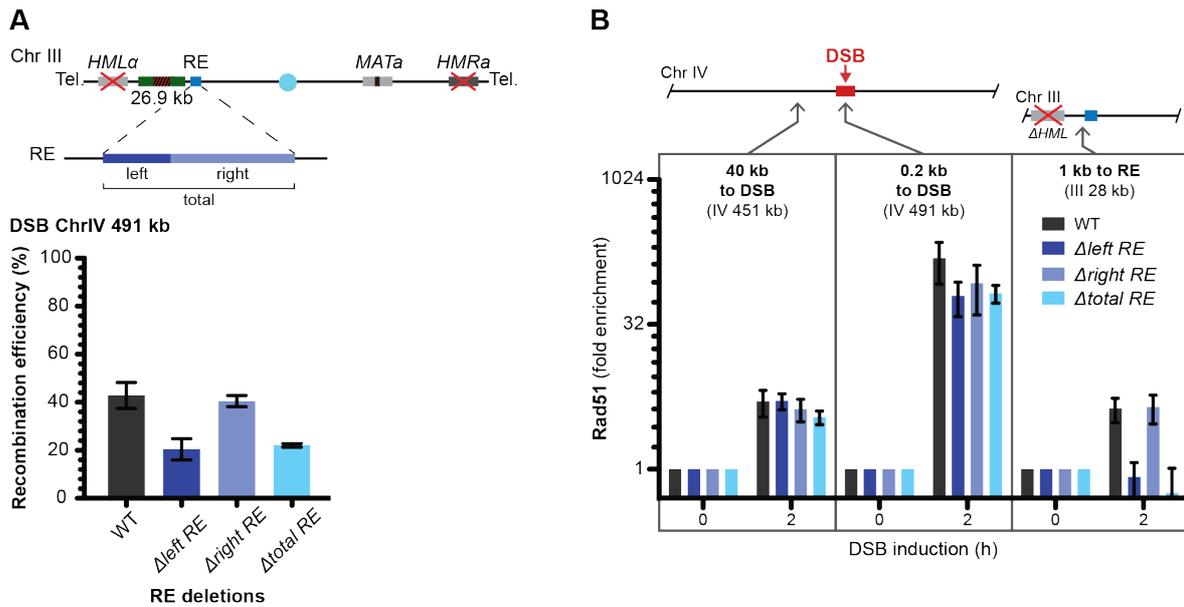
Figure 12 | The left part of the RE guides homology search, but not the right part.
(A) Recombination assay showing the repair efficiency in strains with deleted parts of the RE. In all strains a DSB was induced at ChrIV 491 kb. Additionally, they were carrying a donor site at 26.9 kb on chromosome III, close to the position of the RE. A strain still carrying full-length RE was used as control. The endogenous HO recognition site within the *MAT* locus on ChrIII was mutated and not cleavable. Recombination efficiency data are depicted on a linear scale. Data represent mean ± SEM of two independent experiments. Cells were plated on glucose and galactose containing medium to induce the DSB. Colonies were counted and normalized to cells growing on glucose.
(B) Rad51 enrichment in strains with RE deletions. DSB induction at ChrIV 491 kb was performed via HO overexpression upon addition of galactose. Rad51 enrichment was calculated following Rad51 ChIP-qPCR analysis. Enrichment data are depicted on a log2 scale. qPCR primers were used for the indicated positions. Data represent mean ± SEM of three independent experiments. The qPCR data were normalized to a control locus on ChrX and additionally to the time before DSB induction (0 h).

4.2 DSB-RE interaction significantly depends on Fkh1

4.2.1 Matα2 silences the RE and impairs RE-guided homology search

Early Rad51 filament probing at the RE was only detected in *MATa* cells, but not in *MATα* cells[76]. The *MATα* locus encodes the proteins Matα1 and Matα2. Matα1, together with Mcm1, is involved in the activation of a set of α-specific genes[76,115,159]. In contrast, Matα2 acts together with Mcm1 as a repressor of a-specific genes in *MATα* cells[76,160,168,169]. The general transcription suppressor Tup1 further supports this interaction together with the co-repressor Ssn6[76,117,170]. In *MATα* cells, the Matα2-Mcm1 complex binds to the RE, leading to the covering of the RE with highly positioned nucleosomes, resulting in the silencing of this locus[146,161,162] (Figure 13 A). With a break induction system independent of the *MAT* system, I tested if the RE can be activated in *MATα* cells via a knockout of the RE repressing factor Matα2. For this purpose I constructed a *Δmatα2* strain with a *MATα* mating type. A DSB was induced on chromosome IV by overexpression of SceI (Figure 13 B). As the main repressor of the RE, a knockout of Matα2 is expected to open the RE for interactions and therefore also for homology search. Indeed, deletion of Matα2 restores Rad51 binding to the RE, reflected as enrichment after a Rad51 ChIP and qPCR analysis (Figure 13 B). The open conformation makes the RE accessible for trans-acting factors like the transcription factor Fkh1 (see section 4.2.2) as well as homology search[25,145].

In contrast to *MATα* cells, Matα2 is not expressed in *MATa* strains. Thus, Mcm1 alone binds to the RE and acts as an activator, allowing trans-acting factors to bind[145]. To test the influence of expressed Matα2 in *MATa* cells, it was amplified from a *MATα* strain and integrated into the *URA3* locus on chromosome V under the control of the *GAL1* promoter. Overexpression was simultaneously induced with HO endonuclease (integrated in *ADE3* locus on chromosome VII) via addition of galactose to the medium. Although both strains show similar Rad51 enrichment directly at the DSB and 40 kb upstream, corresponding to a functional Rad51 filament formation and general homology search, overexpressed Matα2 strongly reduced binding of Rad51 to the RE (Figure 13 C).

These data clearly show that the main repressor of the RE is Matα2, as deletion in *MATα* cells led to a probing of the Rad51 nucleoprotein filament at the RE. Vice versa, expression of Matα2 in *MATa* cells is sufficient to induce repression of the RE and therefore prevents the binding of trans-acting factors like Fkh1[145].
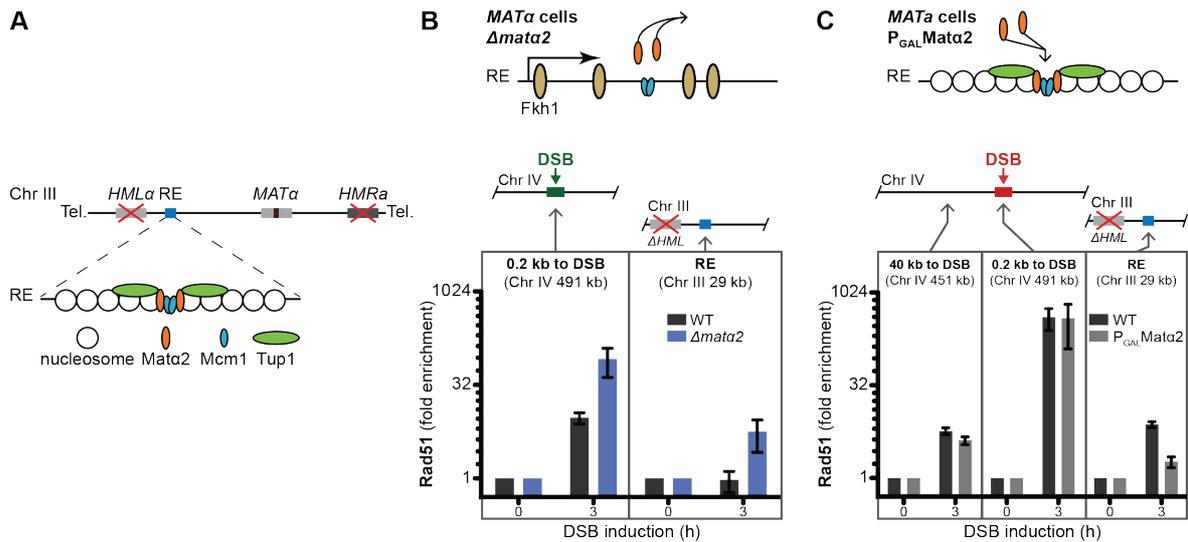
Figure 13 | **Matα2 represses the RE and RE-guided homology search.**
(A) Scheme representing the silencing of the RE on ChrIII. Matα2, together with its co-repressor Mcm1, binds to the RE and recruits the general repressor Tup1, leading to the dense positioning of nucleosomes and the repression of the RE. The endogenous HO recognition site within the *MAT* locus on ChrIII was mutated and not cleavable.
(B) Knockout of Matα2 leads to activation of the RE even in *MATα* cells. A DSB was induced by SceI on ChrIV at 491 kb in a WT or *Δmatα2* strain. Upon deletion of Matα2, Mcm1 alone acts as an activator for the RE, making this region accessible for the binding of trans-acting factors like Fkh1. Activation of the RE is reflected as enrichment of Rad51 at this region.
(C) Overexpression of Matα2 in *MATa* cells leads to the recruitment of repressors and the silencing of the usually activated RE. Overexpression of Matα2 was simultaneously induced with HO endonuclease via galactose. The HO-induced DSB was located on ChrIV. Ongoing homology search was tested by qPCR analysis with a primer pair 40 kb upstream of the DSB. Rad51 signal at the RE decreased compared to the WT.
Rad51 enrichment was calculated following Rad51 ChIP-qPCR analysis. Enrichment data are depicted on a log2 scale. Data represent mean ± SEM of three independent experiments. The qPCR data were normalized to a control locus on ChrX and additionally to the time before DSB induction (0 h).

4.2.2 Fkh1 is essential for RE-guided donor preference regulation

Loop formation between the DSB site and the RE was proposed previously[157]. Although it is well understood how the RE itself is regulated by the Matα2 repressor (see section 2.3.2) and co-factors[168,169], how the regulation of donor preference is established and which factors might contribute, is barely known. However, previous studies indicated that Fkh1 is involved in regulation of mating type switching[145,157]. Thereby it is believed that in *MATa* cells Fkh1 binds to the RE and interacts with one or more factors at the DSB site to mediate spatial proximity between the RE and the break. To confirm these results and as a first approach to further understand how the proposed RE-DSB loop is regulated, I investigated the effect of an *FKH1* deletion in cells where a DSB was induced (Figure 14). Fkh1 also has a paralog, Fkh2, which performs analogous functions[171-173]. Both proteins share a high sequence similarity and recognize similar DNA sequences[154]. Yeast strains with a double knockout of both forkhead transcription factors showed

morphological alterations as well as budding defects, whereas single knockouts did not exhibit this phenotype[171,173,174]. Therefore, I also checked if Fkh2 is involved in the regulation of donor preference. First, a Rad51 ChIP-qPCR was performed with strains harboring an HO recognition site to induce a DSB on chromosome IV at 491 kb (Figure 14 A). In all strains, homology search was ongoing as reflected by Rad51 enrichment 40 kb upstream of the break. An *FKH1* knockout led to a complete loss of Rad51 binding at the RE. Surprisingly, a deletion of its paralog *FKH2* had no influence on enrichment of Rad51 at the RE. A double knockout of both transcription factors consequently showed a similar defect as the *FKH1* single knockout (Figure 14 A).
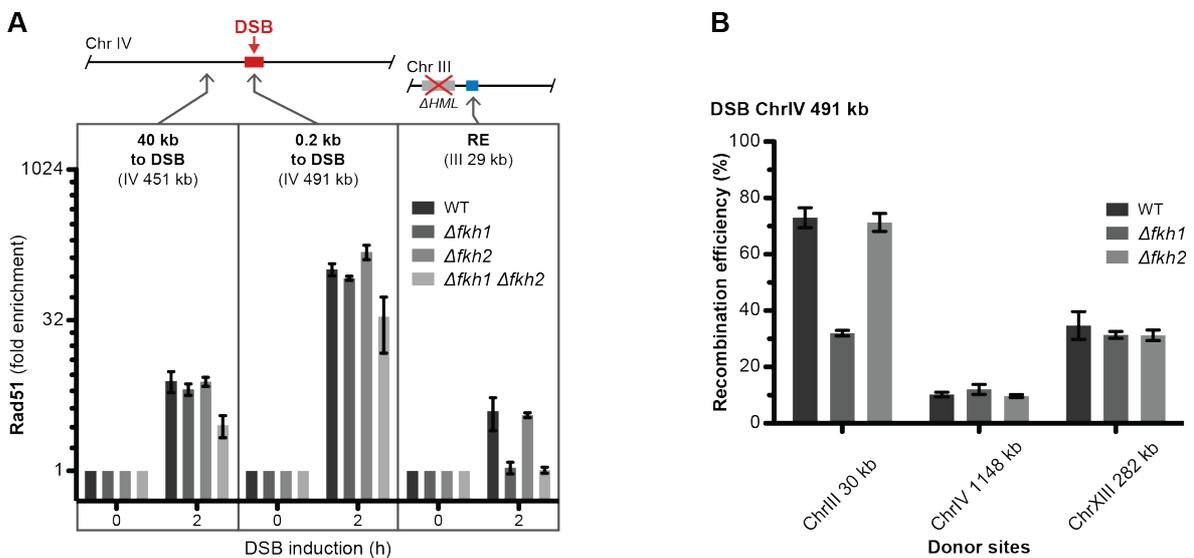
Figure 14 | Fkh1, but not Fkh2, is essential for RE-guided homology search.
(A) Rad51 enrichment in strains bearing either *FKH1*, *FKH2* or double knockout. DSB induction was performed via HO overexpression at the indicated position. Rad51 enrichment was calculated following Rad51 ChIP-qPCR analysis. Enrichment data are depicted on a log2 scale. qPCR primers were used for the indicated positions. Data represent mean ± SEM of three independent experiments. The qPCR data were normalized to a control locus on ChrX and additionally to the time before DSB induction (0 h).
(B) Recombination assay in *FKH1* and *FKH2* knockout strains. A GFP construct bearing the HO recognition site was integrated at ChrIV 491 kb and served as DSB induction site. Donor sites were either inserted close to the RE on ChrIII, on ChrIV or on ChrXIII. Recombination efficiency data are depicted on a linear scale. Data represent mean ± SEM of three independent experiments. Cells were plated on glucose and galactose containing medium to induce the DSB. Colonies were counted and normalized to cells growing on glucose.

As a second experiment to demonstrate the importance of Fkh1 for RE-involved recombination a recombination assay was used (Figure 14 B). Here, a DSB was also induced on chromosome IV and donor sites were integrated at different positions in the genome. Whereas an *FKH2* knockout behaves like wildtype, deletion of *FKH1* strongly decreased recombination efficiency, when the donor is inserted next to the RE. The remaining repair rate in this strain reflected the basal recombination level between the respective loci. Other donor positions are neither impaired by *FKH1* nor by *FKH2*

deletions. These data clearly show that Fkh1 has to be a major player for the regulation of the DSB-RE loop, whereas Fkh2 does not have any influence, neither on ongoing homology search nor on recombination efficiency.

4.2.3 The RE cannot be replaced by an Fkh1-bound promoter region

Besides its role in mating type switching, Fkh1 has also important functions in transcriptional regulation as it binds to many gene promoter regions within the genome[154]. Therefore, I wondered if the RE could be replaced by other Fkh1-binding elements, such as promoters. To examine this hypothesis, I have chosen two promoter regions (*PES4* and *KIP2*), where Fkh1 was found to be highly enriched following Fkh1 ChIP-on-chip[154]. These 500 bp long promoters were inserted next to donor sites on chromosomes IV and XIII (Figure 15). For chromosome IV, insertion of the RE next to the donor site results in a higher recombination efficiency compared to the wildtype situation (Figure 15 A). However, inserting one of the promoter regions next to this site did not lead to increased repair efficiency.

A

DSB ChrIV 491 kb, donor at ChrIV 1148 kb

B

DSB ChrIV 491 kb, donor at ChrXIII 282 kb
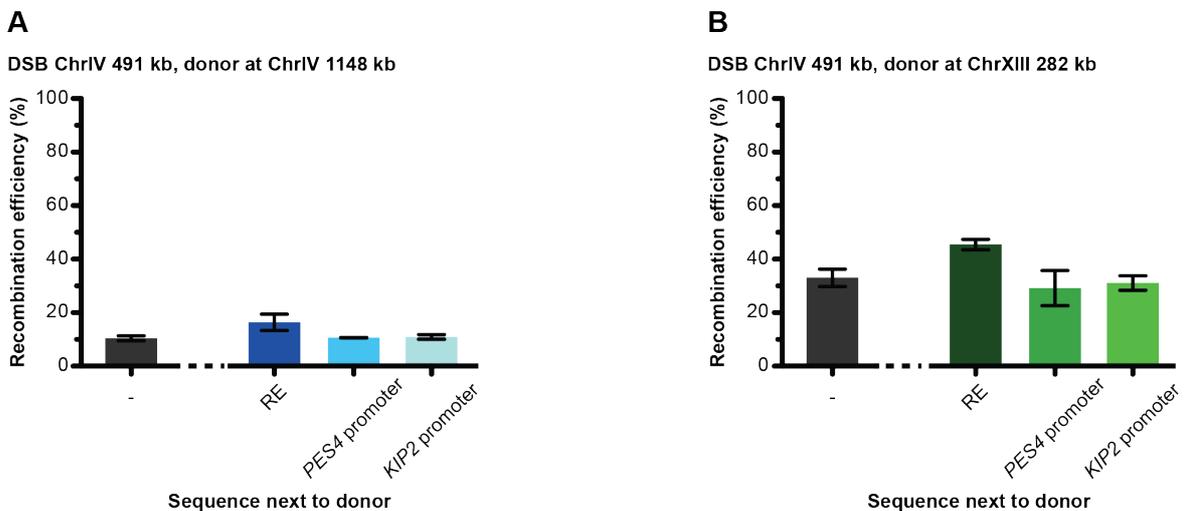
Figure 15 | A promoter region bound by Fkh1 cannot replace the RE.
(A) Recombination efficiency assay with a donor site at ChrIV 1148 kb. Promoter regions were amplified from genomic DNA, cloned into marker plasmids and integrated into the genome via a PCR-based strategy[163,164]. As a control, 754 bp of the RE coding sequence were amplified and integrated next to the donor site.
(B) Recombination efficiency assay with a donor site at ChrXIII 282 kb. Same procedure as in (A). Recombination efficiency data are depicted on a linear scale. Data represent mean ± SEM of three independent experiments. Cells were plated on glucose and galactose containing medium to induce the DSB. Colonies were counted and normalized to cells growing on glucose.

The same scenario was obtained for the donor site on chromosome XIII (Figure 15 B). The RE next to the donor site increased recombination efficiency of the cells. A promoter

region did not have this effect, leaving repair efficiency at wildtype levels. According to these data there has to be a difference between the RE and promoter regions bound by Fkh1, highlighting the fact that loop formation between a DSB and any Fkh1 binding site would be surely unfavorable for the cell. Along this line, one difference between the RE and these promoter sites seems obvious: the RE contains several Fkh1 binding sites[145,147], which could lead to Fkh1 proteins clustering at the RE. Compared to promoter sites, this extensive binding then leads to loop formation.

4.2.4 RE-guided homology search depends on the phosphothreonine-binding domain of Fkh1

Forkhead transcription factors share a common domain, the Forkhead Associated (FHA) domain. These domains have been implicated in binding of phosphothreonine residues[175,176]. FHA domains across all family members have a high degree of sequence diversity, with only a few conserved residues[155]. For Rad53, a mutation of a conserved arginine residue within its FHA domain abolished the function of this domain[177,178]. In Fkh1, this residue corresponds to arginine 80 within the FHA domain. I wondered if a mutation of this residue shows the same strong effect as for the corresponding residue in Rad53. Therefore, *FKH1* was deleted und replaced by a centromeric plasmid harboring either the sequence encoding the wildtype protein or a sequence with a site-directed mutation to change arginine to alanine (R80A). In addition, the effect of an *FKH1* knockout was compared to an RE deletion. First, the repair efficiency of cells was measured, depending on successful recombination between a DSB and a donor site (Figure 16 A). As expected, a deletion of the RE, *FKH1* or both leads to a strong decrease in repair efficiency. When the *FKH1* deletion is compensated by a construct bearing the wildtype sequence, recombination efficiency can be restored to wildtype level. Strikingly, when the same plasmid is used with a sequence coding for Fkh1 R80A, the recombination efficiency of the cells reflects the *FKH1* or *RE* knockout scenario. Other donor sites on chromosome IV and XIII are not affected by the *FKH1* deletion. As a second assay, ongoing homology search was investigated by a Rad51 ChIP-qPCR experiment (Figure 16 B). Here, an *FKH1* deletion was again replaced by a centromeric plasmid bearing either a wildtype or a mutant version of the FHA domain. Similar to an *RE* or *FKH1* deletion, the R80A mutation does not have an influence on ongoing homology search, but instead strongly impairs Rad51 association at a site close to the RE element. Collectively, these data highlight the importance of a functional FHA domain for Fkh1 function at the RE.

A

DSB ChrIV 491 kb

B

C
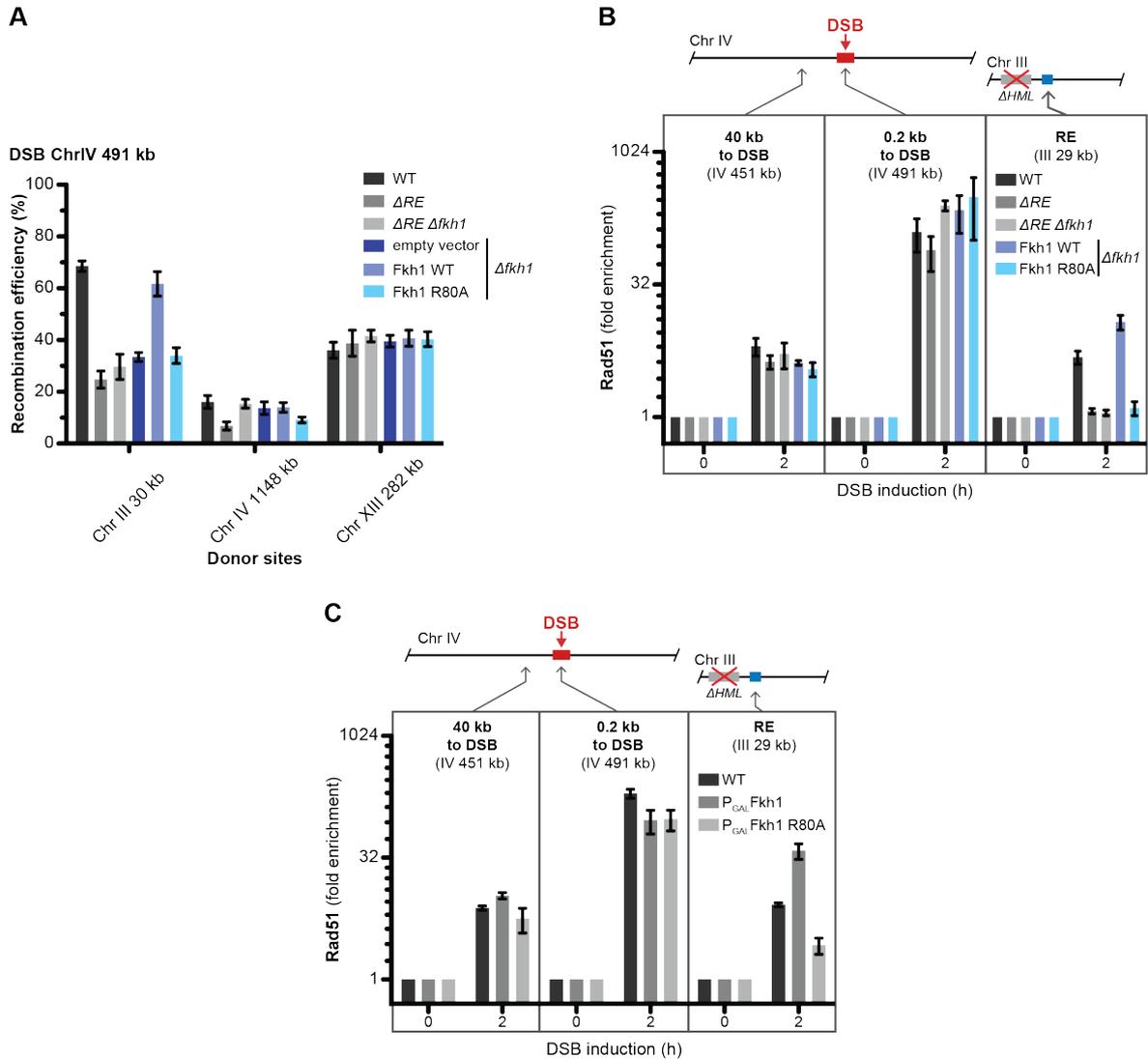
Figure 16 | **Mutation of the phosphopeptide binding pocket of the FHA domain abolishes the function of Fkh1 for the regulation of donor preference.**
(A) Recombination efficiency was calculated in strains harboring different deletions. Cells carrying a single knockout of *FKH1* were carrying either an empty vector or a plasmid bearing the sequence encoding for Fkh1 WT or R80A. A DSB was induced at ChrIV 491 kb and one donor site per strain integrated at different genomic positions. Recombination efficiency data are depicted on a linear scale. Data represent mean ± SEM of four independent experiments. Cells were plated on glucose and galactose containing medium to induce the DSB. Colonies were counted and normalized to cells growing on glucose.
(B) Rad51 enrichment following Rad51 ChIP-qPCR. *Δfkh1* cells were supplemented with an *FKH1* WT or R80A construct.
(C) Rad51 enrichment after overexpression of Fkh1 WT or R80A. *FKH1* WT or R80A under the control of the *GAL1* promoter were integrated into the *URA3* locus on ChrV in *Δfkh1* strains. Overexpression of Fkh1 was induced simultaneously with HO endonuclease upon addition of galactose to the medium.
For (B) and (C): Rad51 enrichment was calculated following Rad51 ChIP-qPCR analysis. Enrichment data are depicted on a log2 scale. qPCR primers were used for the indicated positions. Data represent mean ± SEM of three independent experiments. The qPCR data were normalized to a control locus on ChrX and additionally to the time before DSB induction (0 h).

Next, I wondered if overexpression of Fkh1 could make the RE function more efficient or could compensate for the defect introduced by the R80A mutation. Therefore, either *FKH1*

wildtype or R80A was integrated into the *URA3* locus on chromosome V under the control of the *GAL1* promoter (Figure 16 C). The Fkh1 version was simultaneously overexpressed with HO by galactose addition. While having no effect on Rad51 enrichment around the break site and away from the break, Fkh1 overexpression clearly affected Rad51 signals at the RE. Surprisingly, upon overexpression of wildtype Fkh1, the Rad51 signal at the RE strongly increased. In fact, compared to endogenous expression, the enrichment of the overexpressed version exceeded the wildtype signal by more than 4.5 fold. A stronger binding or covering of the Fkh1 binding sites at the RE can be assumed. In case of the R80A mutant variant, overexpression led to small, but significant enrichment of Rad51 at the RE, not observed at normal expression levels (compare Figure 16 B). For Fkh1 R80A, the overexpression thus partially overcomes the defect introduced by the arginine mutation.

4.2.5 Phosphorylation is critical for RE-guided homology search

It was previously shown that FHA domains in general bind to phosphorylated threonine residues in target proteins[155,177,179]. In Fkh1, the arginine important for interaction with phosphorylated proteins lies within the FHA domain. As shown in this study, mutation of this residue completely abolished the binding of Fkh1 to several interacting factors. In addition, Rad51 binding to the RE was also lost. Furthermore, when transplanting a donor next to the RE, recombination efficiency decreased to a minimum. Therefore, the interaction of Fkh1 with phosphorylated residues of target proteins plays an essential role for the regulation of donor preference. However, the responsible kinase(s) have not been identified by now. A previous study suggested that casein kinase 2 (CK2) has an effect on the regulation of donor preference[157]. CK2 is composed of two α and two β subunits, forming the $\alpha_2\beta_2$ holoenzyme[180]. Thereby the α part has a catalytic and the β part a regulatory function[180]. In this thesis, I checked if a knockout of one of the two catalytic subunits (Cka1/Cka2) would have an effect on Rad51 binding to the RE on chromosome III. Since a knockout of both genes encoding for the catalytic subunit is lethal[181], either *CKA1* or *CKA2* was deleted and the Rad51 enrichment at the RE calculated after DSB induction and Rad51 ChIP-qPCR (Figure 17 A). However, none of the deletions affected Rad51 enrichment at the RE. This is most likely due to the effect that a deletion of one α subunit can be compensated by the other one.

Following DSB induction, several kinases phosphorylate factors involved in DSB repair[182]. One of them is Mec1, the yeast homolog of mammalian ATR (ataxia-telangiectasia mutated and Rad3-related) kinase. Mec1 phosphorylates histone H2A (γ-H2A) at serine 129 as an early response to DSBs[182,183]. Note that a strain carrying a

mutant version of H2A, S129A, did not show any effect on Rad51 enrichment at the RE (data not shown).
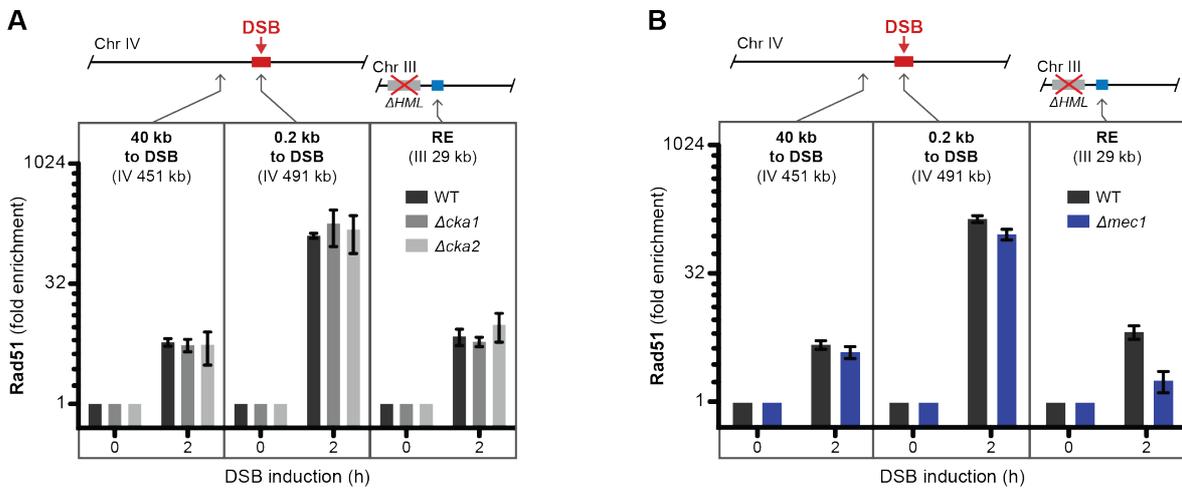
Figure 17 | **Deletion of CK2 catalytic subunits does not affect regulation of donor preference, but deletion of checkpoint kinase Mec1.**
(A) Deletion of a single CK2 catalytic subunit does not affect Rad51 binding at the RE.
(B) Knockout of checkpoint kinase Mec1 leads to a strong decrease of Rad51 binding at the RE. To construct a *MEC1* knockout, deletion of *SML1* was necessary as a single knockout of *MEC1* is lethal.
A DSB was induced at ChrIV 491 kb. Rad51 enrichment was calculated following Rad51 ChIP-qPCR analysis. Enrichment data are depicted on a log2 scale. qPCR primers were used for the indicated positions. Data in (A) represent mean ± SEM of three independent experiments, data in (B) mean ± SEM of five independent experiments. The qPCR data were normalized to a control locus on ChrX and additionally to the time before DSB induction (0 h).

However, previous data did not assign any function to Mec1 for the regulation of donor preference[157]. Nevertheless, I tested this hypothesis by constructing a *MEC1* mutant strain. Since a single *MEC1* knockout is lethal, the sequence coding for Sml1 (suppressor of mec1-lethality) had to be deleted before deleting the *MEC1* sequence[184]. The binding of Rad51 to the RE was measured by calculating Rad51 enrichment after a DSB on chromosome IV at 491 kb and Rad51 ChIP-qPCR (Figure 17 B). Strikingly, a *Δsml1 Δmec1* strain showed a significantly decreased Rad51 enrichment at the RE. These data are contradictory to the previous results for Mec1 function in the regulation of donor preference[157] and clearly showed that Mec1 affects RE function as Rad51 binding to the RE is strongly decreased in a *Δsml1 Δmec1* strain.

4.2.6 Fkh1 interacts with Mph1 and Mte1 to regulate donor preference

Data obtained so far show that Fkh1 is an essential factor for the regulation of donor preference. These findings are supported by publications identifying Fkh1 binding sites within the RE[145,147]. Therefore, Fkh1 is thought to be the factor, which binds to the RE to establish a DSB-RE loop. However, data are missing about potential binding partners at the DSB site, which also contribute to the regulation of donor preference. Such protein binding partners likely exist, as the RE functions irrespective of the DSB location and thus in a sequence-independent manner. As little was known about additional factors involved in donor preference regulation, I conducted an unbiased mass spectrometry-based approach to identify potential interaction partners of Fkh1. I already showed in section 4.2.4 that a functional FHA domain is essential for Fkh1's function during regulation of donor preference. Abolishing the ability of the FHA domain to bind to phosphorylated targets by mutating the relevant arginine (R80) also impaired donor preference regulation (compare Figure 16). Therefore, besides Myc-tagged Fkh1 I also used a tagged Fkh1 R80A mutant to check for phosphorylated binding partners, which should not interact with this mutant version. Performing a Myc-IP, mass spectrometry revealed different binding partners in these strains before and after DSB induction. In addition, the results were also compared to a non-tagged wildtype strain (data not shown). My results confirmed previous findings about general Fkh1 binding partners[185,186]. A previous large-scale study also identified Mph1, an ATP-dependent DNA helicase[187] and yeast's ortholog of the human Fanconi anemia (FA) protein FANCM[188], as a physical interactor of Fkh1[186]. This raised the question if Mph1 might also be involved in regulation of donor preference as an Fkh1 interaction partner. To first confirm the mass spectrometry results, I tagged both proteins, Fkh1 and Mph1, and performed a Co-IP (Figure 18 A). Since interaction of FHA domains with other proteins predominantly depends on the phosphorylation status of binding partners[155,179], I further tested if phosphorylation is also essential for the interaction between Fkh1 and Mph1. Therefore, also an Fkh1 variant carrying the R80A mutation was used for this assay. In addition, the interaction was examined before and after DSB induction to see if it can be enhanced during ongoing DSB repair. Essentially, 6HA-tagged Mph1 could be detected as an Fkh1 interaction partner also in the Co-IP assay[§§].

[§§]While I performed the current studies, another group addressed this independently and showed an interaction between Fkh1 and Mph1[189].

Moreover, an interaction with Fkh1 R80A could not be detected, which supports the mass spectrometry results. Interestingly, binding between Fkh1 and Mph1 was seen even before a DSB and slightly increased after DSB induction. These results clearly show that Mph1 interacts with Fkh1 and that this interaction is dependent on phosphorylation.

In a next step I investigated the influence of Mph1 on homology search and regulation of donor preference (Figure 18 B and C).

Figure 18 | Mph1 interacts with Fkh1 and mildly affects DSB repair.
(A) Mph1 is an Fkh1 interactor. C-terminal tagging of either Fkh1 WT or R80A (indicated in the figure) and Mph1 was done according to a PCR-based strategy[163,164]. Strains expressed either one or two tagged proteins. Cells were grown in lactate medium and a DSB was induced at ChrIV 491 kb by galactose addition. A Co-IP was carried out by pulling on Fkh1 WT or R80A with a Myc-antibody. Samples before and after DSB induction were taken and analyzed by Western blotting and antibodies against the Myc- and the HA-tag.
(B) Rad51 ChIP-qPCR assay shows that the deletion of *MPH1* does not have an influence on Rad51 enrichment at the RE. DSB induction was carried out as described in (A). Rad51 enrichment was calculated following Rad51 ChIP-qPCR analysis. Enrichment data are depicted on a log2 scale. qPCR primers were used for the indicated positions. Data represent mean ± SEM of three independent experiments. The qPCR data were normalized to a control locus on ChrX and additionally to the time before DSB induction (0 h).
(C) An *MPH1* knockout has a minor effect on DSB repair efficiency. Recombination assay showing strains with a DSB induction at ChrIV 491 kb and one donor site per strain inserted at different genomic positions. Recombination efficiency data are depicted on a linear scale. Data represent mean ± SEM of three independent experiments. Cells were plated on glucose and galactose containing medium to induce the DSB. Colonies were counted and normalized to cells growing on glucose.

I tested for Rad51 enrichment after DSB induction (Figure 18 B) as well as recombination efficiency (Figure 18 C). An *MPH1* knockout was compared to an *FKH1* knockout as well as wildtype. Surprisingly, the *MPH1* knockout did not have any influence on Rad51 enrichment at the RE on chromosome III. In fact, same Rad51 levels were obtained as in the wildtype. A double knockout of *MPH1* and *FKH1* consistently led to a loss of Rad51 at the RE, as *FKH1* deletion is sufficient to abolish filament probing at this site. In contrast, in a recombination assay the repair efficiency was slightly reduced in the *MPH1* knockout compared to the wildtype (Figure 18 C). However, this decrease is not as strong as the effect of an *FKH1* knockout, which resulted in a minimum of repair efficiency (31 %, compare Figure 14 B). These data point towards a supporting function of Mph1 within the regulation of mating type switching, however other binding partners of Fkh1 must exist at the DSB.

Among the identified proteins there were also several new interaction partners, which have not been reported so far. One of them has not been described before and had an unknown function: Ygr042w. Two recently published studies identified this protein as Mph1-associated telomere maintenance protein 1 (Mte1), an Mph1 interactor[190,191]. However, I was interested if Mte1 also interacts with Fkh1. Therefore, both proteins were tagged and a Co-IP was performed following DSB induction (Figure 19 A). An interaction could be shown before and after DSB induction. In contrast to Mph1, an increased interaction was not seen with Mte1 after DSB induction. However, interaction is abolished when the Fkh1 FHA defective R80A mutant is used, also pointing towards a phosphorylation-dependent mechanism. To investigate if this interaction also has an influence on DSB repair efficiency, the recombination rate was measured in an *MTE1* knockout strain (Figure 19 B). Whereas the recombination efficiency in wildtype cells is as high as usual, an *MTE1* knockout leads to a mild decrease in repair efficiency. As shown for Mph1, Mte1 thus contributes to the regulation of donor preference as well. However, a mechanism where Mte1 is the main interaction partner of Fkh1 at the break site can be excluded according to the obtained data.

A

B
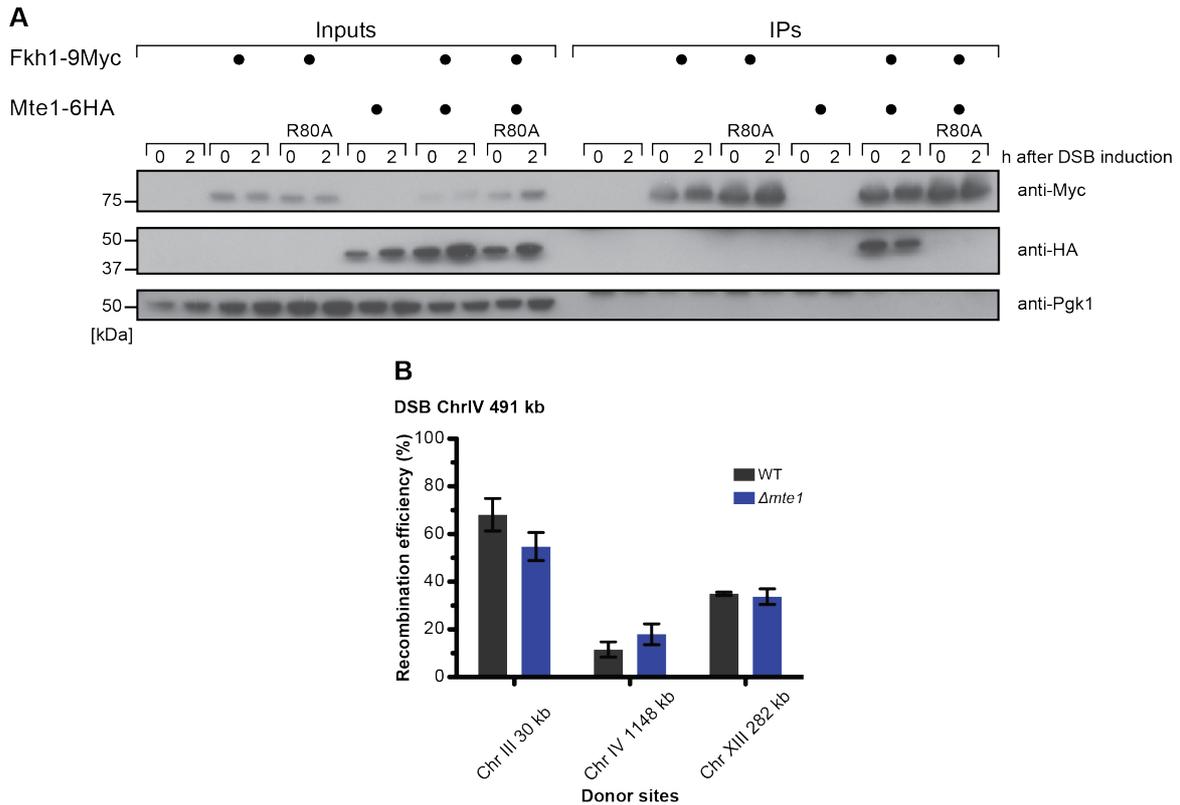
Figure 19 | **Mte1 interacts with Fkh1, but has only a mild effect on DSB repair.**
(A) Mte1 interacts with Fkh1. C-terminal tagging of either Fkh1 WT or R80A (indicated in the figure) and Mte1 was done according to a PCR-based strategy[163,164]. Strains expressed either one or two tagged proteins. Cells were grown in lactate medium and a DSB was induced at ChrIV 491 kb by galactose addition. A Co-IP was carried out by pulling on Fkh1 WT or R80A with a Myc-antibody. Samples before and after DSB induction were taken and analyzed by Western blotting and antibodies against the Myc- and the HA-tag.
(B) Knockout of *MTE1* has only a mild effect on DSB repair efficiency. Recombination assay showing strains with a DSB induction at ChrIV 491 kb and one donor site per strain inserted at different genomic positions. Recombination efficiency data are depicted on a linear scale. Data represent mean ± SEM of three independent experiments. Cells were plated on glucose and galactose containing medium to induce the DSB. Colonies were counted and normalized to cells growing on glucose.

To exclude that the interaction between Fkh1 and Mph1 depends on Mte1 and vice versa, in a final approach the binding to these factors was tested in another Co-IP, independently of the third interaction partner (Figure 20). Fkh1, Mph1 and Mte1 were expressed either with a Myc- or an HA-tag. First of all, the interaction between Fkh1 and Mph1 was further investigated. For this purpose, *MTE1* was deleted in a strain carrying Myc-tagged Fkh1 as well as HA-tagged Mph1 (Figure 20 A). In addition, to check if the interaction is phosphorylation-dependent, I also used an Fkh1 R80A mutant. Notably, absence of Mte1 leads to a weaker interaction between Fkh1 and Mph1 after DSB induction. With functional Mte1 present, the signal was stronger after break induction (compare Figure 18 A). Consequently, this interaction partially seems to depend on a DSB. Next, binding of Mte1 to Fkh1 was examined in the absence of Mph1 (Figure 20 B). Here, the interaction between both proteins stays constant even after a DSB occurred. I assume

that Mte1 also interacts with Fkh1 in other pathways besides the regulation of donor preference.

Figure 20 | **Fkh1, Mph1 and Mte1 interact with each other independently of the third factor.**
(A) Fkh1 interacts with Mph1 in the absence of Mte1. All strains carried an *MTE1* knockout. Fkh1 WT or R80A (indicated in the figure) was 9Myc-tagged and Mph1 was 6HA-tagged.
(B) Fkh1 interacts with Mte1 in the absence of Mph1. All strains carried an *MPH1* knockout. Fkh1 WT or R80A (indicated in the figure) was 9Myc-tagged and Mte1 was 6HA-tagged.
(C) Mte1 interacts with Mph1 in the absence of Fkh1. All strains carried an *FKH1* knockout. Mte1 was 9Myc-tagged and Mph1 was 6HA-tagged.
Proteins were C-terminally tagged as indicated according to a PCR-based strategy[163,164]. Strains expressed either one or two tagged proteins. Cells were grown in lactate medium and a DSB was induced at ChrIV 491 kb via galactose addition. A Co-IP was carried out by pulling on the Myc-tag with a Myc-antibody. Samples before and after DSB induction were taken and analyzed by Western blotting and antibodies against the Myc- and the HA-tag.

Last but not least, *FKH1* was knocked out and Mte1 and Mph1 were tagged with a Myc- and an HA-tag, respectively (Figure 20 C). While Mph1 can be pulled down together with Mte1 before a DSB, the signal is lost after a break was induced. Therefore, this interaction depends on the presence of Fkh1.

Mph1 and Mte1 are newly identified interactors of Fkh1. Both show contributions to the regulation of donor preference as single knockouts led to a decrease in cell recombination efficiency. This raised the question if either Mph1 or Mte1 could complement the function of each other and if double knockout cells would show a synergistic defect. To test this scenario, I wanted to check if a double knockout of *MPH1* and *MTE1* would have an effect. Therefore, a strain with a deletion of both proteins was constructed and Rad51 enrichment was calculated following Rad51 ChIP-qPCR (Figure 21 A). A decrease in Rad51 enrichment was not detected at any position tested. Like wildtype cells, *Δmph1 Δmte1* did not have any effect on the Rad51 filament searching and probing for a homologous sequence. Hence, even a double knockout of *MPH1* and *MTE1* did not show an effect on ongoing homology search.

In a last approach, cells carrying an *MPH1*/*MTE1* double knockout were tested for recombination efficiency after DSB induction (Figure 21 B).
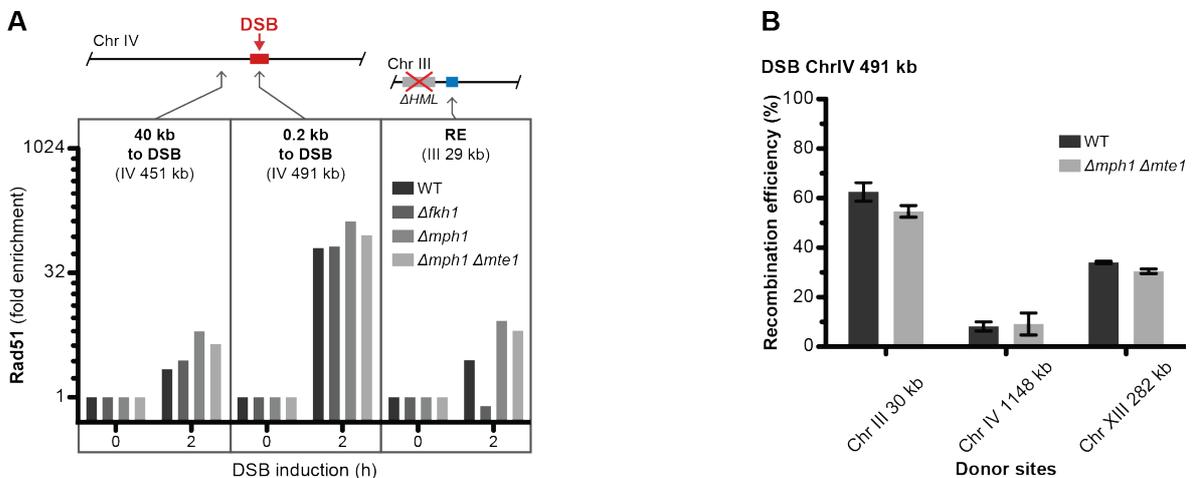
Figure 21 | **Mte1 and Mph1 only mildly impair DSB repair efficiency.**
(A) Preliminary data from Rad51 ChIP-qPCR assay show that a double knockout of *MPH1* and *MTE1* does not have an influence on Rad51 enrichment at the RE. DSB induction was carried out as described. Rad51 enrichment was calculated following Rad51 ChIP-qPCR analysis. Enrichment data are depicted on a log2 scale. qPCR primers were used for the indicated positions. Data represent results from one experiment. The qPCR data were normalized to a control locus on ChrX and additionally to the time before DSB induction (0 h).
(B) Double knockout of *MPH1* and *MTE1* has only a mild effect on DSB repair efficiency. Recombination assay showing strains with a DSB induction at ChrIV 491 kb and one donor site per strain inserted at different genomic positions. Recombination efficiency data are depicted on a linear scale. Data represent mean ± SEM of two independent experiments. Cells were plated on glucose and galactose containing medium to induce the DSB. Colonies were counted and normalized to the cells growing on glucose.

A deletion of both genes only led to a minor reduction in repair efficiency. It rather showed the mild decline in repair efficiency as seen for the *MPH1* and *MTE1* single knockout. Hence, both proteins contribute to the regulation of donor preference, but they are not essential to maintain the mechanism itself.

4.2.7 Fkh1 binds to RPA

Several factors bind to the break site after DSB induction and during the process of homology search. After DNA end resection, the ssDNA is rapidly covered by replication protein A (RPA)[192], whereas RPA is exchanged for Rad51 which then forms the nucleoprotein filament to conduct homology search[10]. RPA is a heterotrimeric protein[10], containing the three subunits Rfa1, Rfa2 and Rfa3. RPA is required for DNA replication, repair and recombination[193]. Due to its high abundance at ssDNA and therefore, at resected DSB sites, it is a good candidate to interact with Fkh1 and establish the RE-DSB loop at the break site. Interestingly, two of the RPA subunits, Rfa1 and Rfa3, were also hits in the mass spectrometry assay conducted for this thesis. To test an interaction between Fkh1 and RPA, first a Co-IP was performed with tagged Fkh1 and Rfa3. However, Rfa3 was not found to bind to Fkh1 (data not shown). A second Co-IP assay was performed with Rfa1 tagged instead (Figure 22). Note that Rfa1 could not be tagged at the C-terminal domain, because the cells were found to be not viable under these conditions. Therefore, it was tagged N-terminally with an HA-tag and expression was controlled by an *ADH1* promoter, integrated upstream of *RFA1* via a PCR-based strategy[163,164].
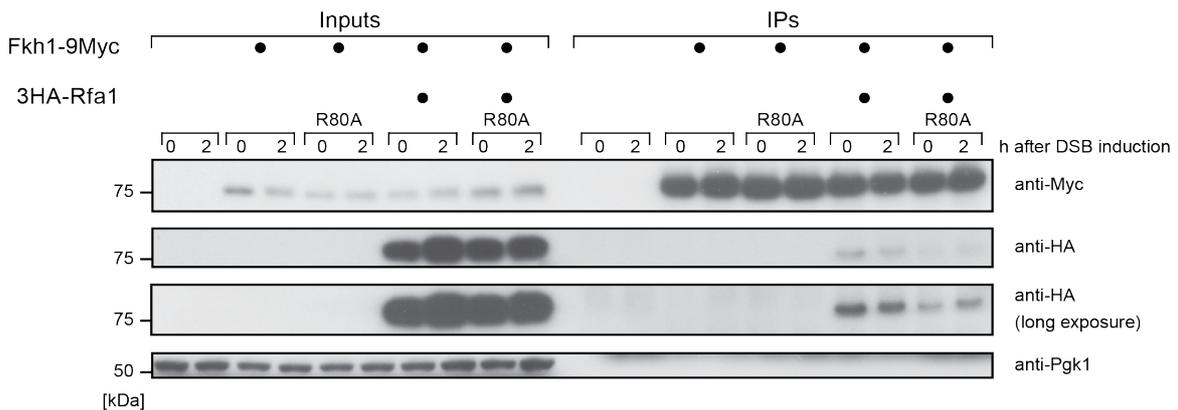
Figure 22 | **Fkh1 interacts with subunit Rfa1 of RPA.**
C-terminal tagging of either Fkh1 WT or R80A (indicated in the figure) and N-terminal tagging of Rfa1 was done as indicated according to a PCR-based strategy[163,164]. Additionally, an *ADH1* promoter was inserted upstream of *RFA1*. Strains expressed either one or two tagged proteins. Cells were grown in lactate medium and a DSB at ChrIV 491 kb was induced via addition of galactose. A Co-IP was carried out by pulling on Fkh1-9Myc with a Myc-antibody. Samples before and after DSB induction were taken and analyzed by Western blotting and antibodies against the Myc- and the HA-tag.

A DSB was induced on chromosome IV at 491 kb via overexpression of HO endonuclease. To determine the importance of a functional FHA domain, a mutant version of Fkh1, R80A, was used. Strikingly, an interaction between Fkh1 and Rfa1 could be confirmed before and after DSB induction. Binding of Rfa1 to Fkh1 R80A was also detected, although the signal was below wildtype level. This confirms the results obtained for the mass spectrometry approach and furthermore highlights a largely phosphorylation-dependent binding mechanism.

4.2.8 Fkh1 and condensin interact phosphorylation-independent

DNA loops within the nucleus can be found during different cellular processes. The regulation of donor preference also requires a loop to enable the homologous recombination between a DSB and a site close to the RE. To maintain this loop during the repair process, factors keeping both DNA strands together are required. At the RE, this factor is the Fkh1 protein, but the counterpart at the DSB remains elusive. Although not identified in the previous mass spectrometry approach, I decided to directly test two further interesting candidates, condensin and cohesin, which are highly important regulators of chromatin organization[194,195]. Both of them are large, evolutionary conserved multisubunit protein complexes which bind to DNA in an ATP-driven mechanism[33,196,197]. A third complex, also responsible for the maintenance of chromosomal architecture, is the Smc5/6 complex, which is also involved in DNA repair and replication[198]. Basically, these protein assemblies consist of a heterodimer of the structural maintenance of chromosomes (SMC) family of ATPases as well as a Kleisin subunit and two HEAT repeats-containing proteins[194,197]. In addition, several co-factors can support their functions[197]. In *S. cerevisiae* the ATPase activity of condensin is covered by Smc2 and Smc4[199], for cohesin by Smc1 and Smc3[200] and for the Smc5/6 complex by Smc5 and Smc6[198,201]. Condensin, cohesin or the Smc5/6 complex might be involved in RE-DSB loop formation. Therefore, I investigated if these complexes also interact with Fkh1. Importantly, none of the complex subunits have been reported so far to interact with Fkh1. Also the mass spectrometry assay conducted for this thesis did not reveal any interaction. Therefore, I decided to do further research and approach this potential interaction with Co-IP assays. For this purpose, Fkh1 was Myc-tagged and one of the Smc proteins HA-tagged. A DSB was induced on chromosome IV at 491 kb. First, the binding of the cohesin subunits Smc1/3 and Fkh1 was examined (data not shown). Pulling on Myc-tagged Fkh1 did neither result in a signal for Smc1 nor for Smc3, independently of the time point investigated (before and after DSB induction). As binding of cohesin subunits to Fkh1 was neither detected in the mass spectrometry nor in the Co-IP assay, an interaction

between Fkh1 and cohesin can be excluded. The same results were obtained when the ATPase subunits of the Smc5/6 complex or its co-factor Mms21, a SUMO (small ubiquitin-like modifier) E3 ligase, were tagged (data not shown).

Figure 23 | Fkh1 interacts with condensin subunit Smc2.
C-terminal tagging of either Fkh1 WT or R80A (indicated in the figure) and Smc2 was done according to a PCR-based strategy[163,164]. Strains expressed either one or two tagged proteins. Cells were grown in lactate medium and a DSB was induced via galactose addition at ChrIV 491 kb. A Co-IP was carried out by pulling on Fkh1-9Myc with a Myc-antibody. Samples before and after DSB induction were taken and analyzed by Western blotting and antibodies against the Myc- and the HA-tag.

In the next step the binding of Fkh1 to condensin was investigated (Figure 23). The ATPase subunit Smc2 was tagged and a Co-IP was performed by pulling on either Myc-tagged Fkh1 wildtype or R80A mutant. Strikingly, a distinct signal for Smc2 was obtained before and after DSB induction (Figure 23). Furthermore, this interaction could also be observed with an Fkh1 R80A mutant. An interaction between Fkh1 and Smc4 could also be detected (data not shown). Similar to Smc2, Smc4 also interacted with Fkh1 R80A, which is deficient for its FHA domain. Interestingly, these data showed that the interaction between Fkh1 and these two condensin subunits does not depend on phosphorylation, but rather on another, yet unknown mechanism.

5 Discussion

5.1 Mating type switching and the regulation of donor preference

Haploid *S. cerevisiae* cells have two mating type alleles: *MATa* and *MATα*. Only one of them is active and determines the mating type of the cell as well as the expression of mating type specific genes[202]. In homothallic strains, haploid cells can switch from one mating type to another via an HO-induced DSB in the *MAT* locus on chromosome III, enabling self-diploidization[110]. In order to conduct the mating type switching, two alleles exist close to each end of chromosome III: *HMLα* and *HMRa*, both harboring a mating type specific sequence (Yα or Ya)[203,204]. Conversion of one mating type to the other is conducted via replacement of the Ya or Yα sequence within the *MAT* locus by using one of the donor loci[205,206]. Surprisingly, the correct donor to repair the break is chosen with an efficiency of 85-90 %[140,141]. This mechanism is described as the regulation of donor preference and serves as a model to study homologous recombination[110]. The high directionality of this regulation was assigned to the cis-acting recombination enhancer, close to *HMLα*[142]. In *MATa* cells, deletion of this sequence results in a loss of specificity to correctly repair the break[142], while *MATα* cells are not affected. Additionally, recent Rad51 ChIP-on-chip experiments, monitoring homology search, performed in our laboratory revealed an early enrichment of Rad51 at sites around the RE upon DSB induction in *MATa* cells, which was abolished upon RE deletion[76]. This might be explained by a loop formed between the RE and the break site, thereby bringing the *HMLα* donor homology close to the *MAT* locus, as suggested in a previous study[157]. It was shown that Fkh1 is involved in this potential loop formation[145], likely by binding directly to the RE. However, the nature of DSB-adjacent components that interact with Fkh1 to establish this loop so far remained enigmatic, just as an answer to the question whether this system could work as a general enhancer of HR also outside the *MAT* system.

In this study, I established a system to study the regulation of donor preference completely independent of the *MAT* system on chromosome III. While inducing a DSB via SceI endonuclease at any genomic position, homology search still probes the endogenous RE on chromosome III. In addition, the RE can also be integrated at different genomic sites and still increases recombination efficiency with nearby donor sites. Importantly, the distance between the RE and a donor site thereby determined recombination efficiency and thus RE function, which can be explained by the random 3-dimensional probing of the homology search, which works efficiently on close-by substrates[207].

By looking at factors contributing to the loop formation between the RE and a DSB, the transcription factor Fkh1 was confirmed to be one major player in the regulation of donor preference, affecting Rad51 nucleoprotein filament probing at the RE. Consequently, Fkh1 also influenced recombination efficiency after a DSB, when a homologous donor site was integrated next to the RE. Especially the phosphothreonine-binding FHA domain of Fkh1 plays an essential role, abolishing the process when mutated to a non-functional version. These data confirm previous studies, which investigated the function of Fkh1's FHA domain in donor preference regulation[157].

Furthermore, a mass spectrometry approach to find phospho-specific interaction partners of Fkh1 revealed a couple of new binding partners, which have not yet been annotated. Among them are very well known factors like RPA and Mph1, which already have been shown to be involved in DNA damage repair pathways[187,192,193,208]. In addition, I also showed that a very recently described factor, Mte1[190,191,209], interacts with Fkh1. Moreover, condensin could be identified as an interaction partner of Fkh1 in this thesis, possibly supporting the stabilization of an RE-DSB loop.

As most of these factors interact with Fkh1 in a phospho-specific manner, various candidate kinases involved in the phosphorylation of relevant factors were analyzed for their contribution to RE function. Among tested candidates, the checkpoint kinase Mec1 had the strongest impact on Rad51 filament probing at the RE.

Altogether, the collected data point towards a more complex regulation of donor preference than assumed. How does the cell manage specific loop formation between the RE and a DSB, when Fkh1 also binds to hundreds of other genomic sites (sections 5.2 and 5.3)? Which mechanisms regulate the interaction between Fkh1 and factors at the break site (section 5.4)? Which factors at the DSB interact with Fkh1 and contribute to the regulation of donor preference (section 5.5)?

In the next sections, I will propose answers to these questions by discussing them in the context of the current literature and presenting a potential mechanistic model.

5.2 The RE as a guide for homology search

One aim of this thesis was to test whether the regulation of donor preference can be completely uncoupled from the *MAT* system. This was achieved via two different means: 1) via integration of the recognition site of either the *MAT*-specific HO or the mitochondrial intron-encoded SceI endonuclease at defined locations in the genome and inducing the break via overexpression of the respective endonuclease. 2) via transplanting the RE to sites different from its natural location and subsequent monitoring of the homology search and recombination with donor sites close by. Regarding the first point I showed that even

with SceI the Rad51 nucleoprotein filament probes at the RE. In conclusion, neither the position of a DSB nor the cutting endonucluease influences regulation of donor preference. In addition, an interaction between the RE and the endonuclease inducing the break can be excluded. In fact, no binding site for HO (or SceI) has been identified within the RE[25]. Recombination efficiency increased after a DSB when an artificially constructed homologous donor site was placed directly downstream of the RE. Regarding the second point, when removed from its endogenous locus and inserted at any other genomic position, the RE still guided homology search. Therefore, no special sequence or chromosomal architecture surrounding the RE on chromosome III seems to be necessary to maintain the function of the RE.

Transplantation of only the left part of the RE, which is defined as the minimal RE[150], guides the homology search and transfers the ability to form a loop and to interact with a DSB to other genomic positions. In detail, integration of the RE at another genomic location guides the Rad51 filament to this position, enabling the interaction of RE-bound Fkh1 with factors binding at the DSB site. Our laboratory clearly showed that homology search spreads along the broken chromosome and the Rad51 enrichment gets diluted with the distance to the DSB[76]. Consistently, when the RE was integrated next to a homologous donor site, recombination efficiency also changed with the variation of the distance between the RE and the donor, thereby decreasing with an increasing RE-donor distance. This was also previously shown within the *MAT* system, when the *HMLα* donor was moved away from the RE on chromosome III[142]. A recent study showed that an RE placed next to a *LEU2* donor site, outside of the *MAT* system on chromosome V, could significantly increase repair efficiency, consistent with my findings[102]. Thus, the RE can be placed in line with other important principles that regulate the recombination efficiency between distant homologies, such as spatial proximity[96] or the length of the homologous donor sequence[102]. However, the increase in recombination efficiency with donor and RE on another chromosome than chromosome III was not as strong as when a donor was integrated at the endogenous RE. A recent publication showed that the conformation of chromosome III is mating type-dependent und controlled by the RE[150]. Other chromosomes are not affected by this mating type specific regulation. The authors could show that the *HMLα* donor is positioned in spatial proximity near the *MAT* locus in *MATa* cells, probably facilitating correct recombination during mating type switching[150]. This effect is lost when the RE is deleted. Therefore, it is possible that the RE-dependent conformation of chromosome III generally influences recombinational events at the RE. A hypothesis could be that the RE transfers flexibility to the left arm of chromosome III, thereby increasing the probability of Rad51 filament probing at the RE and consequently, the formation of a chromosomal loop between the RE and a DSB. As a result, repair

efficiency with a donor next to the endogenous RE would also increase and would be higher compared to an RE-donor system on another chromosome. Homology search is the rate-limiting step during the process of HR. The RE accelerates the homology search via facilitating the probing of the homologous donor sequence and therefore, the recombination with the correct allele during mating type switching. Even in the crowded environment of the nucleus it strongly increases the probability of the probing Rad51 nucleoprotein filament to bind to the correct donor allele.

When I varied the location of a DSB and allowed it to recombine with a donor site on chromosome III, a correlation between the recombination efficiency and the relative distance between DSB and donor was not detected, despite numerous reports showing such a correlation[76,96]. To obtain a correlation between recombination efficiency and the distance between donor and the DSB, two approaches should be used: 1) more DSB and donor sites have to be tested. 2) recombination efficiency has to be investigated not only inter-chromosomally, but also intra-chromosomally. Repair efficiency of inter-chromosomal sites was shown to be low compared to intra-chromosomal recombination[102]. Therefore, further analysis should also include intra-chromosomal DSB and donor sites. Additionally, the distance calculations were based on previously published data analyzing the 3D environment within the static yeast nucleus without DNA damage[30]. Actually, it was shown that upon a DSB the chromosome as well as the DSB mobility increases to facilitate DNA repair[108,109]. Additional chromosomal rearrangements also include the relocalization of DSBs away from heterochromatin[210] or from the nucleolus[97], which was also shown to facilitate repair. Furthermore, another study showed that DNA repair is also supported by movement of the DSB to the nuclear periphery, controlled by the SUMO-targeted ubiquitin ligase Slx5/8[211]. Generally, the DSB repair machinery could benefit from an increased movement to conduct a genome-wide homology search as this also increases the probability for the Rad51 filament to pair with the right donor template[212].

5.3 Fkh1 is essential to RE function

Fkh1 is a transcription factor and was previously shown to be involved in the regulation of donor preference[145,157]. Together with its paralog Fkh2[213], Fkh1 is involved in many cellular processes including transcriptional silencing[174] and cell cycle regulation[172]. My data confirmed the essential role of Fkh1 for the regulation of donor preference. Upon *FKH1* deletion Rad51 did not accumulate at the RE anymore, without influencing ongoing homology search in general. In addition, also RE-associated recombination was deficient in absence of Fkh1. Despite Fkh1 and Fkh2 have overlapping functions and binding

sites[154] and although one Fkh2 binding site was found within the RE[145], an *FKH2* deletion neither affected Rad51 enrichment at the RE nor recombination efficiency, underlining the minuscule function of Fkh2 in donor preference regulation.

As Fkh1 is a transcription factor binding to hundreds of promoter regions[154], the cell has to differentiate between a promoter region and the RE when a DSB is induced. An interaction between the DSB and an Fkh1 binding site such as a promoter region would not be beneficial for the cell and would slow down the process of finding the right donor sequence instead of facilitating it. Indeed, when I integrated promoter regions from two different genes (*KIP2* and *PES4*) next to a homologous donor site, neither of them could increase recombination efficiency as the RE did. What is the difference between an Fkh1-bound promoter region and the RE? Detailed mapping of the RE revealed five well-conserved subdomains, denoted A-E[25,145,147]. Subdomains A, D and E are arrays of Fkh1 binding sites[145,147]. Replacing the entire RE with multimers of one of these subdomains was enough to raise *HMLα* donor usage close to wildtype levels, when a DSB was induced in the *MATa* locus[145]. Binding of Fkh1 to the RE was only detected in *MATa*, but not in *MATα* cells. This is consistent with the fact that the RE is repressed in *MATα* cells by Mcm1 together with Matα2[151] and is not accessible for trans-acting factors like Fkh1. Therefore, it is likely the clustering of Fkh1 binding sites within the RE that allows Fkh1-binding above the required threshold to mediate a stable interaction between a DSB and the RE. To further test this hypothesis, a repetitive array of natural Fkh1 binding sites, such as the *KIP2* or *PES4* promoter, could be integrated into the genome. This array would also offer multiple Fkh1 binding sites, resembling the RE in this function. A donor placed next to this array would then also be used more often due to the enhanced binding of Fkh1 to this site. In addition, one could also investigate this hypothesis by replacing the endogenous RE on chromosome III with one of the Fkh1-bound promoter regions. A potential effect on recombination efficiency with the endogenous *HMLα* locus could then be tested by Fkh1 overexpression. A high Fkh1 expression level could compensate the missing amount of Fkh1 binding sites in the promoter region. In general, probing of the Rad51 filament upon Fkh1 overexpression at Fkh1 binding sites can be tested in a genome-wide assay, as carried out before in our laboratory[76]. An increased Rad51 filament binding to Fkh1-bound regions would also underline that the amount of Fkh1 proteins is critical for loop formation to guide homology search. Importantly, to prove that Fkh1 actually binds to these regions, Fkh1 enrichment at these sites should be investigated.

To show that the cluster of Fkh1 proteins binding to the RE is important for the RE-DSB regulation, I investigated the effect of increased Fkh1 levels on Rad51 filament probing at the RE via overexpression of the protein. In fact, increased Fkh1 levels resulted

in a very strong Rad51 enrichment at the RE. This corroborates my hypothesis that the amount of Fkh1 proteins binding to the RE is the reason why an interaction with the DSB site occurs only with the RE. Fkh1 binds to the RE and interacts with at least one binding partner at the break site, thereby establishing the connection between the RE and a DSB. Increasing amounts of Fkh1 proteins binding at the RE also lead to an increase of available binding sites for factors binding at the break. Fkh1 seems to be the limiting factor in this process. Therefore, the Rad51 nucleoprotein filament probing at the RE also increased with the higher probability of the Rad51 filament to probe the RE for a homologous donor sequence. The question arises why the cell does not further increase Fkh1 expression, as it seems to be beneficial for donor preference regulation. A previous study showed that galactose-induced overexpression of Fkh1 results on the one hand in increased stress resistance and lifespan, but on the other hand vegetative growth is strongly decreased[185]. Therefore, stronger expression levels of Fkh1 could be unfavorable for the cell. Other genes might then also be induced via binding of Fkh1 to their promoter sites. One could approach this hypothesis by measuring transcription levels of genes, whose promoters are bound by Fkh1. Further analysis would then also include investigating the specific effects of this "non-planned" gene expression.

Fkh1, like other proteins of the forkhead family, contains a characteristic FHA domain involved in binding of phosphorylated threonine residues in target proteins[155,175,176]. One well-conserved residue within these domains is an arginine, which lies at position 80 in the amino acid sequence of Fkh1. Mutation of the corresponding residue in the FHA domain of Rad53 abolished the binding of phosphothreonines[177,178]. It seemed obvious that a mutation of R80 would also impair Fkh1's ability to bind target phosphothreonines. In addition, the necessity of this residue and the FHA domain for donor preference regulation could also be tested in this way. When I replaced the *FKH1* gene with a mutant copy, containing the sequence for the R80A mutation, it showed the same effect as an *FKH1* knockout. Thus, abolishing the function of the FHA domain to bind phosphothreonines affects the donor preference mechanism. These results are in line with previously published results by the group of James Haber[157]. Consequently, there must be at least one other factor, which contributes to the loop formation between the RE and a DSB. This factor should be phosphorylated in order to interact with the FHA domain of Fkh1.

5.4 DNA damage response signaling regulates donor preference

I showed that the FHA domain is important for Fkh1's activity in donor preference regulation. FHA domains in general are phosphopeptide recognition domains, with a striking specificity for phosphothreonine residues[177,179]. Mutation of a conserved arginine in this domain completely abolished its function in donor preference regulation. Hence, Fkh1 likely binds a phosphorylated protein at the DSB to mediate loop formation and RE function.

There are two possibilities for the target protein(s) to become phosphorylated: damage-independent or damage-dependent. The first possibility would likely involve a constitutively active protein kinase. Therefore, I wondered if casein kinase 2 (CK2) might be involved in this process. It was previously shown that donor preference partially depends on CK2[157]. As constitutively expressed kinase, CK2 has many target proteins and was shown to be required for cell cycle progression during G1 and G2/M phase in *S. cerevisiae*. In addition, CK2 also promotes DNA repair by phosphorylation of histone H4 after methyl methane sulphonate (MMS)- and phleomycin-induced DSBs[214] as well as after HO-induced DSBs[157]. When I performed Rad51 ChIP experiments with single knockouts of one of the two α subunits of CK2 (Cka1/Cka2), Rad51 enrichment did not change at the RE. Indeed, a single α subunit can compensate the deletion of the other one[181]. To further investigate the influence of CK2 on donor preference, an available temperature-sensitive *CKA2* allele should be used[157]. Another role for CK2 could be that it helps to establish a damage-independent function for the RE. As shown in a recent study, the RE influences the overall structure of chromosome III, even in the absence of DNA damage[150]. CK2 might therefore be the responsible kinase in phosphorylation of factors mediating this conformation. Further studies will identify these CK2 substrates and provide insights how CK2 is involved in donor preference regulation as well as damage-independent, but RE-dependent chromosome III conformation.

In contrast to this damage-independent mechanism, a damage-dependent phosphorylation would likely involve a damage-activated kinase. The two main DNA damage response kinases in yeast are Mec1 and Tel1. Mec1 is the yeast homolog of mammalian ATR kinase and is recruited to DSBs by the recognition of long stretches of RPA-bound ssDNA via its interactor Ddc2[215,216]. Once Mec1 is activated, it phosphorylates a wide variety of substrates[217], giving rise to a global checkpoint response. For my studies it was of interest if the Mec1 kinase activity influences donor preference regulation. A previous study excluded the contribution of Mec1 to this process[157]. However, when I used a strain deleted for *MEC1*, the Rad51 enrichment at and around the DSB remained

unchanged compared to wildtype. Strikingly, the Rad51 enrichment decreased significantly at the RE. I therefore assign a role for Mec1 in donor preference regulation. For Tel1, yeast's homolog of human ataxia-telangiectasia mutated (ATM) kinase, a role in the regulation of donor preference was neither seen in a previous study[157] nor in our laboratory (Claudio Lademann unpublished data). Besides their overlapping substrates, Mec1 seems to be favored over Tel1. This is probably due to the fact that Mec1 is activated and recruited by resected ssDNA (see sections 2.2.2 and 2.2.4)[37]. Resection is a crucial process for HR as well as for mating type switching. Therefore, Mec1 might be better suited for donor preference regulation.

A previous study suggested that donor preference regulation only partially depends on CK2[157], Mec1 might therefore also be involved in phosphorylation of relevant factors for this process. This is also in line with my data that a *MEC1* knockout did not result in complete Rad51 loss at the RE. A strain lacking Mec1 and both CK2 α subunits, supplemented by a previously used temperature-sensitive *CKA2* allele[157], will give further insights into the phosphorylation process affecting donor preference regulation.

5.5 A multi-factorial Fkh1 anchor pad at the DSB contributes to RE function

At the RE, Fkh1 is supposed to be the only binding factor to establish the RE-DSB loop from the RE site. A dimerization can be excluded, because forkhead proteins in general bind DNA as monomers[218] and no internal phosphorylation sites have been reported by now. It was previously assumed that there have to be additional factors binding to Fkh1 to establish the connection between the RE and a DSB[25]. The unbiased mass spectrometry approach that I conducted led to the identification of several interesting Fkh1 interactors potentially involved in RE function. While some of them could not be verified by conventional immunoprecipitation coupled to Western blot, the confirmed interactors could further be sub-classified among damage-dependent and damage-independent binding partners.

As already mentioned above (see section 5.2), it was recently shown that the RE is required for a mating type specific conformation of chromosome III[150], positioning the *HMLα* donor in spatial proximity to the *MAT* locus in *MATa* cells. This conformation is already captured without DNA damage, which might explain the early Rad51 filament probing at the RE after DSB induction shown by our laboratory[76]. However, even in *MATa* cells the *MAT* locus interacts more frequently with *HMRa*[150]. This indicates that the spatial proximity between *MAT* and *HMLα* in *MATa* cells prior to induction of mating type switching might contribute to the selection of correct donor selection, but is not sufficient.

In addition, this special conformation only applies for chromosome III and therefore, damage-dependent factors are required to establish a chromosomal loop by forming a stable tether between the RE and the break site, when both or only one of them are located on different chromosomes. Among those damage-dependent factors falls the Mph1 protein, belonging to the DEAH family of DNA helicases[219]. Mph1 is recruited to DSBs and is involved in the dissociation of Rad51-made D-loops[187]. However, Mph1 did not influence Rad51 filament probing and only had a minor effect when DSB repair efficiency was measured. A recent study identified two closely spaced threonines within the C terminus of Mph1, which were assumed to be phosphorylated and to interact with Fkh1[189]. Mutation of both threonines to alanines abolished the interaction with Fkh1, whereas a single mutation still showed binding to Fkh1[189]. A threonine double mutant resembled an *MPH1* knockout and decreased *HMLα* donor usage by roughly 10 %[189]. Both of these findings are in line with my own data showing that the interaction with Mph1 was lost when a phosphothreonine binding mutant variant of Fkh1 was used and that RE-dependent recombination efficiency is only mildly affected in an *MPH1* knockout strain. Note that the contribution to the donor preference regulation can be uncoupled from the rest of Mph1's activities[189]. Mutation of both relevant threonines did not abolish the helicase activity of Mph1. Vice versa, helicase activity could be stopped and *HMLα* usage was still at wildtype levels as long as the threonines were intact[189]. These data show that Mph1 contributes to the regulation of donor preference, but only plays a minor role.

A mechanism, where more than one protein at the DSB interacts with Fkh1 in order to establish a loop, is very likely. In fact, another factor has recently been identified to be involved in donor preference regulation: Fdo1[189]. With no other reported function by now, an *FDO1* knockout only slightly reduced usage of the *HMLα* donor sequence, when a break was induced in *MATa* cells. A deletion of *FDO1* on top of an *MPH1* knockout showed an additive, but minor effect[189]. These data support my model, whereas Fkh1 interacts with a bundle of proteins to regulate donor preference (Figure 24).

Along this line, one of the top hits in my mass spectrometry data was a protein referred to as Ygr042w, which is meanwhile known as Mte1[190]. By the time I discovered Mte1 as Fkh1 binding partner, the function of the protein was unknown and an interaction with Fkh1 was not annotated in the yeast genome database[220], making it a candidate for donor preference regulation. Interaction between Fkh1 and Mte1 also depended on a functional FHA domain, as Fkh1 R80A did not show any interaction with Mte1 in the mass spectrometry or in the Co-IP experiment. Importantly, in contrast to Mph1 this interaction happened independent of DNA damage induction and therefore, Mte1 is a damage-independent binding partner of Fkh1. Similar to an *MPH1* knockout however, deletion of the sequence coding for Mte1 did only mildly impair recombination efficiency. A knockout

of both *MPH1* and *MTE1* was not additive and only slightly impaired DSB repair efficiency, but did not have an effect on general ongoing homology search represented by Rad51 enrichment at different genomic sites. Mte1 was shown to be an interactor of Mph1, thereby counteracting Mph1's activity in Rad51-made D-loop dissociation and promoting crossover recombination[190,191]. Results of this thesis underline the interaction between Mte1 and Mph1, independently of a DSB. To get a full picture, the target threonines within Mte1 have to be investigated and further research has to be done to understand this new function for Mte1. In summary, Mte1 is another candidate protein potentially contributing to the function of the RE. Yet, also Mph1 and Mte1 together cannot make up for the strong effect of Fkh1, prompting further candidates for the Fkh1 anchor pad at DSBs.

Another interesting candidate in this regard is RPA, which is well-known for its function in DSB repair[70,192,193]. Two of the three subunits of RPA, Rfa1 and Rfa3, were detected in the mass spectrometry experiment, whereas only for Rfa1 an interaction with Fkh1 could be confirmed in a Co-IP assay. Interestingly, the interaction did not change upon DSB induction. It is possible that an interaction between these proteins is generally detected in IP assays independent of DSBs. A single DSB likely leads to posttranslational modifications (see below) only for a small proportion of Rfa1. Therefore, the difference between both time points (before and after DSB induction) is hard to detect. This system could be improved by the induction of multiple breaks, which should increase the amount of posttranslationally modified Rfa1 and should therefore also result in an increased interaction between Fkh1 and Rfa1 upon DSB induction. An important difference to the other Fkh1-binding partners discussed so far however is the partially phosphorylation-independent interaction between both factors, as Rfa1 also showed an interaction with Fkh1 R80A. No phosphothreonines have been identified within Rfa1 and therefore, this needs to be further investigated. One possibility is that the interaction between Fkh1 and Rfa1 does not solely depend on phosphorylation, but also on another mechanism such as SUMOylation. Using a prediction program for SUMO-interaction motifs (SIMs), I could identify two potential SIMs within the FHA domain of Fkh1 (data not shown). Rfa1 is SUMOylated by the SUMO E3 ligase Siz2 and a knockout abolished Rfa1 SUMOylation[221]. However, when I investigated Rad51 filament probing at the RE in a *Δsiz2* strain, no change of Rad51 enrichment at the RE was seen (data not shown). Also a knockout of its paralog, *SIZ1*, did not have an effect (data not shown). At this point it can only be assumed that SUMOylation strengthens the binding of Rfa1 to Fkh1. Further research needs to be done to evaluate this hypothesis. These experiments should then also include SUMOylation-defective variants of Rfa1. A deletion of *RFA1* is not possible, because like the other two RPA subunits, Rfa1 is essential for the *S. cerevisiae* cell[222]. Investigations to the biological relevance of Rfa1 have also relied on hypomorphic alleles.

In terms of donor preference regulation, Rfa1 binds to ssDNA and could act early in the process of the RE-DSB interaction. Indeed, a recent study assigned a role to RPA for the recruitment of the MRX complex, which holds sister chromatids together after a DSB occurred[34]. The authors showed that the interaction between RPA and the MRX complex is essential to keep both sister chromatids and DSB ends together independently of cohesin (see below). Therefore, a mechanism was proposed, where the MRX complex serves as an early structural support holding both sister chromatids together at the DSB[34]. For the regulation of donor preference, Fkh1 could interact with Rfa1 via phosphorylation and SUMOylation and Rfa1 recruits the MRX complex to form an early clamp around the RE and the DSB site. This potential loop would also need to be maintained at later time points in order to keep both sides together.

Different protein complexes could have the competence to fulfill this task. Although not detected as Fkh1 interactor in my mass spectrometry approach or any other large-scale study, the SMC (structural maintenance of chromosomes) complexes are interesting candidates in this respect. SMC complexes include cohesin, condensin as well as the Smc5/6 complex and are conserved from bacteria to humans[195,197]. These ring-shaped complexes encircle DNA in an ATP-driven way, being able to hold more than one strand of DNA together. Among their chromosomal activities, the two most prominent ones are chromosome condensation[223] and sister chromatid cohesion[224]. Furthermore, SMC complexes play an important role in DNA repair[197]. Previous studies already revealed roles for the Smc5/6 complex and cohesin in recombinational DNA repair[225,226], forming a clamp around the broken and the intact DNA strand to complete homologous recombination. In fission yeast *Schizosaccharomyces pombe*, condensin has also been published to play a minor role in DNA repair[227]. Binding to Fkh1 or directly at the RE could therefore be a possible explanation why the RE and a DSB can be kept in spatial proximity during the process of recombination (Figure 24).

While I did not see an interaction of Fkh1 with cohesin or the Smc5/6 complex, I could show that Fkh1 interacts with both large subunits of condensin, Smc2 and Smc4, independently of a DSB. Interestingly, a non-functional FHA domain of Fkh1 did not have any effect on the binding between Fkh1 and Smc2/4. As already mentioned above for Rfa1, SUMOylation could also regulate the Fkh1-condensin interaction. For Smc2 and partially Smc4 SUMOylation was shown to be mediated by the SUMO E3 ligase Mms21[228]. Mms21 is an essential subunit of the Smc5/6 complex[229]. However, when I deleted Mms21's E3 ligase activity, the interaction between Fkh1 and Smc2 remained unaffected (data not shown).

MATa
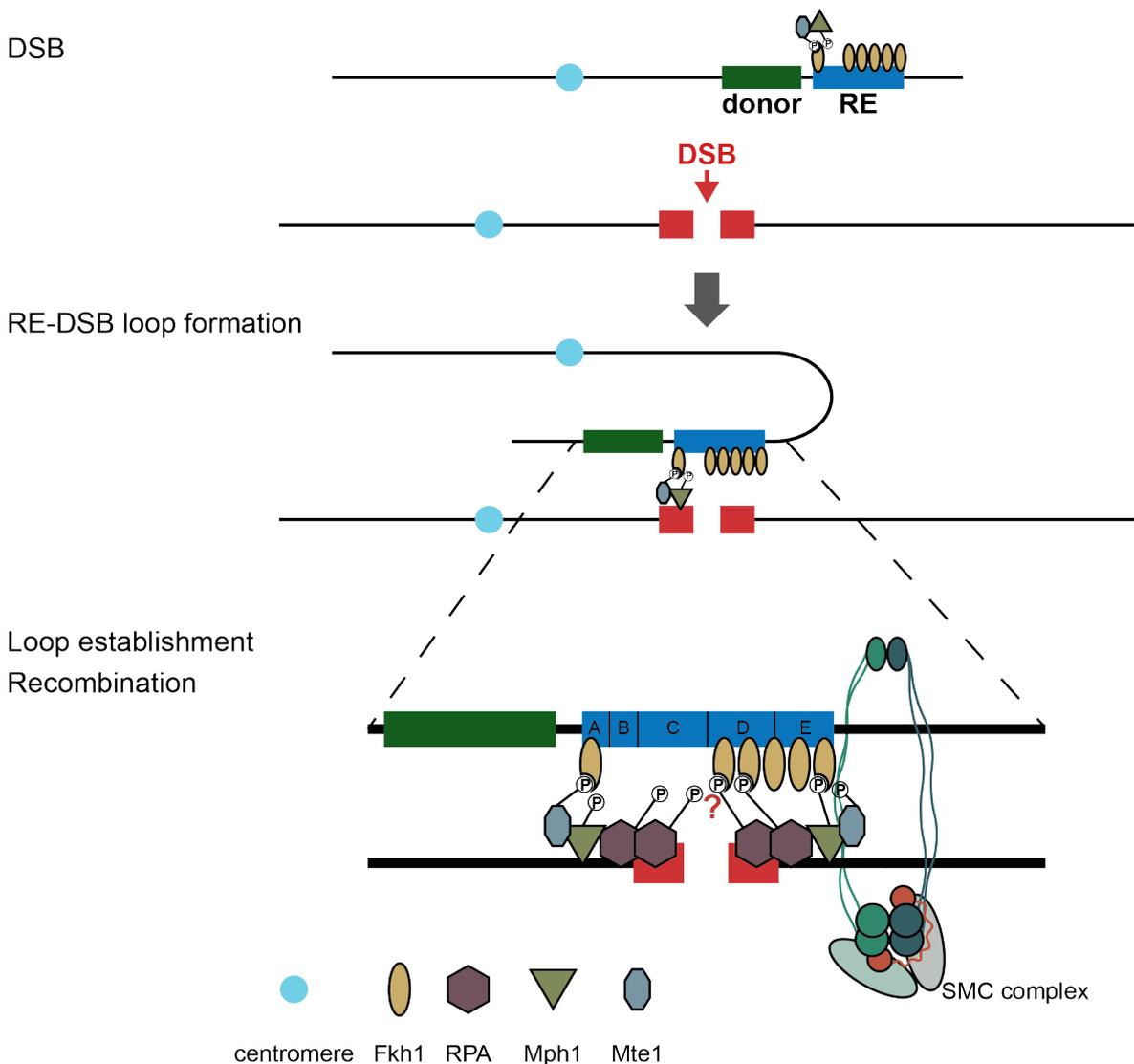
Figure 24 | **General hypothetical model for the regulation of donor preference upon a DSB.**
In _MATa_ cells a DSB is induced at an endogenous locus. The RE was placed next to a donor sequence, homologous to the broken DNA sequence. Fkh1 binds to the RE at multiple binding sites located in RE subdomains A, D and E, leading to clustering of Fkh1. Even in the absence of DNA damage, additional factors like Mte1 bind to Fkh1. Formation of a loop between the RE and the DSB is then induced via interaction of Fkh1 with multiple factors at the break site, thereby bringing the donor sites close to the DSB. Interaction occurs via the FHA domain of Fkh1 and phosphothreonines of binding partners. This mechanism might also regulate the binding of Rfa1 to Fkh1 (red question mark). In addition, an SMC complex binds to both pieces of DNA to maintain the loop. The DSB can now be repaired via homologous recombination with the homologous donor site. Thus the regulation of donor preference requires Fkh1's role at the RE and its interaction with multiple factors at the break site, which together define a DSB. Deletion of any single Fkh1 binding partner only slightly reduces the interaction between the RE and the DSB, resulting in lower recombination efficiency.

A possible explanation could be that the binding of condensin to Fkh1 is mediated by another protein. Generally, condensin is a heteropentameric complex, consisting of two SMC subunits, a Kleisin subunit and two HEAT repeats-containing proteins[197]. All five subunits are essential for chromosome condensation and cell viability[197,230]. The three

non-SMC subunits might also be candidates to contact Fkh1. Therefore, further experiments should include conditional mutants of the condensin subunits or hypomorphic alleles. Although a clear role in DNA repair, especially in HR, has not been reported for condensin by now, the complex may act during the regulation of donor preference, maintaining the loop between the RE and a DSB until recombination is completed. In addition, although an interaction between Fkh1 and cohesin or the Smc5/6 complex was not seen, a role for these complexes cannot be completely excluded in donor preference regulation (Figure 24).

In contrast to the single factor mediating regulation of donor preference at the RE side, Fkh1, multiple factors seem to act at the DSB side to form and establish an RE-DSB loop. Future experiments should test if more factors, which are already involved in DSB repair and especially in HR, also interact with Fkh1.

In summary, the regulation of donor preference is mediated by many factors to ensure successful mating type switching in budding yeast. This study completely uncoupled the function of the RE from mating type switching and shed light on the general function of the RE to guide homology search outside of the *MAT* system. Furthermore, several factors could be identified that contribute to the loop formation between the RE and a DSB. Regulation of donor preference is a more sophisticated mechanism than previously assumed. The future will surely decipher the interplay between all factors involved in loop formation, revealing the bigger picture of donor preference and providing a general model how nuclear architecture influences DNA repair and how this can be applied to the variety of genetic diseases that are linked to HR.

6 Materials and Methods

Unless indicated differently, materials, chemicals and reagents were purchased from Agilent, Becton Dickinson (BD), Biomol, Bioneer, Bio-Rad, Eppendorf, Eurofins Genomics, GE Healthcare, Life Technologies, Merck, Millipore, New England Biolabs (NEB), Promega, Qiagen, Roth, Roche, Sarstedt, Serva, Sigma, Thermo Fisher Scientific or VWR. For all described procedures, sterilized flasks, solutions and de-ionized water were used. Basic microbiological, molecular biological and biochemical techniques followed standard protocols[231,232].

6.1 Microbiology

6.1.1 *Escherichia coli* (*E. coli*) techniques

E. coli strains were cultivated at 37°C, either in liquid LB media or on LB agar plates. Culture density in liquid media was determined photometrically via absorption at 600 nm (OD_{600}).

***E. coli* strains**

Strain	Genotype	Source
DH5α^TM	*F– Φ80lacZΔM15 Δ(lacZYA-argF) U169 recA1 endA1 hsdR17 ($r_{K–,}$ m_{K+}) phoA supE44 λ– thi-1 gyrA96 relA1*	Life Technologies
Mach1^TM **T1**^R	*F⁻Φ80(lacZ)ΔM15 ΔlacX74 hsdR($r_K^- m_K^+$) ΔrecA1398 endA1 tonA*	Life Technologies

***E. coli* media**

LB medium/plates	1 % (w/v) trypton
	0.5 % (w/v) yeast extracts
	1 % (w/v) NaCl
	1.5 % (w/v) agar (only for plates)
	sterilized by autoclaving

For plasmid selection, 100 µg/ml ampicillin were added to media or plates.

Competent *E. coli* cells

Electro-competent *E. coli* cells were prepared by inoculation of 1 l pre-warmed LB medium to an OD_{600} of 0.05 from an overnight culture (commercially available stock was used for this culture). Cells were grown to a final OD_{600} of 0.6-0.8, immediately chilled on ice for 30

min and harvested by centrifugation (2000 g, 10 min, 4°C). The cell pellet was carefully resuspended in 0.5 l of ice-cold water and subsequently washed 4 times with 0.5 l of ice-cold 10 % (v/v) glycerol. After the final washing step with 50 ml of 10 % (v/v) glycerol, bacteria were resuspended in 3 ml 10 % (v/v) glycerol. 50 µl aliquots were frozen in liquid nitrogen and stored at -80°C.

Transformation of *E. coli* cells

E. coli cells were transformed via electroporation. Cells were thawed on ice right before transformation and ~100 ng of plasmid DNA or 10 µl of a dialyzed ligation reaction (see section 6.2.3) added to the cells. The cell-DNA mixture was transferred to pre-cooled electroporation cuvettes (0.1 cm electrode gap; Bio-Rad) and electroporation was carried out by applying a pulse of 1.8 kV and 25 µF at a resistance of 200 Ω using a Gene Pulser X-cell (Bio-Rad). Subsequently after electroporation, 1 ml LB medium was added to the cuvette and the cells were transferred to a 1.5 ml Eppendorf tube and incubated for 30 min at 37°C shaking at 900 rpm. Successfully transformed cells were selected on LB plates containing ampicillin via incubation at 37°C for 12-16 h.

6.1.2 *Saccharomyces cerevisiae* (*S. cerevisiae*) techniques

S. cerevisiae strains were incubated at 30°C either in liquid media or on agar plates. Culture density in liquid media was determined photometrically via absorption at 600 nm (OD_{600}).

S. cerevisiae strains

All yeast strains were isogenic to either JKM179[160] or W303[233]. Strain YCL26 was obtained by crossing YCZ173[234] with W303 *MATα* (Claudio Lademann).

Name	Genotype	Source
JKM179	*Δhml::ADE1, MATα, Δhmr::ADE1, ade1, leu2-3,112 lys5, trp1::hisG', ura3-52, ade3::P$_{GAL}$-HO*	[160]
YCL26	*MATa, ade3::P$_{GAL}$-HO, Δhml::pRS-1 Δhmr::pRS-2*	Claudio Lademann
JoR97	YCL26, *ChrIV$_{491kb}$::HOcs-hphNT1*	[76]
JoR247	*MATα, Δhml::pRS-1 Δhmr::pRS-2, ChrIV$_{491kb}$::SceIcs-kanMX4*	Jörg Renkawitz
BA79	JoR247, *ura3::P$_{GAL}$-SCEI*	This study
BA97	YCL26, *Δade3::natNT2*	This study
BA101	BA97, *ChrIV$_{491kb}$::SceIcs-kanMX4*	This study

BA103	BA97, $ChrIV_{491kb}$::HOcs-hphNT1	This study
BA109	BA101, ura3::P_{GAL}-SCEI	This study
BA120	BA101, ura3::P_{GAL}-HO	This study
BA134	BA97, $ChrXV_{193kb}$::SceIcs-kanMX4	This study
BA146	BA134, ura3::P_{GAL}-SCEI	This study
BA161	BA79, Δmatα2::natNT2	This study
BA172	YCL26, Δade3::URA3	This study
BA174	BA172, URA3 pop out	This study
BA192	BA174, ura3::P_{GAL}-HO	This study
BA193	BA174, ura3::P_{GAL}-SCEI	This study
BA195	BA192, $ChrIV_{491kb}$::HOcs-hphNT1	This study
BA196	BA193, $ChrIV_{491kb}$::SceIcs-hphNT1	This study
BA205	BA195, Δfkh1::natNT2	This study
BA206	BA195, Δfkh2::kanMX4	This study
BA212	BA206, Δfkh1::natNT2	This study
BA248	BA195, $ChrIV_{1148kb}$::RE-natNT2	This study
BA250	BA195, $ChrXIII_{282kb}$::RE-natNT2	This study
BA273	YCL26, $ChrIV_{491kb}$::GFPHOcs-hphNT1	This study
BA278	BA273, $ChrIII_{29kb}$::GFPHOcsmut-kanMX4	This study
BA279	BA273, $ChrIII_{29.4kb}$::GFPHOcsmut-kanMX4	This study
BA280	BA273, $ChrIII_{29.8kb}$::GFPHOcsmut-kanMX4	This study
BA281	BA273, $ChrIII_{30kb}$::GFPHOcsmut-kanMX4	This study
BA282	BA273, $ChrIV_{1148kb}$::GFPHOcsmut-kanMX4	This study
BA283	BA273, $ChrXIII_{282kb}$::GFPHOcsmut-kanMX4	This study
BA285	BA281, Δfkh1::natNT2	This study
BA286	BA282, Δfkh1::natNT2	This study
BA287	BA283, Δfkh1::natNT2	This study
BA293	BA281, Δfkh2::natNT2	This study
BA294	BA282, Δfkh2::natNT2	This study
BA295	BA283, Δfkh2::natNT2	This study
BA298	BA205, pBA34	This study
BA299	BA205, pBA40	This study
BA309	BA285, pBA34	This study
BA310	BA286, pBA34	This study
BA311	BA287, pBA34	This study
BA314	BA285, pBA40	This study
BA315	BA286, pBA40	This study
BA316	BA287, pBA40	This study
BA324	BA285, YCplac111	This study
BA325	BA286, YCplac111	This study
BA326	BA287, YCplac111	This study
BA329	BA281, Δre::c.a.URA3	This study
BA330	BA282, Δre::c.a.URA3	This study
BA331	BA283, Δre::c.a.URA3	This study
BA332	BA285, Δre::c.a.URA3	This study
BA333	BA286, Δre::c.a.URA3	This study
BA334	BA287, Δre::c.a.URA3	This study
BA348	BA282, $RE_{ChrIV\,1148kb}$::natNT2	This study

BA349	BA283, $RE_{ChrXIII\ 283kb}$::*natNT2*	This study
BA374	JoR97, *ura3::P_{GAL}-MATα2*	This study
BA406	JoR97, *fkh1::FKH1-R80A-URA3*	This study
BA407	BA406, *URA3 pop out*	This study
BA412	JoR97, *Δfkh1::kanMX6*	This study
BA415	BA282, $P_{KIP2,\ ChrIV\ 1148\ kb}$::*natNT2*	This study
BA416	BA283, $P_{PES4,\ ChrXIII\ 282\ kb}$::*natNT2*	This study
BA417	BA283, $P_{KIP2,\ ChrXIII\ 282\ kb}$::*natNT2*	This study
BA418	BA282, $P_{PES4,\ ChrIV\ 1148\ kb}$::*natNT2*	This study
BA427	JoR97, *Δmph1::natNT2*	This study
BA428	BA412, *Δmph1::natNT2*	This study
BA429	BA281, *Δmph1::natNT2*	This study
BA430	BA282, *Δmph1::natNT2*	This study
BA431	BA283, *Δmph1::natNT2*	This study
BA432	JoR97, *MPH1-6HA::natNT2*	This study
BA435	JoR97, *FKH1-9Myc::kanMX4*	This study
BA436	BA407, *FKH1-9Myc::kanMX4*	This study
BA440	BA330, $RE_{ChrIV\ 1158kb}$::*natNT2*	This study
BA441	BA330, $RE_{ChrIV\ 1175kb}$::*natNT2*	This study
BA442	BA331, $RE_{ChrXIII\ 290kb}$::*natNT2*	This study
BA443	BA331, $RE_{ChrXIII\ 309kb}$::*natNT2*	This study
BA444	BA331, $RE_{ChrXIII\ 259kb}$::*natNT2*	This study
BA445	BA435, *MPH1-6HA::natNT2*	This study
BA446	BA436, *MPH1-6HA::natNT2*	This study
BA449	JoR97, *ura3::P_{GAL}-MPH1*	This study
BA470	BA427, *Δmte1::kanMX6*	This study
BA472	JoR97, *Δmph1::c.a.URA3*	This study
BA473	JoR97, *MTE1-9Myc::kanMX4*	This study
BA474	BA432, *MTE1-9Myc::kanMX4*	This study
BA475	BA435, *MTE1-6HA::natNT2*	This study
BA477	JoR97, *Δsml1::natNT2*	This study
BA478	JoR97, *Δcka2::natNT2*	This study
BA479	BA477, *Δmec1::c.a.URA3*	This study
BA480	JoR97, *MTE1-6HA::natNT2*	This study
BA481	BA436, *MTE1-6HA::natNT2*	This study
BA484	BA435, *SMC2-6HA::natNT2*	This study
BA487	BA435, *SMC4-6HA::natNT2*	This study
BA492	BA282, *Δmte1::natNT2*	This study
BA493	BA283, *Δmte1::natNT2*	This study
BA495	BA281, *Δmte1::natNT2*	This study
BA496	BA432, *Δmte1::c.a.URA3*	This study
BA497	BA435, *Δmte1::c.a.URA3*	This study
BA498	BA436, *Δmte1::c.a.URA3*	This study
BA499	BA445, *Δmte1::c.a.URA3*	This study
BA500	BA446, *Δmte1::c.a.URA3*	This study
BA501	BA432, *Δfkh1::c.a.URA3*	This study
BA502	BA473, *Δfkh1::c.a.URA3*	This study
BA503	BA474, *Δfkh1::c.a.URA3*	This study

BA504	BA435, *Δmph1::c.a.URA3*	This study
BA505	BA436, *Δmph1::c.a.URA3*	This study
BA506	BA475, *Δmph1::c.a.URA3*	This study
BA507	BA480, *Δmph1::c.a.URA3*	This study
BA508	BA481, *Δmph1::c.a.URA3*	This study
BA509	JoR97, *Δre::natNT2*	This study
BA513	BA436, *SMC4-6HA::natNT2*	This study
BA517	JoR97, *SMC2-6HA::natNT2*	This study
BA520	JoR97, *SMC4-6HA::natNT2*	This study
BA522	BA436, *SMC2-6HA::natNT2*	This study
BA526	BA492, *Δmph1::c.a.URA3*	This study
BA527	BA493, *Δmph1::c.a.URA3*	This study
BA528	BA495, *Δmph1::c.a.URA3*	This study
BA529	BA412, pBA34	This study
BA530	BA412, pBA40	This study
BA536	BA435, *P_{ADH}-3HA-RFA1::natNT2*	This study
BA537	BA436, *P_{ADH}-3HA-RFA1::natNT2*	This study
BA546	JoR97, *Δcka1::natNT2*	This study
BA547	BA479, *Δcka1::kanMX6*	This study
BA548	BA479, *Δcka1::kanMX6*	This study
BA549	JoR97, *Δleft re::natNT2*	This study
BA550	JoR97, *Δright re::natNT2*	This study
BA551	JoR97, *Δtotal re::natNT2*	This study
BA560	BA412, *ura3::P_{GAL}-FKH1*	This study
BA561	BA412, *ura3::P_{GAL}-FKH1 R80A*	This study
BA570	JoR97, *MMS21ΔC terminus::c.a.URA3*	This study

S. cerevisiae vectors

Type	Name (Marker)	Purpose	Source
Centromeric	YCplac111 (*LEU2*)	Expression of protein of interest under *LEU2* marker	[235]
Integrative	YIplac211 (*URA3*)	Expression of protein of interest at the *URA3* locus	[235]

S. cerevisiae plasmids

Name	Plasmid (Marker)	Source
D4135	*pFA6A-HOcs (hphNT1)*	Jörg Renkawitz
D4136	*pFA6A-SceIcs (hphNT1)*	Jörg Renkawitz
pCL1	*YIplac211-P_{GAL}-HO (URA3)*	Claudio Lademann
pCL23	*GFPHOcs (hphNT1)*	Claudio Lademann
pCL24	*GFPHOmut (kanMX6)*	Claudio Lademann
pBA6	*P_{GAL}-SCEI (URA3)*	This study
pBA34	*YCplac111-FKH1, endogenous promoter and terminator (LEU2)*	This study

pBA40	*YCplac111-FKH1 R80A, endogenous promoter and terminator (LEU2)*	This study
pBA52	*pCL1-P_{GAL}-MATα2 (URA3)*	This study
pBA56	*Ylplac211-FKH1 R80A, endogenous promoter and terminator (URA3)*	This study
pBA60	*pCL1-P_{GAL}-MPH1 (URA3)*	This study
pBA134	*pCL1-P_{GAL}-FKH1 (URA3)*	This study
pBA135	*pCL1-P_{GAL}-FKH1 R80A (URA3)*	This study

S. cerevisiae media and buffers

YPD/YP-Gal/YP-Raf	1 % (w/v) yeast extract 2 % (w/v) bacto-peptone 2 % (w/v) carbon source (glucose, galactose, raffinose) 2 % (w/v) agar (only for plates) sterilized by autoclaving
YP-lactate	1 % (w/v) yeast extract 2 % (w/v) bacto-peptone 3 % (w/v) lactic acid adjusted to pH 5.5 with NaOH (ca. 12 g/l final) sterilized by autoclaving
YPD G418/NAT/HYG plates	after autoclaving, YPD medium with 2 % agar was cooled to 50°C and 200 mg/l G418 (geneticine disulfate, PAA Laboratories), 100 mg/l NAT (nourseothricin, HK Jena) or 500 mg/l HYG (hygromycin B, PAA Laboratories) were added.
SC media	0.67 % (w/v) yeast nitrogen base 0.2 % (w/v) amino acid drop out mix (except amino acids selected for auxotrophy markers) 2 % (w/v) glucose 2 % agar (w/v) (only for plates) sterilized by autoclaving
Drop out amino acid mix	20 mg Ade, Ura, Trp, His 30 mg Arg, Tyr, Leu, Lys 50 mg Phe 100 mg Glu, Asp 150 mg Val 200 mg Thr 400 mg Ser

SORB   100 mM LiOAc
                                        10 mM Tris-HCl, pH 8.0
                                        1 mM EDTA, pH 8.0
                                        1 M sorbitol
                                        sterilized by filtration

PEG   100 mM LiOAc
                                        10 mM Tris-HCl, pH 8.0
                                        1 mM EDTA, pH 8.0
                                        40 % (w/v) PEG-3350
                                        sterilized by filtration, stored at 4°C

Storage and cultivation of *S. cerevisiae*

For long-term storage of *S. cerevisiae*, single colonies were inoculated in YPD or the selective SC media for 12-16 h, mixed with 50 % (v/v) glycerol (final concentration 15 %) and frozen at -80°C. Prior to an experiment, cells were freshly streaked out from glycerol stocks onto agar plates using a sterile glass pipette. Single colonies were used to inoculate liquid cultures and grown 12-16 h on a shaking platform (220 rpm). These pre-cultures were then used to inoculate main cultures to an OD_{600} of 0.1. For experiments using YP-lactate, cells had to undergo two sequential pre-culture steps to fully inhibit glucose metabolism. The main cultures were then grown on a shaking platform (110-140 rpm) to mid-log phase (OD_{600} of 0.6-0.8) and further processed according to the experimental protocol.

Preparation of competent *S. cerevisiae* cells

S. cerevisiae cells were grown in a 50 ml YPD culture to mid-log phase and harvested by centrifugation (500 g, 5 min, RT). Cells were washed with 5 ml SORB buffer, finally resuspended in 360 µl SORB buffer and 50 µl carrier DNA (hering sperm DNA, Life Technologies, 10 mg/ml, heat-denatured at 99°C for 10 min) were added. Cells were then either used directly for transformation or stored in 50 µl aliquots at -80°C.

Transformation of *S. cerevisiae* cells

S. cerevisiae cells were transformed via mixing with the respective DNA (for plasmids: 10 µl cells + ~100 ng plasmid DNA, for linearized plasmids: 50 µl cells + ~500 ng DNA, for PCR-amplified DNA: 50 µl cells + 15 µl PCR product (see section 6.2.2)) and 6 volumes of PEG buffer. The cells-DNA mixture was incubated for 30 min at RT, DMSO was then added to a final concentration of 10 % and the cells were heat shocked at 42°C for 10 min in a water bath. Cells were harvested by centrifugation (500 g, 3 min, RT), resuspended in 3 ml of YPD, recovered for 2 h at 30°C under constant shaking (220 rpm; recovery was

only carried out in case of antibiotic selection markers) and then streaked out on plates containing the respective selective media. Selection was carried out via incubation at 30°C for 2-3 days.

Genetic manipulation of *S. cerevisiae*

S. cerevisiae genes were deleted, replaced or tagged using selection cassettes generated by a PCR-based strategy[163,164]. The selection cassettes contained different marker genes (*kanMX4/6, hphNT1, natNT2, c.a.URA3*[236]) and were amplified using gene specific overhangs to integrate them at the endogenous locus, thereby replacing the original gene. Correct integration of the selection cassettes was determined by colony PCR (see below). Chromosomal taggings were additionally confirmed by Western blotting (see section 6.3.1).

Seamless deletions resulted in marker-free integration of genes and cassettes. Therefore, cassettes containing the *URA3* marker were processed as described previously[237]. The chromosomal locus chosen for seamless deletion was replaced by a construct containing the *URA3* ORF, flanked by 50 bp of the endogenous sequence downstream of the integration site. After integration was confirmed by colony PCR, the *URA3* marker was counter-selected on plates containing 5'-Fluoroorotic acid (5'FOA). This results in the deletion of the *URA3* marker via an intra-chromosomal recombination between the 50 bp flanking and the endogenous sequence.

For construction of cassettes bearing an *HO$_{cs}$*, *GFP-HO$_{cs}$* or an *SceI$_{cs}$*, either a 36 bp HO endonuclease recognition sequence (5'-AGTTTCAGCTTTCCGCAACAGTATAATT TTATAAAC-3')[238] or a 30 bp SceI recognition sequence (5'-TTACGCTAGGGATAACAGGGTAATATAGCG-3')[239] was cloned via oligonucleotide annealing (see section 6.2.3) next to a marker gene in the pFA6a backbone (for *HO$_{cs}$* and *SceI$_{cs}$*) or inside the *GFP* ORF of pYM25 (for *GFP-HO$_{cs}$*). This construct was amplified by PCR with site-specific overhangs for the chromosomal integration site. For *GFP-HO$_{csmut}$*, the approach was the same, but using a mutated HO endonuclease recognition site (5'-AGTTTCAGCTTTCCaCAAtAGTATAATTTTATAAAC-3', mutations in lowercase)[165].

Yeast colony PCR

Colony PCR was carried out by dissolving a small toothpick of cells (picked from selective plate) in 20 μl of 20 mM NaOH. Glass beads (0.25-0.5 mm, Roth) were added to the mixture and the samples were incubated at 99°C under constant shaking in a Thermomixer (Eppendorf) for 6 min. Subsequently, the cell debris was pelleted by a quick

spin in a small benchtop centrifuge. 1.6 µl of the supernatant were then taken as template for the PCR reaction (see section 6.2.2).

Induction of single DSBs in vivo

A single and site-specific DSB could be induced by overexpression of either HO or SceI endonuclease under control of the *GAL* promoter[240] in yeast strains harboring an integrated HO or SceI recognition sequence (see above). These strains were grown in YP-lactate medium to avoid repressive effects of glucose metabolism. Cells were grown to mid-log phase (OD_{600} 0.6-0.8) and endonuclease overexpression was induced by the addition of galactose to the YP-lactate medium (final concentration: 2 % (w/v)).

Recombination survival assay

Cells were directly streaked out from glycerol stocks onto YP-Raf plates and incubated for 3 days at 30°C. Afterwards cells were serially diluted to an OD of 10^{-5} and 100 µl or 200 µl were plated onto YPD and YP-Gal plates, respectively. Plates were incubated at 30°C for 3 days and single colonies were counted. The ratio between colonies on YPD and YP-Gal plates was calculated as recombination efficiency.

6.2 Molecular biology techniques

6.2.1 DNA isolation, purification and sequencing

Isolation of plasmid DNA from *E. coli*

Single *E. coli* colonies were inoculated in 5 ml LB supplemented with ampicillin and grown for 12-16 h at 37°C. Cells were harvested and plasmid DNA was isolated using the AccuPrep® Plasmid Mini Extraction Kit (Bioneer) according to the manufacturer's instructions.

Purification of PCR DNA

Linear DNA fragments generated by PCR amplification were purified using the QIAquick PCR purification Kit (Qiagen) according to the manufacturer's instructions.

Purification of DNA fragments from agarose gels

DNA fragments separated via agarose gel electrophoresis were purified using the QIAquick Gel Extraction Kit (Qiagen) according to the manufacturer's instructions.

Isolation of genomic DNA from *S. cerevisiae*

Genomic DNA from *S. cerevisiae* was isolated using the MasterPure™ Yeast DNA Purification Kit (Epicentre) according to the manufacturer's instructions.

Measuring of DNA concentration

DNA concentration of plasmids or genomic DNA was determined photometrically using a NanoDrop ND-1000 spectrophotometer (Thermo Fisher Scientific). The absorbance at a wavelength of 260 nm (OD_{260}) was measured, whereas an OD_{260} of 1 equals a concentration of 50 µg/ml double-stranded DNA.

Separation of DNA fragments by agarose gel electrophoresis

DNA fragments were separated for analytical or preparative purposes via agarose gel electrophoresis. Therefore, 0.5-1.5 % (w/v) gels containing ultra-pure agarose in TBE buffer (89 mM Tris, 89 mM boric acid, 2 mM EDTA), supplemented with ethidium bromide (final concentration 1 µg/ml), were prepared. Ethidium bromide allowed the visualization of the DNA using an UV transilluminator (Raytest). Before loading, DNA samples were mixed with 5 x DNA loading buffer (30 % glycerol, 0.5 % SDS, 25 mM EDTA and bromophenol blue) and electrically separated at 110 volts (12 V/cm) in TBE buffer. Using a standard size marker (1 Kb PLUS DNA Ladder, Life Technologies) running on the same gel, the size of the DNA fragments was estimated.

DNA sequencing

The core facility of the MPI of Biochemistry performed the sequencing analysis of purified plasmid DNA or PCR products using an ABI 3730 DNA analyzer (Applied Biosystems) and ABI Big Dye 3.1 sequencing chemistry. Otherwise, samples were also sequenced as value reads by Eurofins Genomics.

6.2.2 Polymerase Chain Reaction (PCR)

PCR was used to amplify DNA fragments from genomic and plasmid DNA for cloning, amplification of targeting cassettes for chromosomal integration as well as epitope tagging, to test for genomic recombination events and to analyze ChIP experiments via quantitative real-time PCR.

Amplification of genomic and plasmid DNA fragments

For the amplification of genomic or plasmid DNA the Phusion® High-Fidelity DNA Polymerase (NEB) was used. The final reaction volume of 50 µl consisted of 200 ng DNA, 0.6 µM of each primer, 0.8 mM dNTP mix, 1 x Phusion HF buffer and 2 units Phusion polymerase. For amplification, a Veriti® Thermal Cycler (Applied Biosystems) and the following PCR program were used: 1 min initial denaturation step at 98°C, followed by 30 cycles of 20 s 98°C denaturation, 20 s 55°C primer annealing and an elongation step at 72°C adjusted to the length of the desired DNA fragment (15 s/kb for plasmid DNA, 30 s/kb for genomic DNA plus additional 20 s). Final extension was carried out for 10 min at 72°C, samples were subsequently stored at 4°C or -20°C.

Amplification of marker cassettes for genomic integration

Marker cassettes were amplified using a mixture of Taq (made in-house by the MPI core facility) and Vent® polymerase (NEB) as described previously[163,164]. The PCR program was not adjusted for natNT2 marker cassettes.

Amplification of DNA for yeast colony PCR

Yeast colony PCR was performed to test for correct genomic integration of marker cassettes and epitope tagging. The DNA template was generated as described above and amplified using the Taq polymerase (made in-house by the MPI core facility). Alternatively, mi-Taq only polymerase (Metabion) was used. A 20 µl reaction consisted of 1.6 µl template DNA, 0.64 µM of each primer, 1.4 mM dNTP mix, 1 x ThermoPol Reaction Buffer (NEB) or 1 x Complete mi-Taq reaction buffer (Metabion) and 2 units of Taq or mi-Taq only polymerase. Amplification was carried out in a Veriti® Thermal Cycler (Applied Biosystems) with initial denaturation at 94°C for 5 min, followed by 30 cycles of 30 s 94°C denaturation, 30 s 55°C primer annealing and an elongation step adjusted to the length of the DNA product (60 s/kb) at 72°C. Final extension lasted 5 min at 72°C, samples were subsequently stored at 4°C or -20°C.

Quantitative real-time PCR (qPCR)

For quantitative real-time PCR (qPCR), the LightCycler 480 system (Roche) was used. For ChIP experiments (see section 6.3.2) the SYBR Green-based mixture consisted of the KAPA SYBR® FAST qPCR Kit (KAPA Biosystems, "KAPA Mix"). The qPCR reaction mix contained 2 µl of the ChIP (non-diluted) or input DNA (1:10 diluted), 10 µl of the KAPA mix and 0.2 µM of each primer. Reactions were performed in technical triplicates in 384-well

plates (Roche) and pipetted by a CAS-1200 PCR setup robot (Corbett Lifescience). The PCR program contained an initial denaturation step for 3 min 95°C, followed by 40 amplification/detection cycles with 10 s 95°C denaturation, 20 s 57°C primer annealing and 1 s 72°C elongation. Melting curve analysis was performed for 5 s 95°C, 1 min 65°C, followed by an increase from 65°C to 97°C, with 0.11°C/s and 5 acquisitions/°C. Samples were then cooled down to 4°C. PCR reaction was followed by a quantification using the "second-derivative maximum" method of the LightCycler 480 software. The relative concentrations of the template DNA was determined by fitting these calculated values with a primer-specific standard curve, generated by a dilution series of one input sample (1:5, 1:50, 1:500 and 1:5000 dilution) measured with each primer pair. Those samples showing multiple products in the melting curve analysis at the end of the amplification or clear differences within the technical triplicates were removed from the analysis as quality control. The IP/input ratios were calculated and normalized to the IP/input ratios of a control primer pair on chromosome X (see table qPCR primer).

qPCR primer

Name	Sequence	Genomic position	Usage
BA050	GACTGTCAAGGAGGGTATTCTG	Marker cassette	DSB induction
BA069	CAATGGACGAGGAAACAAGAGCGATT	ChrIV_509kb	ChIP filament
BA070	ACCATACCAGACCTTTTCCAGTCTGT	ChrIV_509kb	ChIP filament
BA160	TGACCATCCGACAAATAGTTCCCTCA	ChrIV_491kb	ChIP DSB
BA161	CCGCGGAACAATATTTGAAATCGTGAA	ChrIV_491kb	ChIP DSB
BA175	GAAGATACATGGAAACCGTCTCTGG	ChrXII_498kb	DSB induction
BA178	CGTGTTTGCATCAATCAACACGTCA	ChrXII_498kb	ChIP DSB
BA179	ACTATTGAAAACGGACAATTTCCTGGGC	ChrXII_498kb	ChIP DSB
BA220	CAGTAGCTGCTTCTACAGTGGCTCTT	ChrXV_193kb	ChIP DSB
BA221	CCTATTTCATCTCTCAAGGCCCACCC	ChrXV_193kb	ChIP DSB
BA222	CGATTAATTCAGTGGCCACATCACC	ChrXV_193kb	DSB induction
BA223	GCTTTTACGCAGGGCAATTTCGGG	ChrXIII_282kb	ChIP DSB
BA224	ACAAGCGCAGGTTAATAAAGGGTTCT	ChrXIII_282kb	ChIP DSB
BA226	GCAATTGCAGCCCCAATAAATCCAAC	ChrIV_1148kb	ChIP DSB
BA227	TTCGATGCAGGCATCTACGTTTTGAC	ChrIV_1148kb	ChIP DSB
BA228	GTCCAAATACTAGTATGCAGCAATTG	ChrIV_1148kb	DSB induction
BA414	GACGTTGTTCGACAGAACGGATTGAT	ChrXIII_339kb	ChIP DSB
BA415	GGATACAAAAGGACGCTCAAGCAGAC	ChrXIII_339kb	ChIP DSB
BA658	ATTGTTGTTGCGTAGTTCGACGGTAG	ChrIV_742kb	ChIP DSB
BA659	ATCAACAACGAGGTGGAAGTACTGGT	ChrIV_742kb	ChIP DSB
BA660	GCATGCTCGGTAGAGGTTTCGAATTT	ChrVII_110kb	ChIP DSB
BA661	ACAGAGGGTTCGAAGGAAAACAGGAA	ChrVII_110kb	ChIP DSB
BA662	ATGAAAAGGTTAAACCGCAGATCCCG	ChrXIII_209kb	ChIP DSB
BA663	GCTATAGATGGGGAAGATGAGGGACG	ChrXIII_209kb	ChIP DSB
CL279	CTCTAACGCCACGGTCATGAAGAA	ChrIV_451kb	ChIP filament
CL280	TCCTAACGGTCTCGGTATTCCTCC	ChrIV_451kb	ChIP filament

JoR138	CTTTTCGTGTTCTAGCGTGTTCAC	ChrIII_29kb	ChIP filament
JoR139	CTATCCAAAACCCTGGGCAA	ChrIII_29kb	ChIP filament
JoR161	CGCCATTTGGGTGTAAAATCG	ChrIII_28kb	ChIP filament
JoR162	GGAAACCTGGTTTGGAGATCAATC	ChrIII_28kb	ChIP filament
JoR163	ATTGTTCCAATGAAGCCGATG	ChrIII_31kb	ChIP filament
JoR164	GTTCACCACCAAATTTTCGACG	ChrIII_31kb	ChIP filament
JoR187	GCGTGCCTGGTCACAGGTTCATACGAC	ChrX_207kb	Standard control
JoR188	TCATACGGCCCAAATATTTACGTCCC	ChrX_207kb	Standard control
JoR330	AGGGCCAACACCTAGTCCAA	ChrIV_496kb	ChIP filament
JoR331	AGGCGAAGTTAGTGCTGAACA	ChrIV_496kb	ChIP filament

6.2.3 Molecular Cloning

Restriction digest

Digestion of DNA was performed using site-specific restriction enzymes (NEB) according to the manufacturer's instructions. In brief, ~1.5 µg of plasmid DNA or 30 µl of a purified PCR reaction were mixed with the desired restriction enzymes and the recommended buffer to give a total volume of 30 µl. The reaction mixture was incubated for 2 h at 37°C and subsequently purified via column-based purification.

De-phosphorylation of linearized plasmid DNA

Plasmid vectors used for cloning were digested as mentioned above. The de-phosphorylation of the free 5'-ends of the linearized and purified vector backbone DNA (~1.5 µg) was performed with 2 units of rAPid Alkaline Phosphatase (Roche) in the provided reaction buffer for 1 h at 37°C. The Alkaline Phosphatase was then heat-inactivated at 75°C for 5 min. The vector backbone was then used for the ligation reaction.

Oligonucleotide annealing

DNA inserts with less than 120 bp were generated using oligonucleotide annealing instead of PCR amplification. Complementary oligonucleotides were designed with overhangs specific to the favored restriction enzyme and dissolved to reach a concentration of 100 µM in 50 mM Tris-HCl (pH 8.0), 100 mM NaCl and 1 mM EDTA. Annealing was carried out by mixing 10 µl of each oligonucleotide and incubation in a PCR reaction tube, denaturation at 95°C for 90 s, followed by a gradual decrease of the temperature at a rate of 1°C per 20 s until 4°C was reached (Veriti[®] Thermal Cycler, Applied Biosystems). 2 µl of the reaction were used as insert for the ligation reaction.

DNA ligation

DNA ligation was performed in a total volume of 20 µl, containing linearized and de-phosphorylated vector DNA and digested PCR product in a ratio of 1:4, 1 x T4 DNA ligase buffer and 400 units of T4 DNA ligase (NEB). The reaction mix was incubated at RT for 20 min, followed by 10 min at 65°C to heat-inactivate the ligase. The ligation mixture was then dialyzed for 20 min against de-ionized water using a nitrocellulose filter (pore size 0.05 µm). 8 µl were used to transform electro-competent *E. coli* cells.

Gibson cloning

For some constructs, ligation did not give the desired results. Therefore, Gibson cloning was performed[241]. Briefly, the vector backbone was linearized and de-phosphorylated as described above. For the insert, primer pairs were designed with overhangs to the desired vector backbone including the restriction sites. The PCR was purified via column-based purification. Restriction digest was not performed. Instead, the vector backbone and the PCR product were mixed in a ratio of 1:5 in a total volume of 5 µl. Then 5 µl of Gibson Assembly® Master Mix (NEB) were added and the mixture was incubated for 45 min at 50°C in a Thermomixer (Eppendorf) without shaking. Afterwards the mixture was diluted 1:4 with water and dialyzed against de-ionized water (see above). 20 µl of the reaction mix was then used for transformation of electro-competent *E. coli*.

Site-directed mutagenesis

Specific mutations could be introduced into plasmid DNA using the PCR-based QuikChange® Site-Directed Mutagenesis Kit (Agilent Technologies). Complementary oligonucleotides were designed with 20-25 bp flanking each side of the mutation. For PCR reaction, PfuTurbo polymerase (Agilent technologies) and 10 ng of input DNA were used. Directly after the reaction, Dam-methylated and non-mutagenized input DNA was removed by the addition of 10 units of the DpnI restriction endonuclease (NEB) and incubation for 2 h at 37°C. Column-based purification was then followed by dialysis as described above. 8 µl of the reaction were used to transform electro-competent *E. coli* cells. Purified plasmid DNA was analyzed by DNA sequencing to verify the desired mutated site.

6.3 Biochemical and cell biological techniques

6.3.1 Protein methods

General buffers and solutions

HU sample buffer

$\qquad$ 200 mM Tris-HCl, pH 6.8

8 M urea

5 % (w/v) SDS

1 mM EDTA

0.1 % (w/v) bromophenol blue

100 mM DTT (freshly added before use)

MOPS running buffer

$\qquad$ 50 mM MOPS

50 mM Tris base

3.5 mM SDS

1 mM EDTA

Blotting buffer (self-made)

$\qquad$ 250 mM Tris base

1.92 M glycine

0.1 % (w/v) SDS

20 % (v/v) methanol

Swift blotting buffer

$\qquad$ 5 % (v/v) 20 x Swift buffer (G-Bioscience)

10 % (v/v) Methanol

TBS-T solution

$\qquad$ 25 mM Tris-HCl, pH 7.5

137 mM NaCl

2.6 mM KCl

0.1 % (v/v) Tween 20

PBS

$\qquad$ 10 mM phosphate, pH 7.4

137 mM NaCl

2.7 mM KCl

IP lysis buffer

$\qquad$ 10 % (v/v) glycerol

1 x PBS

0.5 % NP-40

1 mM NEM (freshly added before use)

IP wash buffer

$\qquad$ 10 % (v/v) glycerol

1 x PBS

0.5 % NP-40

Preparation of denatured protein extracts (TCA precipitation)

Denatured protein extracts were generated by harvesting a cell amount corresponding to one OD_{600} via centrifugation (3500 g, 3 min, RT). The supernatant was discarded and the

cell pellet was resuspended in 1 ml of ice-cold water. 150 µl of 1.85 M NaOH/7.5 % β-mercaptoethanol (β-ME) were added and the mixture was incubated for 15 min on ice. Protein precipitation was performed by addition of 150 µl 55 % cold TCA (trichloroacetic acid) and incubation for 10 min on ice, followed by a centrifugation step for 10 min at 20000 g, 4°C. TCA supernatant was completely removed and the protein pellet was resuspended in 100 µl HU buffer. Samples were incubated for 10 min at 65°C under constant shaking (1400 rpm, Thermomixer, Eppendorf) prior to SDS-PAGE analysis.

SDS-polyacrylamide gel electrophoresis (SDS-PAGE)

Protein samples in HU buffer were loaded on pre-cast 4-12 % NuPage Bis-Tris gels (Thermo Fisher Scientific). Gel electrophoresis was carried out in MOPS buffer at a constant voltage of 120 V for 2 h. Size of the protein samples was compared to the standard size marker Precision Plus Protein All Blue Standard (Bio-Rad) loaded on the same gel.

Western blot analysis

Proteins separated by SDS-PAGE were subsequently transferred to polyvinylidene fluoride (PVDF) membranes (Immobilon-P, Millipore) and blotting was performed via wet blotting in an electric tank blotter (Hoefer) at a constant voltage of 75 V for 2 h at 4°C. Efficient Western blotting was determined by transfer of the standard size marker. Afterwards, membranes were blocked in TBS-T + 5 % milk powder at RT for 20-30 min, followed by incubation with the respective antibody (see table "antibodies" below) diluted in TBS-T + 5 % milk powder overnight at 4°C or for 3 h at RT. Subsequently, membranes were washed 3 times with TBS-T for 10 min. The secondary antibody (Dianova), coupled to horseradish peroxidase (HRP), was diluted in TBS-T + 5 % milk powder, added to the membranes and incubated for 1 h at RT. After 3 washing steps with TBS-T (each 10 min), signal detection was performed with chemiluminescence kits ECL or ECL-plus (GE Healthcare) and exposure of the membranes to chemiluminescence sensitive films (Amersham Hyperfilms ECL, GE Healthcare). Exposure times were varied and the films were developed. If needed, membranes were stripped with a Restore™ PLUS Western Blot Stripping Buffer (Thermo Fisher Scientific) for 10-15 min at RT, then washed 3 times with TBS-T and blocked with TBS-T + 5 % milk powder for 20-30 min and a new primary antibody was added.

Determination of protein interactions by immunoprecipitation (IP)

For immunoprecipitation (IP) experiments 200 OD_{600} of yeast cells were harvested from cultures at desired time points, washed once with ice-cold PBS and transferred to 2 ml reaction tubes. The cell pellets were either snap-frozen in liquid nitrogen and stored at -80°C or 800 µl of IP lysis buffer, freshly supplemented with 1 mM NEM and a protease inhibitor mix (1 x EDTA-free complete cocktail, Roche), was added to the cell pellets. An equal volume of Zirconia/Silica beads (BioSpec, Inc.) was added and lysis was performed at 4°C in a bead-beater (MM301, Retsch GmbH) in 6 intervals of 1 min shaking (frequency 30/s) and 5 min pausing for cool-down. Samples were separated from the beads via piggyback elution and collected in fresh tubes. For Benzonase treatment, cells were incubated with 500 units of Benzonase (Sigma), supplemented with 2 mM $MgCl_2$, for 15 min at 4°C on a rotating wheel. Cell debris was pelleted in a benchtop centrifuge for 5 min, 2600 g, 4°C. For pre-clearing, the supernatant was transferred to fresh tubes and 30 µl of pre-swollen Protein A Sepharose CL-4B (GE Healthcare) slurry, washed twice (500 g, 2 min, 4°C) with 500 µl IP lysis buffer, were added. The mixture was incubated for 30-60 min at 4°C on a rotating wheel and beads were then pelleted at 500 g, 2 min, 4°C. 5 µl of the lysate were taken as input and mixed with 30-40 µl of HU buffer prior to a denaturing step at 65°C for 10 min. 800 µl of the lysate were transferred to fresh tubes, the antibody (see table below) was added and incubated for 60 min at 4°C on a rotating wheel, followed by addition of 30 µl of pre-swollen Protein A Sepharose CL-4B slurry and further incubated at 4°C for 30-60 min. Next, the beads were pelleted by centrifugation (100 g, 2 min, 4°C) and washed three times with 600 µl IP wash buffer. For the last washing step, the IP samples were transferred to fresh tubes. The remaining buffer was aspirated, 30-40 µl of HU buffer was added to the IPs and the samples were denatured for 10 min at 65°C (see above). Input and IP samples were then stored at -20°C or subsequently analyzed by SDS-PAGE and Western blot analysis (see above).

Antibodies

Antibody	Type	Use	Source
Myc (9E10)	primary (mouse IgG)	IP (4 µl)	Sigma
c-Myc (A-14)	primary (rabbit IgG)	Western (1:2500)	Santa Cruz
HA	primary (mouse IgG)	Western (1:1000)	Santa Cruz
HRP-coupled α-mouse	secondary (goat IgG)	Western (1:5000)	Dianova
HRP-coupled α-rabbit	secondary (goat IgG)	Western (1:5000)	Dianova
Pgk1	primary (mouse IgG)	Western (1:5000)	Thermo Fisher
Rad51 (y-180)	primary (rabbit IgG)	ChIP (4 µl)	Santa Cruz
RPA (RFA)	primary (rabbit IgG)	ChIP (1.5 µl)	Agrisera

6.3.2 Chromatin immunoprecipitation (ChIP)

Buffers and solutions

FA lysis buffer	50 mM Hepes-KOH, pH 7.5
	150 mM NaCl
	1 mM EDTA
	1 % (v/v) Triton X-100
	0.1 % (w/v) Deoxycholic acid, Na-salt
	0.1 % (w/v) SDS
FA lysis buffer 500 (high salt)	50 mM Hepes-KOH, pH 7.5
	500 mM NaCl
	1 mM EDTA
	1 % (v/v) Triton X-100
	0.1 % (w/v) Deoxycholic acid, Na-salt
	0.1 % (w/v) SDS
ChIP wash buffer	10 mM Tris-HCl, pH 8
	250 mM LiCl
	1 mM EDTA
	0.5 % (v/v) NP-40
	0.5 % (w/v) Deoxycholic acid, Na-salt
TE	10 mM Tris-HCl, pH 8
	1 mM EDTA
ChIP elution buffer	50 mM Tris-HCl, pH 7.5
	10 mM EDTA
	1 % (w/v) SDS

Chromatin immunoprecipitation (ChIP)

The procedure of chromatin immunoprecipitation (ChIP) was already previously described[76,242]. In this study, formaldehyde (37 % solution, Roth) was added to 200 ml cultures resulting in a final concentration of 1 % (v/v). Crosslinking was carried out for 16 min at RT shaking at 130 rpm, followed by termination via addition of 2.5 M glycine (final concentration 375 mM). The crosslinked cultures were kept shaking for at least 20 min and 180 OD_{600} were harvested by centrifugation (3500 g, 5 min, 4°C). The cells were washed once with ice-cold PBS and transferred to a 2 ml reaction tube. Cell pellets were subsequently snap-frozen in liquid nitrogen and stored at -80°C for further processing. For cell lysis, pellets were thawed on ice and 800 µl of FA lysis buffer, freshly supplemented with protease inhibitors (1 x EDTA-free complete cocktail and 1 mg/ml Pefabloc SC, Roche), were added. An equal volume of Zirconia/Silica beads (BioSpec Inc.) was added and lysis was carried out at 4°C in a bead-beater (MM301, Retsch GmbH) in 6 intervals of

3 min shaking (frequency 30/s) with cool-downs of 3 min. Subsequently, the lysate was transferred to a fresh tube via piggyback elution and pelleted at 20000 g for 15 min at 4°C. The supernatant was discarded and the pellet was resuspended in 900 µl of FA lysis buffer and transferred to hard plastic TPX tubes (Diagenode). Then, chromatin was sheared in a water/ice bath by sonication in a Bioruptor UCD-200 sonication system (Diagenode). 40 cycles were conducted with an output of 200 W and 30 s/cycle with a 30 s break to shear the DNA to an average length of 250-500 bp. After 10 cycles, 200 ml of water were exchanged for an equal amount of ice to cool the samples during the sonication. Subsequently, 1.1 ml of FA lysis buffer were added to the sheared chromatin samples and cell debris pelleted via centrifugation (6150 g, 30 min, 4°C). 20 µl of the chromatin lysate were taken as input reference and 800 µl of the lysate were used for IP. The lysate was incubated with the primary antibody of choice (see table "antibodies" in section 6.3.1) for 1.5 h at RT on a rotating wheel, followed by addition of 100 µl of pre-swollen Protein A Sepharose CL-4B (GE Healthcare) slurry and further incubation for 30 min. For washing, the beads were pellet by centrifugation (150 g, 1 min, RT) and the supernatant was removed via aspiration. The beads were then washed 4 times with 400 µl FA lysis buffer and once with FA lysis buffer 500, ChIP wash buffer and TE. After final aspiration, 110 µl of ChIP elution buffer were added to elute the IP material from the beads. The samples were incubated for 10 min at 65°C under constant shaking (1400 rpm) in a Thermomixer (Eppendorf). In a final centrifugation step (8000 g, 2 min, RT), the beads were pelleted and 100 µl of the IP was transferred to a fresh 0.5 ml reaction tube. Digestion with Proteinase K (Sigma, final concentration 2 mg/ml) was performed in a total volume of 200 µl with a final SDS concentration of 0.5 % for 2 h at 42°C, followed by reversal of the cross-links via incubation at 65°C for 8 h. Final purification was carried out with the QIAquick PCR purification kit (Qiagen), whereas the DNA samples were eluted in 100 µl of EB buffer. Afterwards, samples were used for qPCR (see section 6.2.2).

6.4 Bioinformatics

6.4.1 General Bioinformatics

Literature research and work was performed using databases related to the National Center of Biotechnology Information (www.ncbi.nlm.nih.gov) and Papers2 (http://papersapp.com/mac/).

For information about *S. cerevisiae* genomic sequences and proteins the Saccharomyces Genome Database (www.yeastgenome.org) was used[220]. Analysis and

manipulation of DNA sequences was performed using DNASTAR software (DNA Star Inc.).

Statistical evaluation and representation were carried out with GraphPad Prism (www.graphpad.com/scientific-software/prism/). Western blots were level- and contrast-adjusted as well as cropped using Adobe Photoshop (Adobe Systems Inc.)

Figures were designed, labeled and arranged using Adobe Illustrator software (Adobe System Inc.). For general text and table generation, the Microsoft Office software package (Microsoft Corp.) was used.

6.4.2 Calculation of the distance between two genomic sites

The distance between two genomic loci was calculated based on data obtained from 3D modeling of the *S. cerevisiae* genome[98]. The formula to calculate the distance was as follows:

Distance between two loci = $\sqrt{(x1 - x2)^2 + (y1 - y2)^2 + (z1 - z2)^2}$

x1/y1/z1 corresponds to the coordinates of one locus, x2/y2/z2 of the other locus

7 References

1. Lindahl, T. Instability and decay of the primary structure of DNA. *Nature* **362,** 709–715 (1993).
2. Branzei, D. & Foiani, M. Maintaining genome stability at the replication fork. *Nat. Rev. Mol. Cell Biol.* **11,** 208–219 (2010).
3. Kim, N. & Jinks-Robertson, S. Transcription as a source of genome instability. *Nat. Rev. Genet.* **13,** 204–214 (2012).
4. Lindahl, T. The Croonian Lecture, 1996: endogenous damage to DNA. *Philosophical transactions of the Royal Society of London. Series B, Biological sciences* **351,** 1529–1538 (1996).
5. Hoeijmakers, J. H. J. DNA damage, aging, and cancer. *N. Engl. J. Med.* **361,** 1475–1485 (2009).
6. Lindahl, T. The Intrinsic Fragility of DNA (Nobel Lecture). *Angew. Chem. Int. Ed. Engl.* **55,** 8528–8534 (2016).
7. Friedberg, E. C. DNA damage and repair. *Nature* **421,** 436–440 (2003).
8. Aguilera, A. & Gómez-González, B. Genome instability: a mechanistic view of its causes and consequences. *Nat. Rev. Genet.* **9,** 204–217 (2008).
9. Barnes, D. E. & Lindahl, T. Repair and genetic consequences of endogenous DNA base damage in mammalian cells. *Annu. Rev. Genet.* **38,** 445–476 (2004).
10. San Filippo, J. & Sung, P. Mechanism of eukaryotic homologous recombination. *Nature* **467,** 108–111 (2008).
11. Hoeijmakers, J. H. Genome maintenance mechanisms for preventing cancer. *Nature* **411,** 366–374 (2001).
12. Mehta, A. & Haber, J. E. Sources of DNA Double-Strand Breaks and Models of Recombinational DNA Repair. *Cold Spring Harb Perspect Biol* **6,** (2014).
13. Thompson, L. H. Recognition, signaling, and repair of DNA double-strand breaks produced by ionizing radiation in mammalian cells: The molecular choreography. *Mutat. Res.* **751,** 158–246 (2012).
14. Lomax, M. E., Folkes, L. K. & O'Neill, P. Biological Consequences of Radiation-induced DNA Damage: Relevance to Radiotherapy. *Clin Oncol (R Coll Radiol)* **25,** 578–585 (2013).
15. Champoux, J. J. DNA topoisomerases: Structure, function, and mechanism. *Annual Review of Biochemistry* **70,** 369–413 (2001).
16. Milligan, J. R. *et al.* Dna-Repair by Thiols in Air Shows 2 Radicals Make a Double-Strand Break. *Radiat. Res.* **143,** 273–280 (1995).
17. Ma, W., Halweg, C. J., Menendez, D. & Resnick, M. A. Differential effects of poly(ADP-ribose) polymerase inhibition on DNA break repair in human cells are revealed with Epstein-Barr virus. *Proc. Natl. Acad. Sci. U.S.A.* **109,** 6590–6595 (2012).
18. Vilenchik, M. M. & Knudson, A. G. Endogenous DNA double-strand breaks: production, fidelity of repair, and induction of cancer. *Proc. Natl. Acad. Sci. U.S.A.* **100,** 12871–12876 (2003).
19. Bennett, C. B., Lewis, A. L., Baldwin, K. K. & Resnick, M. A. Lethality Induced by a Single Site-Specific Double-Strand Break in a Dispensable Yeast Plasmid. *Proc. Natl. Acad. Sci. U.S.A.* **90,** 5613–5617 (1993).
20. Huang, L. C., Clarkin, K. C. & Wahl, G. M. Sensitivity and selectivity of the DNA damage sensor responsible for activating p53-dependent G(1) arrest. *Proc. Natl. Acad. Sci. U.S.A.* **93,** 4827–4832 (1996).
21. Berti, M. & Vindigni, A. Replication stress: getting back on track. *Nat. Struct. Mol. Biol.* **23,** 103–109 (2016).
22. Helleday, T., Petermann, E., Lundin, C., Hodgson, B. & Sharma, R. A. DNA repair pathways as targets for cancer therapy. *Nat. Rev. Cancer* **8,** 193–204 (2008).
23. de Massy, B. Initiation of Meiotic Recombination: How and Where? Conservation

and Specificities Among Eukaryotes. *Annu. Rev. Genet.* **47,** 563–599 (2013).

24. Keeney, S., Giroux, C. N. & Kleckner, N. Meiosis-specific DNA double-strand breaks are catalyzed by Spo11, a member of a widely conserved protein family. *Cell* **88,** 375–384 (1997).

25. Haber, J. E. Mating-type genes and MAT switching in Saccharomyces cerevisiae. *Genetics* **191,** 33–64 (2012).

26. Helmink, B. A. & Sleckman, B. P. The Response to and Repair of RAG-Mediated DNA Double-Strand Breaks. *Annu. Rev. Immunol.* **30,** 175–202 (2012).

27. Alt, F. W., Zhang, Y., Meng, F.-L., Guo, C. & Schwer, B. Mechanisms of Programmed DNA Lesions and Genomic Instability in the Immune System. *Cell* **152,** 417–429 (2013).

28. Symington, L. S. End resection at double-strand breaks: mechanism and regulation. *Cold Spring Harb Perspect Biol* **6,** (2014).

29. Harper, J. W. & Elledge, S. J. The DNA damage response: ten years after. *Molecular Cell* **28,** 739–745 (2007).

30. Stracker, T. H. & Petrini, J. H. J. The MRE11 complex: starting from the ends. *Nat. Rev. Mol. Cell Biol.* **12,** 90–103 (2011).

31. Trujillo, K. M. *et al.* Yeast xrs2 binds DNA and helps target rad50 and mre11 to DNA ends. *J. Biol. Chem.* **278,** 48957–48964 (2003).

32. Lisby, M., Barlow, J. H., Burgess, R. C. & Rothstein, R. Choreography of the DNA damage response: spatiotemporal relationships among checkpoint and repair proteins. *Cell* **118,** 699–713 (2004).

33. Lammens, A., Schele, A. & Hopfner, K. P. Structural biochemistry of ATP-driven dimerization and DNA-stimulated activation of SMC ATPases. *Curr. Biol.* **14,** 1778–1782 (2004).

34. Seeber, A. *et al.* RPA Mediates Recruitment of MRX to Forks and Double-Strand Breaks to Hold Sister Chromatids Together. *Molecular Cell* (2016). doi:10.1016/j.molcel.2016.10.032

35. Ciccia, A. & Elledge, S. J. The DNA damage response: making it safe to play with knives. *Molecular Cell* **40,** 179–204 (2010).

36. Paciotti, V., Clerici, M., Lucchini, G. & Longhese, M. P. The checkpoint protein Ddc2, functionally related to S. pombe Rad26, interacts with Mec1 and is regulated by Mec1-dependent phosphorylation in budding yeast. *Genes Dev.* **14,** 2046–2059 (2000).

37. Friedel, A. M., Pike, B. L. & Gasser, S. M. ATR/Mec1: coordinating fork stability and repair. *FEBS Lett.* **513,** 237–244 (2009).

38. Nakada, D., Matsumoto, K. & Sugimoto, K. ATM-related Tel1 associates with double-strand breaks through an Xrs2-dependent mechanism. *Genes Dev.* **17,** 1957–1962 (2003).

39. Lee, J. H. & Paull, T. T. ATM activation by DNA double-strand breaks through the Mre11-Rad50-Nbs1 complex. *Science* **308,** 551–554 (2005).

40. Villa, M., Cassani, C., Gobbini, E., Bonetti, D. & Longhese, M. P. Coupling end resection with the checkpoint response at DNA double-strand breaks. *Cell. Mol. Life Sci.* **73,** 3655–3663 (2016).

41. Cassani, C. *et al.* Tel1 and Rif2 Regulate MRX Functions in End-Tethering and Repair of DNA Double-Strand Breaks. *PLoS Biol.* **14,** e1002387 (2016).

42. Sanchez, Y. *et al.* Regulation of RAD53 by the ATM-like kinases MEC1 and TEL1 in yeast cell cycle checkpoint pathways. *Science* **271,** 357–360 (1996).

43. Lieber, M. R. The mechanism of double-strand DNA break repair by the nonhomologous DNA end-joining pathway. *Annu. Rev. Biochem.* **79,** 181–211 (2010).

44. Aravind, L. & Koonin, E. V. Prokaryotic homologs of the eukaryotic DNA-end-binding protein Ku, novel domains in the Ku protein and prediction of a prokaryotic double-strand break repair system. *Genome Res.* **11,** 1365–1374 (2001).

45. Doherty, A. J., Jackson, S. P. & Weller, G. R. Identification of bacterial homologues of the Ku DNA repair proteins. *FEBS Lett.* **500,** 186–188 (2001).

46. Boulton, S. J. & Jackson, S. P. Saccharomyces cerevisiae Ku70 potentiates illegitimate DNA double-strand break repair and serves as a barrier to error-prone DNA repair pathways. *EMBO J.* **15,** 5093–5103 (1996).

47. Milne, G. T., Jin, S., Shannon, K. B. & Weaver, D. T. Mutations in two Ku homologs define a DNA end-joining repair pathway in Saccharomyces cerevisiae. *Mol. Cell. Biol.* **16,** 4189–4198 (1996).

48. Herrmann, G., Lindahl, T. & Schär, P. Saccharomyces cerevisiae LIF1: a function involved in DNA double-strand break repair related to mammalian XRCC4. *EMBO J.* **17,** 4188–4198 (1998).

49. Teo, S. H. & Jackson, S. P. Lif1p targets the DNA ligase Lig4p to sites of DNA double-strand breaks. *Curr. Biol.* **10,** 165–168 (2000).

50. Chen, L., Trujillo, K., Ramos, W., Sung, P. & Tomkinson, A. E. Promotion of Dnl4-catalyzed DNA end-joining by the Rad50/Mre11/Xrs2 and Hdf1/Hdf2 complexes. *Molecular Cell* **8,** 1105–1115 (2001).

51. Wilson, T. E., Grawunder, U. & Lieber, M. R. Yeast DNA ligase IV mediates non-homologous DNA end joining. *Nature* **388,** 495–498 (1997).

52. Graham, T. G. W., Walter, J. C. & Loparo, J. J. Two-Stage Synapsis of DNA Ends during Non-homologous End Joining. *Molecular Cell* **61,** 850–858 (2016).

53. Wilson, T. E. & Lieber, M. R. Efficient processing of DNA ends during yeast nonhomologous end joining. Evidence for a DNA polymerase beta (Pol4)-dependent pathway. *J. Biol. Chem.* **274,** 23599–23609 (1999).

54. Wu, X., Wilson, T. E. & Lieber, M. R. A role for FEN-1 in nonhomologous DNA end joining: the order of strand annealing and nucleolytic processing events. *Proc. Natl. Acad. Sci. U.S.A.* **96,** 1303–1308 (1999).

55. Tseng, H.-M. & Tomkinson, A. E. Processing and joining of DNA ends coordinated by interactions among Dnl4/Lif1, Pol4, and FEN-1. *J. Biol. Chem.* **279,** 47580–47588 (2004).

56. McVey, M. & Lee, S. E. MMEJ repair of double-strand breaks (director's cut): deleted sequences and alternative endings. *Trends Genet.* **24,** 529–538 (2008).

57. Sfeir, A. & Symington, L. S. Microhomology-Mediated End Joining: A Back-up Survival Mechanism or Dedicated Pathway? *Trends in Biochemical Sciences* **40,** 701–714 (2015).

58. Cannavo, E. & Cejka, P. Sae2 promotes dsDNA endonuclease activity within Mre11-Rad50-Xrs2 to resect DNA breaks. *Nature* **514,** 122–125 (2014).

59. Lee, K. & Lee, S. E. Saccharomyces cerevisiae Sae2- and Tel1-dependent single-strand DNA formation at DNA break promotes microhomology-mediated end joining. *Genetics* **176,** 2003–2014 (2007).

60. Mateos-Gomez, P. A. *et al.* Mammalian polymerase θ promotes alternative NHEJ and suppresses recombination. *Nature* **518,** 254–257 (2015).

61. Wang, H. C. *et al.* DNA ligase III as a candidate component of backup pathways of nonhomologous end joining. *Cancer Res.* **65,** 4020–4030 (2005).

62. Huertas, P. DNA resection in eukaryotes: deciding how to fix the break. *Nat. Struct. Mol. Biol.* **17,** 11–16 (2010).

63. Heyer, W.-D., Ehmsen, K. T. & Liu, J. Regulation of homologous recombination in eukaryotes. *Annu. Rev. Genet.* **44,** 113–139 (2010).

64. Kadyk, L. C. & Hartwell, L. H. Sister chromatids are preferred over homologs as substrates for recombinational repair in Saccharomyces cerevisiae. *Genetics* **132,** 387–402 (1992).

65. Nasmyth, K. & Haering, C. H. Cohesin: its roles and mechanisms. *Annu. Rev. Genet.* **43,** 525–558 (2009).

66. Huertas, P., Cortés-Ledesma, F., Sartori, A. A., Aguilera, A. & Jackson, S. P. CDK targets Sae2 to control DNA-end resection and homologous recombination. *Nature* **455,** 689–692 (2008).

67. Dynan, W. S. & Yoo, S. Interaction of Ku protein and DNA-dependent protein kinase catalytic subunit with nucleic acids. *Nucleic Acids Research* **26,** 1551–1559 (1998).

68. Zhu, Z., Chung, W.-H., Shim, E. Y., Lee, S. E. & Ira, G. Sgs1 helicase and two nucleases Dna2 and Exo1 resect DNA double-strand break ends. *Cell* **134,** 981–994 (2008).

69. Mimitou, E. P. & Symington, L. S. Sae2, Exo1 and Sgs1 collaborate in DNA double-strand break processing. *Nature* **455,** 770–774 (2008).

70. Chen, H., Lisby, M. & Symington, L. S. RPA Coordinates DNA End Resection and Prevents Formation of DNA Hairpins. *Molecular Cell* **50,** 589–600 (2013).

71. Deng, S. K., Gibb, B., de Almeida, M. J., Greene, E. C. & Symington, L. S. RPA antagonizes microhomology-mediated repair of DNA double-strand breaks. *Nat. Struct. Mol. Biol.* **21,** 405–U152 (2014).

72. New, J. H., Sugiyama, T., Zaitseva, E. & Kowalczykowski, S. C. Rad52 protein stimulates DNA strand exchange by Rad51 and replication protein A. *Nature* **391,** 407–410 (1998).

73. Shinohara, A. & Ogawa, T. Stimulation by Rad52 of yeast Rad51-mediated recombination. *Nature* **391,** 404–407 (1998).

74. Barzel, A. & Kupiec, M. Finding a match: how do homologous sequences get together for recombination? *Nat. Rev. Genet.* **9,** 27–37 (2008).

75. Weiner, A., Zauberman, N. & Minsky, A. Recombinational DNA repair in a cellular context: a search for the homology search. *Nat. Rev. Microbiol.* **7,** 748–755 (2009).

76. Renkawitz, J., Lademann, C. A., Kalocsay, M. & Jentsch, S. Monitoring Homology Search during DNA Double-Strand Break Repair In Vivo. *Molecular Cell* (2013). doi:10.1016/j.molcel.2013.02.020

77. Aylon, Y., Liefshitz, B., Bitan-Banin, G. & Kupiec, M. Molecular dissection of mitotic recombination in the yeast Saccharomyces cerevisiae. *Mol. Cell. Biol.* **23,** 1403–1417 (2003).

78. Maloisel, L., Fabre, F. & Gangloff, S. DNA polymerase delta is preferentially recruited during homologous recombination to promote heteroduplex DNA extension. *Mol. Cell. Biol.* **28,** 1373–1382 (2008).

79. Wright, W. D. & Heyer, W.-D. Rad54 functions as a heteroduplex DNA pump modulated by its DNA substrates and Rad51 during D loop formation. *Molecular Cell* **53,** 420–432 (2014).

80. Llorente, B., Smith, C. E. & Symington, L. S. Break-induced replication - What is it and what is it for? *Cell Cycle* **7,** 859–864 (2008).

81. Saini, N. *et al.* Migrating bubble during break-induced replication drives conservative DNA synthesis. *Nature* **502,** 389–+ (2013).

82. Bishop, D. K., Park, D., Xu, L. & Kleckner, N. DMC1: a meiosis-specific yeast homolog of E. coli recA required for recombination, synaptonemal complex formation, and cell cycle progression. *Cell* **69,** 439–456 (1992).

83. Sarbajna, S. & West, S. C. Holliday junction processing enzymes as guardians of genome stability. *Trends in Biochemical Sciences* **39,** 409–419 (2014).

84. Wu, L. & Hickson, I. D. The Bloom's syndrome helicase suppresses crossing over during homologous recombination. *Nature* **426,** 870–874 (2003).

85. Bhargava, R., Onyango, D. O. & Stark, J. M. Regulation of Single-Strand Annealing and its Role in Genome Maintenance. *Trends Genet.* **32,** 566–575 (2016).

86. Rothenberg, E., Grimme, J. M., Spies, M. & Ha, T. Human Rad52-mediated homology search and annealing occurs by continuous interactions between overlapping nucleoprotein complexes. *Proc. Natl. Acad. Sci. U.S.A.* **105,** 20274–20279 (2008).

87. Cremer, T. & Cremer, C. Chromosome territories, nuclear architecture and gene regulation in mammalian cells. *Nat. Rev. Genet.* **2,** 292–301 (2001).

88. Wang, X., Montero Llopis, P. & Rudner, D. Z. Organization and segregation of bacterial chromosomes. *Nat. Rev. Genet.* **14,** 191–203 (2013).

89. Sharma, R. & Meister, P. Nuclear organization in the nematode C. elegans. *Curr. Opin. Cell Biol.* **25,** 395–402 (2013).

90. Gibcus, J. H. & Dekker, J. The hierarchy of the 3D genome. *Molecular Cell* **49,** 773–782 (2013).

91. Lanctot, C., Cheutin, T., Cremer, M., Cavalli, G. & Cremer, T. Dynamic genome architecture in the nuclear space: regulation of gene expression in three dimensions. *Nat. Rev. Genet.* **8,** 104–115 (2007).

92. Cremer, T. *et al.* Chromosome territories - a functional nuclear landscape. *Curr. Opin. Cell Biol.* **18,** 307–316 (2006).

93. Cremer, T. & Cremer, M. Chromosome Territories. *Cold Spring Harb Perspect Biol* **2,** (2010).

94. Taddei, A., Schober, H. & Gasser, S. M. The budding yeast nucleus. *Cold Spring Harb Perspect Biol* **2,** a000612 (2010).

95. Zimmer, C. & Fabre, E. Principles of chromosomal organization: lessons from yeast. *J. Cell Biol.* **192,** 723–733 (2011).

96. Agmon, N., Liefshitz, B., Zimmer, C., Fabre, E. & Kupiec, M. Effect of nuclear architecture on the efficiency of double-strand break repair. *Nat Cell Biol* (2013). doi:10.1038/ncb2745

97. Torres-Rosell, J. *et al.* The Smc5-Smc6 complex and SUMO modification of Rad52 regulates recombinational repair at the ribosomal gene locus. *Nat Cell Biol* **9,** 923–931 (2007).

98. Duan, Z. *et al.* A three-dimensional model of the yeast genome. *Nature* **465,** 363–367 (2010).

99. Hakim, O. *et al.* DNA damage defines sites of recurrent chromosomal translocations in B lymphocytes. *Nature* **484,** 69–74 (2012).

100. Roukos, V. *et al.* Spatial dynamics of chromosome translocations in living cells. *Science* **341,** 660–664 (2013).

101. Roukos, V., Burman, B. & Misteli, T. The cellular etiology of chromosome translocations. *Curr. Opin. Cell Biol.* **25,** 357–364 (2013).

102. Lee, C.-S. *et al.* Chromosome position determines the success of double-strand break repair. *Proc. Natl. Acad. Sci. U.S.A.* (2015). doi:10.1073/pnas.1523660113

103. Loidl, J. The hidden talents of SPO11. *Dev. Cell* **24,** 123–124 (2013).

104. Renkawitz, J., Lademann, C. A. & Jentsch, S. Mechanisms and principles of homology search during recombination. *Nat. Rev. Mol. Cell Biol.* **15,** 369–383 (2014).

105. Agmon, N., Pur, S., Liefshitz, B. & Kupiec, M. Analysis of repair mechanism choice during homologous recombination. *Nucleic Acids Research* **37,** 5081–5092 (2009).

106. Hoang, M. L. *et al.* Competitive repair by naturally dispersed repetitive DNA during non-allelic homologous recombination. *PLoS Genet.* **6,** e1001228 (2010).

107. Burgess, S. M. & Kleckner, N. Collisions between yeast chromosomal loci in vivo are governed by three layers of organization. *Genes Dev.* **13,** 1871–1883 (1999).

108. Miné-Hattab, J. & Rothstein, R. Increased chromosome mobility facilitates homology search during recombination. *Nat Cell Biol* (2012). doi:10.1038/ncb2472

109. Dion, V., Kalck, V., Horigome, C., Towbin, B. D. & Gasser, S. M. Increased mobility of double-strand breaks requires Mec1, Rad9 and the homologous recombination machinery. *Nat Cell Biol* **14,** 1–9 (2012).

110. Haber, J. E. Mating-type gene switching in Saccharomyces cerevisiae. *Annu. Rev. Genet.* **32,** 561–599 (1998).

111. Wilson, A. M. *et al.* Homothallism: an umbrella term for describing diverse sexual behaviours. *IMA Fungus* **6,** 207–214 (2015).

112. Klar, A. J. Determination of the yeast cell lineage. *Cell* **49,** 433–435 (1987).

113. Herskowitz, I. Life cycle of the budding yeast Saccharomyces cerevisiae. *Microbiol. Rev.* **52,** 536–553 (1988).

114. Haber, J. E. Transpositions and translocations induced by site-specific double-strand breaks in budding yeast. *DNA Repair* **5,** 998–1009 (2006).

115. Hagen, D., Bruhn, L., Westby, C. & Sprague, G. Transcription of Alpha-Specific Genes in Saccharomyces-Cerevisiae - Dna-Sequence Requirements for Activity of the Coregulator Alpha-1. *Mol. Cell. Biol.* **13,** 6866–6875 (1993).

116. Strathern, J., Shafer, B., Hicks, J. & McGill, C. a/Alpha-specific repression by MAT alpha 2. *Genetics* **120,** 75–81 (1988).

117. Herschbach, B., Arnaud, M. & Johnson, A. Transcriptional Repression Directed by the Yeast Alpha-2 Protein in-Vitro. *Nature* **370,** 309–311 (1994).

118. Patterton, H. G. & Simpson, R. T. Nucleosomal location of the STE6 TATA box and Mat alpha 2p-mediated repression. *Mol. Cell. Biol.* **14,** 4002–4010 (1994).

119. Smith, R. L. & Johnson, A. D. Turning genes off by Ssn6-Tup1: a conserved system of transcriptional repression in eukaryotes. *Trends in Biochemical Sciences* **25,** 325–330 (2000).

120. Strathern, J., Hicks, J. & Herskowitz, I. Control of Cell Type in Yeast by the Mating Type Locus - the Alpha-1-Alpha-2 Hypothesis. *J. Mol. Biol.* **147,** 357–372 (1981).

121. Johnson, P. R., Swanson, R., Rakhilina, L. & Hochstrasser, M. Degradation signal masking by heterodimerization of MATalpha2 and MATa1 blocks their mutual destruction by the ubiquitin-proteasome pathway. *Cell* **94,** 217–227 (1998).

122. Strathern, J. N., Klar, A., Hicks, J. B., Abraham, J. A. & Ivy, J. M. Homothallic switching of yeast mating type cassettes is initiated by a double-stranded cut in the MAT locus. *Cell* (1982).

123. Kostriken, R., Strathern, J. N., Klar, A. J., Hicks, J. B. & Heffron, F. A site-specific endonuclease essential for mating-type switching in Saccharomyces cerevisiae. *Cell* **35,** 167–174 (1983).

124. Nasmyth, K. A. Molecular-Genetics of Yeast Mating Type. *Annu. Rev. Genet.* **16,** 439–500 (1982).

125. Weiss, K. & Simpson, R. T. High-resolution structural analysis of chromatin at specific loci: Saccharomyces cerevisiae silent mating type locus HML alpha. *Mol. Cell. Biol.* **18,** 5392–5403 (1998).

126. Connolly, B., White, C. I. & Haber, J. E. Physical Monitoring of Mating Type Switching in Saccharomyces-Cerevisiae. *Mol. Cell. Biol.* **8,** 2342–2349 (1988).

127. Loo, S. & Rine, J. Silencers and Domains of Generalized Repression. *Science* **264,** 1768–1771 (1994).

128. Imai, S., Armstrong, C. M., Kaeberlein, M. & Guarente, L. Transcriptional silencing and longevity protein Sir2 is an NAD-dependent histone deacetylase. *Nature* **403,** 795–800 (2000).

129. Moazed, D., Kistler, A., Axelrod, A., Rine, J. & Johnson, A. D. Silent information regulator protein complexes in Saccharomyces cerevisiae: A SIR2/SIR4 complex and evidence for a regulatory domain in SIR4 that inhibits its interaction with SIR3. *Proc. Natl. Acad. Sci. U.S.A.* **94,** 2186–2191 (1997).

130. Gasser, S. M. & Cockell, M. M. The molecular biology of the SIR proteins. *Gene* **279,** 1–16 (2001).

131. Abraham, J., Nasmyth, K. A., Strathern, J. N., Klar, A. & Hicks, J. B. Regulation of Mating-Type Information in Yeast - Negative Control Requiring Sequences Both 5' and 3' to the Regulated Region. *J. Mol. Biol.* **176,** 307–331 (1984).

132. Brand, A. H., Breeden, L., Abraham, R., Sternglanz, R. & Nasmyth, K. Characterization of a Silencer in Yeast - a Dna-Sequence with Properties Opposite to Those of a Transcriptional Enhancer. *Cell* **41,** 41–48 (1985).

133. Mahoney, D. J. & Broach, J. R. The HML mating-type cassette of Saccharomyces cerevisiae is regulated by two separate but functionally equivalent silencers. *Mol. Cell. Biol.* **9,** 4621–4630 (1989).

134. Nasmyth, K. The determination of mother cell-specific mating type switching in yeast by a specific regulator of HO transcription. *EMBO J.* **6,** 243–248 (1987).

135. Rudin, N. & Haber, J. E. Efficient repair of HO-induced chromosomal breaks in Saccharomyces cerevisiae by recombination between flanking homologous sequences. *Mol. Cell. Biol.* **8,** 3918–3928 (1988).

136. Krogh, B. O. & Symington, L. S. Recombination proteins in yeast. *Annu. Rev. Genet.* **38,** 233–271 (2004).

137. Hicks, W. M., Yamaguchi, M. & Haber, J. E. Real-time analysis of double-strand DNA break repair by homologous recombination. *Proc. Natl. Acad. Sci. U.S.A.* **108,** 3108–3115 (2011).

138. Nickoloff, J. A., Chen, E. Y. & Heffron, F. A 24-base-pair DNA sequence from the MAT locus stimulates intergenic recombination in yeast. *Proc. Natl. Acad. Sci. U.S.A.* **83,** 7831–7835 (1986).

139. McGill, C., Shafer, B. & Strathern, J. Coconversion of flanking sequences with homothallic switching. *Cell* **57,** 459–467 (1989).

140. Klar, A. J., Hicks, J. B. & Strathern, J. N. Directionality of yeast mating-type interconversion. *Cell* **28,** 551–561 (1982).

141. Weiler, K. S. & Broach, J. R. Donor locus selection during Saccharomyces cerevisiae mating type interconversion responds to distant regulatory signals. *Genetics* **132,** 929–942 (1992).

142. Wu, X. & Haber, J. E. A 700 bp cis-acting region controls mating-type dependent recombination along the entire left arm of yeast chromosome III. *Cell* **87,** 277–285 (1996).

143. Wu, X., Moore, J. K. & Haber, J. E. Mechanism of MAT alpha donor preference during mating-type switching of Saccharomyces cerevisiae. *Mol. Cell. Biol.* **16,** 657–668 (1996).

144. Wu, X., Wu, C. & Haber, J. E. Rules of donor preference in saccharomyces mating-type gene switching revealed by a competition assay involving two types of recombination. *Genetics* **147,** 399–407 (1997).

145. Sun, K., Coïc, E., Zhou, Z., Durrens, P. & Haber, J. E. Saccharomyces forkhead protein Fkh1 regulates donor preference during mating-type switching through the recombination enhancer. *Genes Dev.* **16,** 2085–2096 (2002).

146. Weiss, K. & Simpson, R. T. Cell type-specific chromatin organization of the region that governs directionality of yeast mating type switching. *EMBO J.* **16,** 4352–4360 (1997).

147. Wu, C. & Haber, J. E. Mcm1 regulates donor preference controlled by the recombination enhancer in Saccharomyces mating-type switching. *Genes Dev.* 1–12 (1998).

148. Smith, D. L. & Johnson, A. D. Operator-Constitutive Mutations in a Dna-Sequence Recognized by a Yeast Homeodomain. *EMBO J.* **13,** 2378–2387 (1994).

149. Tan, S. & Richmond, T. J. Crystal structure of the yeast MATalpha2/MCM1/DNA ternary complex. *Nature* **391,** 660–666 (1998).

150. Belton, J.-M. *et al.* The Conformation of Yeast Chromosome III Is Mating Type Dependent and Controlled by the Recombination Enhancer. *Cell Reports* (2015). doi:10.1016/j.celrep.2015.10.063

151. Szeto, L., Fafalios, M. K., Zhong, H., Vershon, A. K. & Broach, J. R. Alpha2p controls donor preference during mating type interconversion in yeast by inactivating a recombinational enhancer of chromosome III. *Genes Dev.* **11,** 1899–1911 (1997).

152. Coïc, E., Sun, K., Wu, C. & Haber, J. E. Cell cycle-dependent regulation of Saccharomyces cerevisiae donor preference during mating-type switching by SBF (Swi4/Swi6) and Fkh1. *Mol. Cell. Biol.* **26,** 5470–5480 (2006).

153. Spellman, P. T. *et al.* Comprehensive identification of cell cycle-regulated genes of the yeast Saccharomyces cerevisiae by microarray hybridization. *Mol. Biol. Cell* **9,** 3273–3297 (1998).

154. Ostrow, A. Z. *et al.* Fkh1 and Fkh2 Bind Multiple Chromosomal Elements in the S. cerevisiae Genome with Distinct Specificities and Cell Cycle Dynamics. *PLoS ONE* **9,** e87647 (2014).

155. Hammet, A. *et al.* FHA domains as phospho-threonine binding modules in cell signaling. *IUBMB Life* **55,** 23–27 (2003).

156. Pennell, S. *et al.* Structural and functional analysis of phosphothreonine-dependent FHA domain interactions. *Structure* **18,** 1587–1595 (2010).

157. Li, J. *et al.* Regulation of Budding Yeast Mating-Type Switching Donor Preference by the FHA Domain of Fkh1. *PLoS Genet.* **8,** e1002630 (2012).

158. Coïc, E., Richard, G.-F. & Haber, J. E. Saccharomyces cerevisiae donor preference during mating-type switching is dependent on chromosome architecture and organization. *Genetics* **173,** 1197–1206 (2006).

159. Kalocsay, M., Hiller, N. J. & Jentsch, S. Chromosome-wide Rad51 spreading and SUMO-H2A.Z-dependent chromosome fixation in response to a persistent DNA double-strand break. *Molecular Cell* **33,** 335–343 (2009).

160. Lee, S. E. *et al.* Saccharomyces Ku70, mre11/rad50 and RPA proteins regulate adaptation to G2/M arrest after DNA damage. *Cell* **94,** 399–409 (1998).

161. Jacquier, A. & Dujon, B. An intron-encoded protein is active in a gene conversion process that spreads an intron into a mitochondrial gene. *Cell* **41,** 383–394 (1985).

162. Choulika, A., Perrin, A., Dujon, B. & Nicolas, J. F. Induction of homologous recombination in mammalian chromosomes by using the I-SceI system of Saccharomyces cerevisiae. *Mol. Cell. Biol.* **15,** 1968–1973 (1995).

163. Knop, M. *et al.* Epitope tagging of yeast genes using a PCR-based strategy: more tags and improved practical routines. *Yeast* **15,** 963–972 (1999).

164. Janke, C. *et al.* A versatile toolbox for PCR-based tagging of yeast genes: new fluorescent proteins, more markers and promoter substitution cassettes. *Yeast* 1–16 (2004). doi:10.1002/yea.1142

165. Nickoloff, J. A., Singer, J. D. & Heffron, F. In vivo analysis of the Saccharomyces cerevisiae HO nuclease recognition site by site-directed mutagenesis. *Mol. Cell. Biol.* **10,** 1174–1179 (1990).

166. Jin, Q., Trelles-Sticken, E., Scherthan, H. & Loidl, J. Yeast nuclei display prominent centromere clustering that is reduced in nondividing cells and in meiotic prophase. *J. Cell Biol.* **141,** 21–29 (1998).

167. Jin, Q. W., Fuchs, J. & Loidl, J. Centromere clustering is a major determinant of yeast interphase nuclear organization. *J. Cell. Sci.* **113 (Pt 11),** 1903–1912 (2000).

168. Smith, D. & Johnson, A. A Molecular Mechanism for Combinatorial Control in Yeast - Mcm1 Protein Sets the Spacing and Orientation of the Homeodomains of an Alpha-2 Dimer. *Cell* **68,** 133–142 (1992).

169. Keleher, C., Passmore, S. & Johnson, A. Yeast Repressor Alpha-2 Binds to Its Operator Cooperatively with Yeast Protein Mcm1. *Mol. Cell. Biol.* **9,** 5228–5230 (1989).

170. Laney, J. D., Mobley, E. F. & Hochstrasser, M. The short-lived Matalpha2 transcriptional repressor is protected from degradation in vivo by interactions with its corepressors Tup1 and Ssn6. *Mol. Cell. Biol.* **26,** 371–380 (2006).

171. Kumar, R. *et al.* Forkhead transcription factors, Fkh1p and Fkh2p, collaborate with Mcm1p to control transcription required for M-phase. *Curr. Biol.* **10,** 896–906 (2000).

172. Hollenhorst, P. C. Mechanisms controlling differential promoter-occupancy by the yeast forkhead proteins Fkh1p and Fkh2p: implications for regulating the cell cycle and differentiation. *Genes Dev.* **15,** 2445–2456 (2001).

173. Zhu, G. *et al.* Two yeast forkhead genes regulate the cell cycle and pseudohyphal growth. *Nature* **406,** 90–94 (2000).

174. Hollenhorst, P. C., Bose, M. E., Mielke, M. R., Müller, U. & Fox, C. A. Forkhead

genes in transcriptional silencing, cell morphology and the cell cycle. Overlapping and distinct functions for FKH1 and FKH2 in Saccharomyces cerevisiae. *Genetics* **154,** 1533–1548 (2000).

175. Stone, J., Collinge, M., Smith, R., Horn, M. & Walker, J. Interaction of a Protein Phosphatase with an Arabidopsis Serine-Threonine Receptor Kinase. *Science* **266,** 793–795 (1994).

176. Sun, Z. X., Hsiao, J., Fay, D. S. & Stern, D. F. Rad53 FHA domain associated with phosphorylated Rad9 in the DNA damage checkpoint. *Science* **281,** 272–274 (1998).

177. Durocher, D. *et al.* The Molecular Basis of FHA Domain:Phosphopeptide Binding Specificity and Implications for Phospho-Dependent Signaling Mechanisms. *Molecular Cell* **6,** 1169–1182 (1999).

178. Liao, H., Byeon, I. & Tsai, M. D. Structure and function of a new phosphopeptide-binding domain containing the FHA2 of Rad53. *J. Mol. Biol.* **294,** 1041–1049 (1999).

179. Durocher, D., Henckel, J., Fersht, A. R. & Jackson, S. P. The FHA domain is a modular phosphopeptide recognition motif. *Molecular Cell* **4,** 387–394 (1999).

180. Hanna, D. E., Rethinaswamy, A. & Glover, C. V. Casein kinase II is required for cell cycle progression during G1 and G2/M in Saccharomyces cerevisiae. *J. Biol. Chem.* **270,** 25905–25914 (1995).

181. Padmanabha, R., Chen-Wu, J. L., Hanna, D. E. & Glover, C. V. Isolation, sequencing, and disruption of the yeast CKA2 gene: casein kinase II is essential for viability in Saccharomyces cerevisiae. *Mol. Cell. Biol.* **10,** 4089–4099 (1990).

182. Rossetto, D., Truman, A. W., Kron, S. J. & Cote, J. Epigenetic Modifications in Double-Strand Break DNA Damage Signaling and Repair. *Clin. Cancer Res.* **16,** 4543–4552 (2010).

183. Harrison, J. C. & Haber, J. E. Surviving the breakup: the DNA damage checkpoint. *Annu. Rev. Genet.* **40,** 209–235 (2006).

184. Zhao, X., Muller, E. G. & Rothstein, R. A suppressor of two essential checkpoint genes identifies a novel protein that negatively affects dNTP pools. *Molecular Cell* **2,** 329–340 (1998).

185. Postnikoff, S. D. L., Malo, M. E., Wong, B. & Harkness, T. A. A. The yeast forkhead transcription factors fkh1 and fkh2 regulate lifespan and stress response together with the anaphase-promoting complex. *PLoS Genet.* **8,** e1002583 (2012).

186. Ho, Y. *et al.* Systematic identification of protein complexes in Saccharomyces cerevisiae by mass spectrometry. *Nature* **415,** 180–183 (2002).

187. Prakash, R. *et al.* Yeast Mph1 helicase dissociates Rad51-made D-loops: implications for crossover control in mitotic recombination. *genesdev.cshlp.org* (2008).

188. Whitby, M. C. The FANCM family of DNA helicases/translocases. *DNA Repair* **9,** 224–236 (2010).

189. Dummer, A. M. *et al.* Binding of the Fkh1 Forkhead Associated Domain to a Phosphopeptide within the Mph1 DNA Helicase Regulates Mating-Type Switching in Budding Yeast. *PLoS Genet.* **12,** e1006094 (2016).

190. Silva, S. *et al.* Mte1 interacts with Mph1 and promotes crossover recombination and telomere maintenance. *Genes Dev.* **30,** 700–717 (2016).

191. Xue, X. *et al.* Differential regulation of the anti-crossover and replication fork regression activities of Mph1 by Mte1. *Genes Dev.* **30,** 687–699 (2016).

192. Chen, R. & Wold, M. S. Replication protein A: Single-stranded DNA's first responder Dynamic DNA-interactions allow replication protein A to direct single-strand DNA intermediates into different pathways for synthesis or repair. *Bioessays* **36,** 1156–1161 (2014).

193. Longhese, M., Plevani, P. & Lucchini, G. Replication Factor-a Is Required in-Vivo for Dna-Replication, Repair, and Recombination. *Mol. Cell. Biol.* **14,** 7884–7890

(1994).

194.   Thadani, R., Uhlmann, F. & Heeger, S. Condensin, chromatin crossbarring and chromosome condensation. *Curr. Biol.* **22,** R1012–21 (2012).

195.   Hirano, T. SMC-mediated chromosome mechanics: a conserved scheme from bacteria to vertebrates? *Genes Dev.* **13,** 11–19 (1999).

196.   Wilhelm, L. *et al.* SMC condensin entraps chromosomal DNA by an ATP hydrolysis dependent loading mechanism in Bacillus subtilis. *Elife* **4,** (2015).

197.   Uhlmann, F. SMC complexes: from DNA to chromosomes. *Nat. Rev. Mol. Cell Biol.* **17,** 399–412 (2016).

198.   Murray, J. M. & Carr, A. M. Smc5/6: a link between DNA repair and unidirectional replication? *Nat. Rev. Mol. Cell Biol.* **9,** 177–182 (2008).

199.   Stray, J. E. & Lindsley, J. E. Biochemical analysis of the yeast condensin Smc2/4 complex - An ATPase that promotes knotting of circular DNA. *J. Biol. Chem.* **278,** 26238–26248 (2003).

200.   Sun, M., Nishino, T. & Marko, J. F. The SMC1-SMC3 cohesin heterodimer structures DNA through supercoiling-dependent loop formation. *Nucleic Acids Research* **41,** 6149–6160 (2013).

201.   Fousteri, M. I. & LEHMANN, A. R. A novel SMC protein complex in Schizosaccharomyces pombe contains the Rad18 DNA repair protein. *EMBO J.* **19,** 1691–1702 (2000).

202.   Haber, J. E. Mating-Type Gene Switching in Saccharomyces-Cerevisiae. *Trends Genet.* **8,** 446–452 (1992).

203.   Takano, I. & Oshima, Y. An allele specific and a complementary determinant controlling homothallism in Saccharomyces oviformis. *Genetics* **57,** 875–885 (1967).

204.   Oshima, Y. & Takano, I. Mating types in Saccharomyces: their convertibility and homothallism. *Genetics* **67,** 327–335 (1971).

205.   Astell, C. R. *et al.* The sequence of the DNAs coding for the mating-type loci of Saccharomyces cerevisiae. *Cell* **27,** 15–23 (1981).

206.   Tatchell, K., Nasmyth, K. A., Hall, B. D., Astell, C. & Smith, M. In vitro mutation analysis of the mating-type locus in yeast. *Cell* **27,** 25–35 (1981).

207.   Forget, A. L. & Kowalczykowski, S. C. Single-molecule imaging of DNA pairing by RecA reveals a three-dimensional homology search. *Nature* **482,** 423–427 (2012).

208.   Štafa, A., Donnianni, R. A., Timashev, L. A., Lam, A. F. & Symington, L. S. Template Switching During Break-Induced Replication Is Promoted by the Mph1 Helicase in Saccharomyces cerevisiae. *Genetics* **196,** 1017–1028 (2014).

209.   Yimit, A., Kim, T., Anand, R. & Meister, S. YGR042W/MTE1 Functions in Double-Strand Break Repair with MPH1. *Nucleic Acids …* (2015). doi:10.1101/032581

210.   Chiolo, I. *et al.* Double-Strand Breaks in Heterochromatin Move Outside of a Dynamic HP1a Domain to Complete Recombinational Repair. *Cell* **144,** 732–744 (2011).

211.   Nagai, S. *et al.* Functional targeting of DNA damage to a nuclear pore-associated SUMO-dependent ubiquitin ligase. *Science* **322,** 597–602 (2008).

212.   Gehlen, L. R., Gasser, S. M. & Dion, V. How Broken DNA Finds Its Template for Repair: A Computational Approach. *Progress of Theoretical Physics Supplement* 20–29 (2011).

213.   Byrne, K. P. & Wolfe, K. H. The Yeast Gene Order Browser: Combining curated homology and syntenic context reveals gene fate in polyploid species. *Genome Res.* **15,** 1456–1461 (2005).

214.   Cheung, W. L. *et al.* Phosphorylation of histone H4 serine 1 during DNA damage requires casein kinase II in S. cerevisiae. *Curr. Biol.* **15,** 656–660 (2005).

215.   Costanzo, V. *et al.* An ATR- and Cdc7-dependent DNA damage checkpoint that inhibits initiation of DNA replication. *Molecular Cell* **11,** 203–213 (2003).

216.   Zou, L. & Elledge, S. J. Sensing DNA damage through ATRIP recognition of RPA-

ssDNA complexes. *Science* **300,** 1542–1548 (2003).

217. Matsuoka, S. *et al.* ATM and ATR substrate analysis reveals extensive protein networks responsive to DNA damage. *Science* **316,** 1160–1166 (2007).

218. Carlsson, P. & Mahlapuu, M. Forkhead transcription factors: key players in development and metabolism. *Dev. Biol.* **250,** 1–23 (2002).

219. Scheller, J., Schürer, A., Rudolph, C., Hettwer, S. & Kramer, W. MPH1, a yeast gene encoding a DEAH protein, plays a role in protection of the genome from spontaneous and chemically induced damage. *Genetics* **155,** 1069–1081 (2000).

220. Cherry, J. M. *et al.* Saccharomyces Genome Database: the genomics resource of budding yeast. *Nucleic Acids Research* **40,** D700–5 (2012).

221. Psakhye, I. & Jentsch, S. Protein Group Modification and Synergy in the SUMO Pathway as Exemplified in DNA Repair. *Cell* **151,** 807–820 (2012).

222. Brill, S. J. & Stillman, B. Replication Factor-a From Saccharomyces-Cerevisiae Is Encoded by 3 Essential Genes Coordinately Expressed at S-Phase. *Genes Dev.* **5,** 1589–1600 (1991).

223. Kagami, Y. & Yoshida, K. The functional role for condensin in the regulation of chromosomal organization during the cell cycle. *Cell. Mol. Life Sci.* (2016). doi:10.1007/s00018-016-2305-z

224. Remeseiro, S. & Losada, A. Cohesin, a chromatin engagement ring. *Curr. Opin. Cell Biol.* **25,** 63–71 (2013).

225. Sjogren, C. & Nasmyth, K. Sister chromatid cohesion is required for postreplicative double-strand break repair in Saccharomyces cerevisiae. *Curr. Biol.* **11,** 991–995 (2001).

226. De Piccoli, G. *et al.* Smc5-Smc6 mediate DNA double-strand-break repair by promoting sister-chromatid recombination. *Nat Cell Biol* **8,** 1032–1034 (2006).

227. Aono, N., Sutani, T., Tomonaga, T., Mochida, S. & Yanagida, M. Cnd2 has dual roles in mitotic condensation and interphase. *Nature* **417,** 197–202 (2002).

228. Takahashi, Y. *et al.* Cooperation of Sumoylated Chromosomal Proteins in rDNA Maintenance. *PLoS genetics* (2008). Available at: (Accessed: 27 July 2016)

229. Zhao, X. L. & Blobel, G. A SUMO ligase is part of a nuclear multiprotein complex that affects DNA repair and chromosomal organization. *Proc. Natl. Acad. Sci. U.S.A.* **102,** 4777–4782 (2005).

230. Kinoshita, K., Kobayashi, T. J. & Hirano, T. Balancing acts of two HEAT subunits of condensin I support dynamic assembly of chromosome axes. *Dev. Cell* **33,** 94–106 (2015).

231. Ausubel, F. M. *Current Protocols in Molecular Biology*. (John Wiley & Sons, 2010).

232. Sambrook, J., Fritsch, E. F. & Maniatis, T. *Molecular Cloning: A Laboratory Manual*. (Cold Spring Harbor Laboratory Press, 1989).

233. Thomas, B. J. & Rothstein, R. Elevated recombination rates in transcriptionally active DNA. *Cell* **56,** 619–630 (1989).

234. Zierhut, C. & Diffley, J. F. X. Break dosage, cell cycle stage and DNA replication influence DNA double strand break response. *EMBO J.* **27,** 1875–1885 (2008).

235. Gietz, R. D. & Sugino, A. New yeast-Escherichia coli shuttle vectors constructed with in vitro mutagenized yeast genes lacking six-base pair restriction sites. *Gene* **74,** 527–534 (1988).

236. Goldstein, A. L., Pan, X. & McCusker, J. H. Heterologous URA3MX cassettes for gene replacement in Saccharomyces cerevisiae. *Yeast* **15,** 507–511 (1999).

237. Akada, R. *et al.* PCR-mediated seamless gene deletion and marker recycling in Saccharomyces cerevisiae. *Yeast* **23,** 399–405 (2006).

238. Pâques, F. & Haber, J. E. Two pathways for removal of nonhomologous DNA ends during double-strand break repair in Saccharomyces cerevisiae. *Mol. Cell. Biol.* **17,** 6765–6771 (1997).

239. Lisby, M., Mortensen, U. H. & Rothstein, R. Colocalization of multiple DNA double-strand breaks at a single Rad52 repair centre. *Nat Cell Biol* **5,** 572–577

(2003).

240. Sugawara, N. & Haber, J. E. Monitoring DNA recombination initiated by HO endonuclease. *Methods Mol. Biol.* **920,** 349–370 (2012).
241. Gibson, D. G. *et al.* Enzymatic assembly of DNA molecules up to several hundred kilobases. *Nat. Methods* **6,** 343–345 (2009).
242. Aparicio, O. *et al.* Chromatin immunoprecipitation for determining the association of proteins with specific genomic sequences in vivo. *Curr Protoc Mol Biol* **Chapter 21,** Unit 21.3 (2005).

8 Abbreviations

3D	Three-dimensional
5'FOA	5'-Fluoroorotic acid
A	Alanine
AMP	Ampicillin
AU	Arbitrary unit
β-ME	β-mercaptoethanol
BER	base-excision repair
BIR	Break-induced replication
Bp	Base pairs
CDK	Cyclin-dependent kinase
CEN	Centromere
ChIP	Chromatin immunoprecipitation
ChIP-on-chip	ChIP analyzed by genome-wide tiling arrays
Chr	Chromosome
Da	Dalton
DDR	DNA damage response
dHJ	Double Holliday junction
DNA	Desoxyribonucleic acid
dNTP	Desoxynucleoside triphosphate
D-loop	Displacement loop
DSB	DNA double-strand break
DSBR	DNA double-strand break repair
E. coli	*Escherichia coli*
EDTA	Ethylenediaminetetraacetic acid
G	relative centrifugal force (RCF)
G1 phase	Gap 1 phase
G2 phase	Gap 2 phase
G418	Geneticine disulfate
Gal	Galactose
GFP	Green fluorescent protein
H	Hour
H2A	Histone 2 A
H3	Histone 3
H4	Histone 4
HA	Human influenza hemagglutinin
HML	Hidden *MAT* left, silent mating type locus
HMR	Hidden *MAT* right, silent mating type locus
HO	HO (homothallic switching) endonuclease
HO-cs	HO endonuclease DNA cleavage site
HphNT1	Gene conferring resistance to hygromycin
HR	Homologous recombination
HRP	Horseradish peroxidase
Hyg	Hygromycin
IP	Immunoprecipitation
Kan	Kanamycin
KanMX6	Gene conferring resistance to G418
Kb	Kilobase pairs
LB	Lysogeny broth
Log	Logarithmic
M	Molar
MAT	Mating type locus
MATα	*MAT* locus containing α information

MATa	*MAT* locus containing a information
Min	Minute
MMEJ	Microhomology-mediated end joining
MMR	Mismatch repair
MRX	MRX complex consisting of Rad50, Mre11 and Xrs2
Myc	Epitope derived from c-myc
N	Number of independent experiments
NaOH	Sodium hydroxide
Nat	Nourseothricin
NatNT2	Gene conferring resistance to nourseothricin
NER	Nucleotide-excision repair
NHEJ	Non-homologous end joining
Nt	Nucleotide
PAGE	Polyacrylamide gel electrophoresis
PCNA	Proliferating cell nuclear antigen
PCR	Polymerase chain reaction
qPCR	Quantitative real-time PCR
RPA	Replication protein A
R	Arginine
Rad	Radiation
Raf	Raffinose
rDNA	DNA coding for ribosomal RNA
RE	Recombination enhancer element
RNA	Ribonucleic acid
RT	Room temperature
S phase	Synthesis phase
SceI	SceI endonuclease
Sce-cs	SceI endonuclease DNA cleavage site
S. cerevisiae	*Saccharomyces cerevisiae*
SC media	Synthetic complete media
SDS	Sodium dodecylsulfate
SDSA	Synthesis-dependent strand annealing
SEM	Standard error of the mean
SPB	Spindle pole body
SSA	Single-strand annealing
ssDNA	Single-stranded DNA
SUMO	Small ubiquitin-like modifier
TCA	Trichloroacetic acid
Tel	Telomere
UV	Ultraviolet
V(D)J	Variable, diversity and joining genes
WT	Wildtype
γH2A	Histone 2 A phosphorylated on serine 129 (*S. cerevisiae*) or H2A.X phosphorylated on serine 139 in mammalian cells
YPD	Yeast bactopeptone dextrose

9 Acknowledgements

I thank Stefan Jentsch, my PhD supervisor, for the scientific freedom, creativity and possibilities he provided during the last years. He stimulated my own scientific ideas and his door was always open for questions and discussions. Stefan, I will never forget our first meeting, when you were wearing your characteristic Chucks and I got to know you as a truly inspiring person. Also I will never forget your sense of black humor and the overall great time in your lab.
You will always be remembered.

I would like to thank Prof Peter Becker for being my first referee. In addition, I thank Prof Marc Bramkamp for accepting to be the co-referee of this work. Furthermore, I want to kindly acknowledge all other members of my thesis committee at the LMU: Prof Angelika Böttger, Prof John Parsch, Prof Charles David and Prof Michael Boshart for reading and evaluating my thesis. Besides my thesis committee, I also thank my TAC: Prof Karl-Peter Hopfner and Dr Philipp Korber, for their support and ideas during our meetings.

I express my sincere gratitude to Claudio and Jörg, for their great support at the beginning and during my thesis. Thank you both for your inspiring discussions concerning homology search and the recombination enhancer. Also thank you for the fun in the lab. In addition, I thank Claudio for fruitful discussions about important details of the Marvel Universe…we are Groot! Moreover, I would like to thank Max for the experimental discussions at the beginning of my thesis as well as being the second half of the Jentsch FCB fan base. Irina, Sean, Sven and Alex: thanks a lot for the fun in the lab and the great time. Furthermore, I would also like to thank Markus and André, my favorite Mexican postdoc Matias and all the other members of the Jentsch department, especially highlighting Flo for discussing figures, titles and everything else of my thesis during the writing of this thesis and Ramazan, for discussions and being the first one to be instructed by me in recreational diving. I also thank Claudio, Jörg and Boris for critical reading of this thesis. Boris also has my gratitude for being supportive especially during the last months of my thesis.

Also thanks to the IMPRS coordination office, Hans-Jörg, Ingrid, Maxi and Amy, for your excellent support and organization of all the workshops.

I want to express my sincere gratitude to my mother for her ongoing support and honest encouragement, for everything she has done for me to make all this possible.

Finally I thank Carolin. You always supported and encouraged me to pursue my goals. Thank you for your motivational speeches, your patience and understanding. I am grateful to have you at my side. Thank you for your love.

10 Curriculum vitae

Personal Data

Name	Benjamin Anstett
Date and place of birth	20.03.1987, Pirmasens
Nationality	German
Profession	Biologist (M.Sc.)

Education

Since 01/2012	PhD studies in the group of Prof Dr Stefan Jentsch, Max Planck Institute of Biochemistry, Martinsried
	Thesis title: "Homology Search Guidance by the Yeast Recombination Enhancer"
10/2009 – 11/2011	Master studies "Molecular Biosciences", Ruprecht-Karls-University Heidelberg
	Thesis title: "Analysis of the Positioning of M Domain Motif 1 of the Disaggregase ClpB"
10/2006 – 09/2009	Bachelor studies "Biology", Technical University of Kaiserslautern
	Thesis title: "Investigations to the Redox State and Redox Regulation of Mitochondrial Proteins"
03/2006	A-levels (Abitur), Immanuel-Kant-Gymnasium Pirmasens

Publications

Oguchi Y, Kummer E, Seyffer F, Berynskyy M, Anstett B, Zahn R, Wade RC, Mogk A, Bukau B (2012): A tightly regulated molecular toggle controls AAA+ disaggregase.
Nature Structural and Molecular Biology (12):1338-46